

SVD-based Causal Emergence for Gaussian Iterative Systems

Kaiwei Liu¹, Linli Pan¹, Zhipeng Wang¹, Mingzhe Yang¹, Bing Yuan² and Jiang Zhang^{* 1,2}

¹ School of Systems Science, Beijing Normal University, 100875, Beijing, China

²Swarma Research, 102300, Beijing, China

Abstract

Causal emergence (CE) based on effective information (EI) demonstrates that macro-states can exhibit stronger causal effects than micro-states in dynamics. However, the identification of CE and the maximization of EI both rely on coarse-graining strategies, which is a key challenge. A recently proposed CE framework based on approximate dynamical reversibility, utilizing singular value decomposition (SVD), is independent of coarse-graining. Still, it is limited to transition probability matrices (TPM) in discrete states. To address this, this article proposes a novel CE quantification framework for Gaussian iterative systems (GIS), based on approximate dynamical reversibility derived from the SVD of inverse covariance matrices in forward and backward dynamics. The positive correlation between SVD-based and EI-based CE, along with the equivalence condition, is given analytically. After that, we provide precise coarse-graining strategies directly from singular value spectra and orthogonal matrices. This new framework can be applied to any dynamical system with continuous states and Gaussian noise, such as auto-regressive growth models, Markov-Gaussian systems, and even SIR modeling using neural networks (NN). Numerical simulations on typical cases validate our theory and offer a new approach to studying the CE phenomenon, emphasizing noise and covariance over dynamical functions in both known models and machine learning.

Keywords: Causal emergence, approximate dynamical reversibility, Gaussian iterative systems, singular value decomposition, inverse covariance matrix.

1 Introduction

Complex systems with dynamics are ubiquitous in the world around us, such as ecosystems [1], organisms [2, 3], brains [4–7], and cells [8, 9]. The interrelations between different dimensions and the accumulation of randomness result in entropy production and disorder, thereby complicating the analysis of dynamics of microscopic composition, such as individuals in society, cells in the human body, and atoms in matter [10, 11]. Many scholars contend that complex systems conceal profound patterns and regularities within their apparent disorder. For example, it is difficult to accurately describe the motion trajectory of microscopic molecules in gases or liquids, but the changes of both can be clearly described macroscopically using temperature and pressure. So they try to derive dynamical models of the systems at the macro-level by coarse-graining the dynamical systems, discovering that the strength of the causal effect [12–15] for macro-states can surpass those of micro-states, a phenomenon called causal emergence (CE) [16–21].

The typical quantitative framework for CE proposed by Hoel et al. [17, 18, 22] is based on effective information (EI) [16], demonstrating that coarse-grained macro-states may have larger EI than micro-states, especially in Boolean networks [17, 23], cellular automata [24, 25], even in Gaussian iterative systems (GIS) [26, 27]. With theoretical support, the study in Neural Information Squeezer plus (NIS+) [28, 29] based on Hoel’s EI framework utilizes neural networks (NN) to maximize EI and identify CE in data of the Boids model [30] or fRMI [31]. However, the dependence on coarse-graining strategies during maximizing EI within Hoel’s framework presents challenges. Because when facing practical problems, we need to find the optimal coarse-graining strategy that maximizes EI, which is difficult in high-dimensional complex systems.

Some research is independent of predefined coarse-graining strategies. A notable example is Rosas’ framework [19], which is based on integrated information decomposition theory [32, 33], and CE is quantified by calculating the synergic information (Syn) across micro-variables. However, this approach is challenging to implement due to the

*Email: zhangjiang@bnu.edu.cn

combinatorial explosion that occurs during the precise calculation of *Syn*. Although Rosas proposed approximate methods [34–36] with results on real-world datasets, such as ECoG [37] or MEG [38], these methods require predefined macro-state variables and representation learning, which also depends on the coarse-graining strategy. In addition, Barnett and Seth proposed a framework [20] for quantifying CE via dynamical independence. Yet, this framework has only been applied to linear systems and also requires predefined coarse-graining strategies [39]. Both methods utilize mutual information, making their results dependent on the distribution of variable states and unable to reflect causality.

To find a more essential quantification of CE, Zhang et al. recently proposed a CE quantification framework based on singular value decomposition (SVD) [40] for probability transition matrices (TPM), which is independent of the optimization of coarse-graining strategies and can simplify max EI calculation using SVD. Besides, the framework introduces the new concept of approximate dynamical reversibility derived from SVD to quantify the strength of the causal effects, which describes the proximity of TPM to a permutation matrix. SVD-based CE can be quantified as the potential maximal efficiency increase of approximate dynamical reversibility. This work also finds that the essence of CE lies in redundancy, represented by irreversible and correlated information pathways. What’s more, this article demonstrates a strong correlation between the SVD-based and maximized EI-based CE. However, this method only applies to discrete Markov chains [41] or complex networks [42, 43] and lacks an analytical and exact relation between the two quantifications of CE. More research is needed to extend this framework to continuous systems.

Based on the above theory, the motivation for this paper is to derive a new theory of CE for GIS based on dynamical reversibility and SVD, and prove that this theory is approximately equivalent to Hoel’s CE theory based on maximizing EI. To illustrate our theoretical framework, after briefly introducing linear GIS (Section Appendix A), we first introduce the concepts of causality and approximate dynamical reversibility in Sections 2.2 and 2.3, respectively. We then present the SVD-based CE framework and compare its equivalence to the EI-based CE (Section 2.3), as well as a coarse-graining strategy derived from SVD. Finally, we use 3 examples to illustrate how to use SVD to analyze the causal emergence properties of a dynamical system (Section 3).

2 Theories

2.1 Linear Gaussian iterative systems

Many real-world complex systems, whether physical, biological, economic, or social, exhibit dynamical behavior constructed by the interplay of deterministic laws and random disturbances as

$$x_{t+1} = f(x_t) + \eta_t, \eta_t \sim \mathcal{N}(0, \Sigma), \quad (2.1)$$

$x_t \in \mathcal{R}^n, \Sigma \in \mathcal{R}^{n \times n}$, which we called Gaussian iterative systems (GIS) [44, 45]. $f(x_t) : \mathcal{R}^n \rightarrow \mathcal{R}^n$ captures deterministic dynamics, η_t denotes random noise. Like Logistic map [46], Hénon map [47], including some continuous dynamic systems (such as Kuramoto [48], SIR [49], Lotka-Volterra [50]), can be approximated in this form.

For nonlinear functions, we usually linearize them to analyze their local properties. For any function $f(x_t) : \mathcal{R}^n \rightarrow \mathcal{R}^n$, it can be locally linearized by Taylor expansion as

$$x_{t+1} = a_0 + Ax_t + \eta_t, \eta_t \sim \mathcal{N}(0, \Sigma), \quad (2.2)$$

which we called linear GIS, where $a_0, x_t \in \mathcal{R}^n$, and $A, \Sigma \in \mathcal{R}^{n \times n}$. $A = \nabla f(x_t)$ corresponds to the Jacobian matrix around x_t . This equation can also be written in the form of a transition probability as

$$p(x_{t+1}|x_t) = \mathcal{N}(Ax_t + a_0, \Sigma). \quad (2.3)$$

This is the physical model we mainly analyze in this article, several one-dimensional cases of which are shown in Fig.1.

2.2 Causality and reversibility for linear systems

2.2.1 Causality

Dynamics expressed in equations Eq.(D.1) or Eq.(2.3) can be considered a causal model, the state x_t at time t causes changes in state x_{t+1} at the subsequent time $t + 1$. Thus, x_t is the cause variable and x_{t+1} is the effect variable. The causality discussed in this paper refers specifically to the strength of the causal effect of cause variables

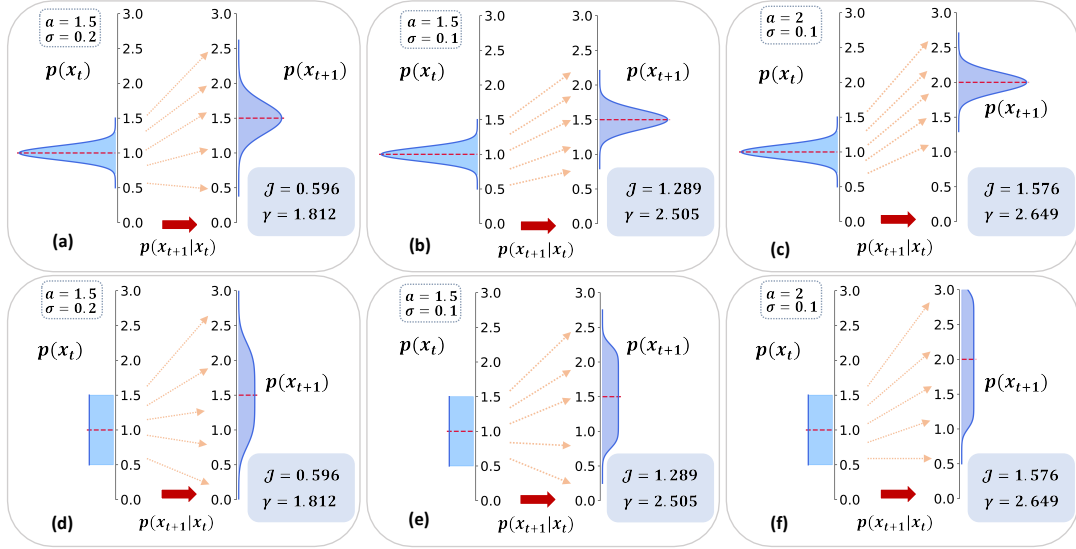


Figure 1: For 1-dimensional Gaussian information system $x_{t+1} = ax_t + \eta_t$, $\eta_t \sim \mathcal{N}(0, \sigma^2)$, we examine the dynamics under three different parameter settings and two distinct intervention distributions of $p(x_t)$, showing the resulting distributions $p(x_{t+1})$ and the corresponding measures of dimension averaged causal effect (\mathcal{J}) and approximate reversible information ($\gamma \equiv \gamma_1$). For any given probability density $p(x_t)$ at time t , the conditional probability $p(x_{t+1}|x_t) = \mathcal{N}(ax_t, \Sigma)$ corresponding to the forward dynamics gives the probability density $p(x_{t+1})$ at the next time step $t + 1$. In (a) and (d), when we stipulate $a = 1.5, \sigma = 0.2$, the dimensionally averaged EI $\mathcal{J} = 0.596$ and the dimensional average reversible information $\gamma = 1.812$ are satisfied. In (b) and (e), we decrease σ to $\sigma = 0.1$. Due to the increase in determinism, the dimensionally averaged EI increases to $\mathcal{J} = 1.289$, and the dimensional average reversible information increases to $\gamma = 2.505$, indicating that the approximate reversibility and causal effect strength are increased simultaneously. Then increase a in (c) (f) to $a = 2$. Due to the increase in non-degeneracy, the dimensionally averaged EI increases to $\mathcal{J} = 1.576$, and the dimensional average reversible information increases to $\gamma = 2.649$. From these simple cases, we can initially obtain three pieces of information: (1) \mathcal{J} and γ are only related to $p(x_{t+1}|x_t)$, and independent on the probability density $p(x_t)$ of x_t can be defined arbitrarily; (2) \mathcal{J} and γ are both positively correlated with determinism and non-degeneracy, and increase synchronously with the increase of a and decrease synchronously with the increase of σ ; (3) \mathcal{J} and γ are positively correlated.

on effect variables when given their causal relationship, which is the degree of certainty that when the cause changes, the effect will also change accordingly.

Fig.1 shows several examples of 1-dimensional linear GIS in Eq.(D.1), demonstrating the process of causality change from left to right. Specifically, when the dynamic parameter a in Eq.(D.1) is larger or the noise standard deviation σ is smaller, it is generally believed that the strength of the causal effect will be greater. Moreover, the strength of the causal effect should be independent of the input state distribution $p(x_t)$ and only related to the dynamics (or causal mechanism) $p(x_{t+1}|x_t)$ (compare the upper and lower figures in each column in Fig.1).

Tononi et al. and Hoel et al.[16, 17] invented effective information ($EI = I(x_t, x_{t+1}|do(x_t))$) to quantify the strength of causal effect for transitional matrices. Then Hoel et al. and Liu et al. [26, 27] extended EI to continuous systems. For linear GIS defined in Eq.(D.1) and Eq.(2.3), the dimensionally averaged EI (derived in Appendix B.1-B.2) is defined as

$$\mathcal{J} \equiv \frac{1}{n} I(x_{t+1}|do(x_t \sim \mathcal{U}([-L/2, L/2]^n))) = \ln \frac{\text{pdet}(A^T \Sigma^{-1} A)^{\frac{1}{2n}} L}{(2\pi e)^{\frac{1}{2}}} = \frac{1}{2n} \sum_{i=1}^{r_s} \ln s_i + \ln \frac{L}{(2\pi e)^{\frac{1}{2}}}, \quad (2.4)$$

where, $\text{pdet}(\cdot)$ represents the pseudo-determinant [51] of matrix \cdot . The operator $do(\cdot)$ signifies manual intervention, where $x_t \sim \mathcal{U}([-L/2, L/2]^n)$ after applying $do(\cdot)$ on x_t , with L being the interval size. Eq.(B.6) expands \mathcal{J} into the sum of $\ln s_i$, where $s_1 \geq \dots \geq s_{r_s}$ are the singular values of $A^T \Sigma^{-1} A$, and r_s is its rank. By comparing a-c and d-f in Fig.1, we can see that \mathcal{J} decreases as the standard deviation σ increases and increases as the parameter a increases. By comparing the upper and lower rows (Fig.1a and e, b and f, c and g), we can see that \mathcal{J} is independent of the distribution $p(x_t)$ of the state x_t , so \mathcal{J} can well measure the strength of the causal effect.

\mathcal{J} in Eq.(B.6) can be divided into two terms [17, 27]: **determinism** $Det = \ln \left[(2\pi e)^{-\frac{1}{2}} \text{pdet}(\Sigma^{-1})^{\frac{1}{2n}} \right]$ and **non-**

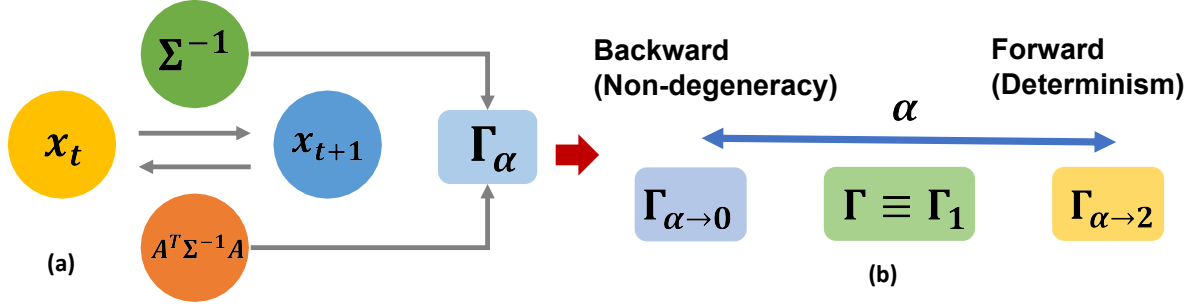


Figure 2: (a) For $p(x_{t+1}|x_t) = \mathcal{N}(Ax_t + a_0, \Sigma)$, the inverse covariance matrices of forward dynamics $x_{t+1} = a_0 + Ax_t + \eta_t$ and backward dynamics $x_t = A^\dagger x_{t+1} - A^\dagger a_0 - A^\dagger \eta_t$ are Σ^{-1} and $A^T \Sigma^{-1} A$, respectively. Σ^{-1} and $A^T \Sigma^{-1} A$ determine the approximate dynamical reversibility as Γ_α together. (b) $\alpha = 1$ is often chosen to balance Γ_α 's emphasis on both forward (determinism) and backward (non-degeneracy) dynamics. For $\alpha < 1$, Γ_α tends to capture more information about backward dynamics $p(x_t|x_{t+1})$ (non-degeneracy). For $\alpha > 1$, Γ_α emphasizes more information about forward dynamics $p(x_{t+1}|x_t)$ (determinism).

degeneracy $Nondeg = \ln \left[\text{pdet}(A^T \Sigma^{-1} A)^{\frac{1}{2n}} \text{pdet}(\Sigma)^{\frac{1}{2n}} L \right]$. These two indicators describe the degree of uncertainty of the effect variable when given the cause variable and the degree of uncertainty of the cause variable when given the effect variable.

2.2.2 Approximate dynamical reversibility

Another important property of dynamics that people are concerned about is dynamical reversibility. It is generally believed that the dynamics of the microscopic physical world (such as Newton's second law or the Schrödinger equation [52] in quantum mechanics) are dynamically reversible, while the second law of thermodynamics in the macroscopic world stems from the irreversibility of macroscopic dynamic processes [53, 54]. In Eq.(D.1), when $\eta_t = 0$ and $f(x_t) = a_0 + Ax_t$ is a reversible bijection mapping on \mathcal{R}^n , we assume that the dynamics of GIS described by Eq.(D.1) is strictly reversible as $x_{t+1} = a_0 + Ax_t$, and the corresponding backward dynamics of Eq.(D.1) can be directly established as $x_t = A^{-1}(x_{t+1} - a_0)$. However, real-world dynamical systems around us are not so simple and perfect.

The presence of random noise and the irreversibility of the matrix A in mapping $f : \mathcal{R}^n \rightarrow \mathcal{R}^n$ can make the dynamics irreversible. However, systems may still exhibit approximate reversibility when noise is small. If $f(x_t)$ is bijective, then the dynamics with a smaller noise variance are closer to reversible. Therefore, we can use approximate dynamical reversibility to measure their closeness to reversible dynamics. In [40], approximate dynamical reversibility can be quantified by the α -powered sum of the singular values of the TPM (Appendix C.1). Here, we extend this concept to GIS like Eq.(D.1) using singular value spectra from functional analysis [55] and Fourier methods [56]. We then derive the corresponding approximate dynamical reversibility indicator for GIS (derived in Appendix C.2-C.3), which is

$$\Gamma_\alpha = \left(\frac{2\pi}{\alpha} \right)^{\frac{n}{2}} \text{pdet}(A^T \Sigma^{-1} A)^{\frac{1}{2} - \frac{\alpha}{4}} \text{pdet}(\Sigma^{-1})^{\frac{\alpha}{4}}. \quad (2.5)$$

Apart from the constant term, the other two terms correspond to the pseudo-determinants of the inverse covariance matrices, i.e., Σ^{-1} and $A^T \Sigma^{-1} A$, of forward and backward dynamics, respectively (see Fig.2a).

$\alpha \in (0, 2)$ is a parameter to control the relative weight of the forward and backward inverse covariance matrices in Γ_α (see Fig.2b). When $\alpha \rightarrow 0$, $\Gamma_{\alpha \rightarrow 0} = \left(\frac{2\pi}{\alpha} \right)^{\frac{n}{2}}_{\alpha \rightarrow 0} \text{pdet}(A^T \Sigma^{-1} A)^{\frac{1}{2}}$ is dominated by the backward dynamics and reflects non-degeneracy after removing forward covariance interference. When $\alpha \rightarrow 2$, $\Gamma_{\alpha \rightarrow 2} = (\pi)^{\frac{n}{2}} \text{pdet}(\Sigma^{-1})^{\frac{1}{2}}$ is dominated by the forward dynamics and reflects determinism. In general, we set $\alpha = 1$ gives $\Gamma \equiv \Gamma_1$, where both directions contribute equally.

Γ_α quantifies approximate dynamical reversibility because when the uncertainties of the forward and backward dynamics are large, the pseudo-determinants of Σ^{-1} and $A^T \Sigma^{-1} A$ are small, indicating strong irreversibility. Conversely, when these uncertainties are small (approaching zero), the pseudo-determinants grow large, implying approximate reversible dynamics.

To avoid the excessive influence of variable dimension on the reversibility of dynamics, we can use the dimensional average reversible information $\hat{\gamma}_\alpha \equiv \frac{1}{n} \ln \Gamma_\alpha$ to more effectively quantify the approximate dynamical reversibility.

After removing the constant term, $\gamma_\alpha = \hat{\gamma}_\alpha - \frac{1}{2} \ln \left(\frac{2\pi}{\alpha} \right)$ is a variable only determined by the singular values after the SVD of Σ^{-1} and $A^T \Sigma^{-1} A$ (Lemma 2 in Appendix) as

$$\gamma_\alpha = \frac{1}{n} \left[\left(\frac{1}{2} - \frac{\alpha}{4} \right) \sum_{i=1}^{r_s} \ln s_i + \frac{\alpha}{4} \sum_{i=1}^{r_\kappa} \ln \kappa_i \right]. \quad (2.6)$$

Here r_s, r_κ denote the ranks of $A^T \Sigma^{-1} A$ and Σ^{-1} , respectively. s_i and κ_i denote the i -th singular value of $A^T \Sigma^{-1} A$ and Σ^{-1} respectively. Generally, we also set $\alpha = 1$ and $\gamma \equiv \gamma_1$.

Below each \mathcal{J} indicator in Fig.1, the corresponding γ for each mapping is also shown (where $\alpha = 1$). It can be seen that, same as \mathcal{J} , γ decreases with the increase of the standard deviation σ and increases with the increase of the dynamic parameter a . It is only related to the dynamics (the causal mechanism $p(x_{t+1}|x_t)$) and independent of the distribution $p(x_t)$.

2.2.3 Nearly linear relationship

This observation is not accidental. In fact, we have a general conclusion: γ_α is approximately linearly related to \mathcal{J} (Theorem 5 in Appendix). When the backward dynamics $p(x_t|x_{t+1})$ is close to a normalized normal distribution as $A^T \Sigma^{-1} A \approx I_n$, \mathcal{J} and γ_α satisfies

$$\gamma_\alpha \simeq \left(1 - \frac{\alpha}{4}\right) \mathcal{J} + C, \quad (2.7)$$

where $C = \left(1 - \frac{\alpha}{4}\right) \ln \left(\frac{L}{\sqrt{2\pi e}} \right)$ is a constant, and \simeq denotes approximate equality, this equality holds strictly when A is of full rank and $A^T \Sigma^{-1} A = I_n$, meaning the backward dynamics $p(x_t|x_{t+1})$ is a normalized normal distribution. Numerical experiments of randomly sampled A and Σ verify this linear relation, which is shown in Appendix C.4 and Figure 2 in the Appendix.

2.3 Causal emergence (CE)

CE refers to a special property of Markov dynamics: if the system's dynamics can yield a macroscopic dynamics with larger EI under a predefined coarse-graining strategy, then the system exhibits CE. However, this definition relies on the selection of coarse-graining strategies. Hoel et al. proposed the principle of maximizing EI [17, 18, 27, 29] to eliminate the arbitrariness of coarse-graining. However, this approach requires solving an often intractable optimization problem to obtain the optimal coarse-graining strategy and derive CE. To overcome this difficulty, Zhang et al. [40] introduced a new measure of CE based on approximate dynamical reversibility with SVD. Independent of coarse-graining, CE can be quantified directly from the singular value spectrum of the system's TPM. In the following section, we will extend this framework to GIS.

2.3.1 Causal emergence based on approximate dynamical reversibility with SVD

From the definition of dimensional average reversible information γ_α (Eq.C.37) in the Section 2.2.2, we can obtain that its final value depends only on two spectra, one is the spectrum $s_1 \geq \dots \geq s_n$ of $A^T \Sigma^{-1} A$, and the other is the spectrum $\kappa_1 \geq \dots \geq \kappa_n$ of Σ^{-1} . Thus, CE can be defined using these singular value spectra: it occurs when most reversible information is concentrated in a few dimensions with large singular values, allowing the dynamics to be coarse-grained via SVD-based dimensional reduction.

Thus, we can quantify CE based on approximate dynamical reversibility as follows:

$$\Delta \Gamma_\alpha(\epsilon) \equiv \gamma_\alpha(\epsilon) - \gamma_\alpha = \frac{1}{r_\epsilon} \left[\left(\frac{1}{2} - \frac{\alpha}{4} \right) \sum_{i=1}^{r_\epsilon} \ln s_i + \frac{\alpha}{4} \sum_{i=1}^{r_\epsilon} \ln \kappa_i \right] - \frac{1}{n} \left[\left(\frac{1}{2} - \frac{\alpha}{4} \right) \sum_{i=1}^{r_s} \ln s_i + \frac{\alpha}{4} \sum_{i=1}^{r_\kappa} \ln \kappa_i \right]. \quad (2.8)$$

Here $\epsilon \geq 0$ is a threshold for cutting the small singular values. $\Delta \Gamma_\alpha(\epsilon)$ is the strength of CE, and CE occurs with a threshold ϵ only if $\Delta \Gamma_\alpha(\epsilon) > 0$. Specifically, we call **clear CE** occurs when $\epsilon = 0$ (Definition 5 in Appendix), and **vague CE** occurs in other cases (Definition 6 in Appendix). If $A^T \Sigma^{-1} A$ or Σ^{-1} is not full-rank, clear CE occurs; otherwise, vague CE may occur.

The basic idea behind this definition is that the differences of γ before and after the small singular values (that is, satisfying $\kappa_i \leq \epsilon$ or $s_i \leq \epsilon$) are removed. And the number of remaining dimensions that contain two singular values is the effective rank r_ϵ as the dimension of the new system.

A simple example is given to show the occurrence of vague CE in Fig.3 with $\epsilon = 1.0$. This is a linear dynamical system with the given A and Σ as shown in Fig.3a, and its singular value spectra of forward and backward dynamics

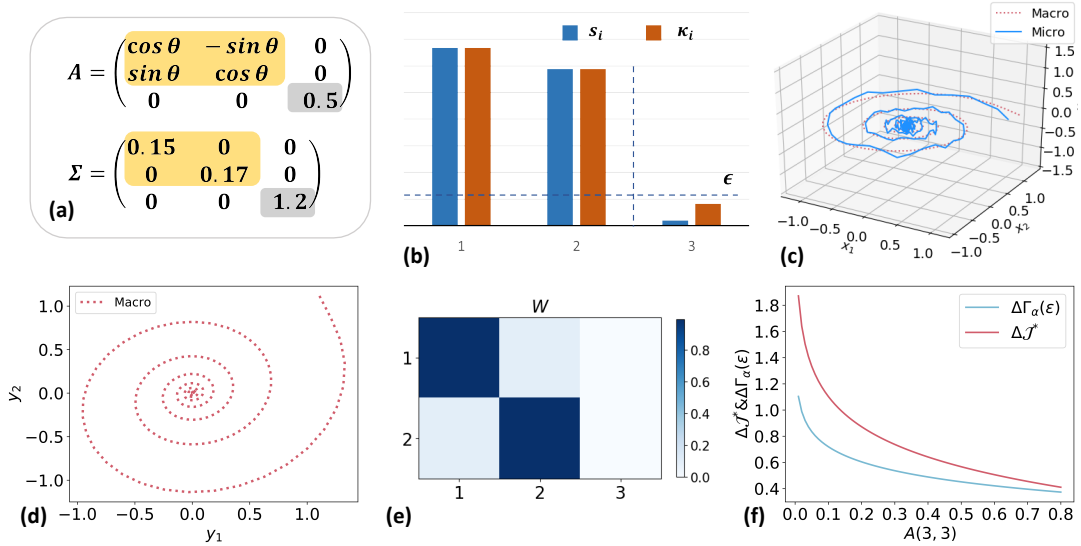


Figure 3: A case where vague CE occurs. A and Σ in (a) construct the GIS dynamics of a rotation model. In (b), the two singular values of the third dimension are less than the threshold $\epsilon = 1.0$, so $\Delta\Gamma_\alpha(\epsilon) > 0$ and vague CE occurs. In (c), the dynamic trajectory of macroscopic states in 3-dimensional Euclidean space \mathcal{R}^3 is shown. (d) and (e) correspond to the macroscopic dynamics trajectory in \mathcal{R}^2 obtained by the SVD method and the coarse-graining strategy based on which. (f) shows that as A_{33} , which represents the element of the 3rd row and 3rd column of A , increases. The strength of CE ($\Delta\Gamma_\alpha$) will decrease due to the decrease in the difference $s_2 - s_3 (> 0)$ between singular values s_2 and s_3 of $A^T \Sigma^{-1} A$. As a comparison, the strength CE based on the maximizing EI framework ($\Delta\mathcal{J}$) also decreases similarly.

are shown in Fig.3b. The trajectory in three-dimensional space is shown in Fig.3c. From Fig.3b, we can observe that the spectra exhibit a sharp decay between dimensions 2 and 3, therefore CE occurs. This phenomenon can be quantified by $\gamma(\epsilon)$ by setting the threshold ϵ (horizontal dashed line) to truncate near-zero singular values (right of the vertical dashed line). Actually, zero or near-zero singular values indicate redundant dimensions with near-zero dimensional average reversible information γ (e.g., the x_3 dimension in Fig.3c). Removing these dimensions through a coarse-graining strategy (which will be mentioned in the following section) enhances γ , and a more informative dynamics (macro-dynamics) can be obtained as shown in Fig.3d. Furthermore, Fig.3f shows the significance of CE decreases with the increase of the value of the right-bottom element in A .

2.3.2 Equivalence between the two frameworks

This framework is reasonable, and the most important reason is that our new definition of CE is consistent with Hoel et al.'s definition [17, 18, 22, 26, 57–59] (Appendix D.1) based on maximizing EI. There is an approximate linear relationship, analytically, between CE based on SVD and CE based on maximizing EI (Theorem 6 in Appendix). When the backward dynamics $p(x_t|x_{t+1})$ is close to a normalized normal distribution as $A^T \Sigma^{-1} A \approx I_n$ and $r_\epsilon = k$, k is the dimension of macro dynamics we set in the framework of maximizing EI (The operational recipe for choosing the macro dimension k is given in Appendix D.1.2), $\Delta\Gamma_\alpha(\epsilon)$ and $\Delta\mathcal{J}^*$ are approximately linear and positively correlated as

$$\Delta\Gamma_\alpha(\epsilon) \simeq \left(1 - \frac{\alpha}{4}\right) \Delta\mathcal{J}^*. \quad (2.9)$$

The equal sign holds when the backward dynamics $p(x_t|x_{t+1})$ is a normalized normal distribution as $A^T \Sigma^{-1} A = I_n$. Numerical experiments of randomly sampled A and Σ verify this linear relation, which is shown in Appendix D.3 and Figure 2 in the Appendix. In Eq.(D.19), $\Delta\mathcal{J}^*$ is the optimal result of CE based on the EI maximization framework proposed by Hoel et al. and Liu et al. [17, 18, 27, 29] defined as

$$\Delta\mathcal{J}^* = \frac{1}{2k} \sum_{i=1}^k \ln s_i - \frac{1}{2n} \sum_{i=1}^r \ln s_i, \quad (2.10)$$

in which $s_1 \geq \dots \geq s_n$ represents the singular values of the matrix $A^T \Sigma^{-1} A$, r is its rank. In the simple example of CE shown in Fig. 3, both $\Delta\Gamma_\alpha$ and $\Delta\mathcal{J}^*$ decrease with increasing A_{33} , which is the value of the 3-row and 3-column

element of A .

From another perspective, our definition of CE is actually an approximate necessary condition for maximizing EI-based CE as defined by Hoel et al. [17, 18]. In other words, for any Markov dynamics, if we want to find a coarse-graining strategy that maximizes EI, we can actually perform SVD on the dynamics first. Although there is a high likelihood that the two frameworks overlap, they are not entirely equivalent because the coarse-graining strategy obtained by maximizing EI ignores the covariance of forward dynamics. So, we need to propose a method that constructs a coarse-graining strategy based on SVD, in which both forward and backward dynamics are taken into account.

2.3.3 Coarse-graining strategy based on SVD

For any GIS, we can first perform SVD on both $A^T \Sigma^{-1} A$ and Σ^{-1} to obtain the two spectra $s_1 > \dots > s_n$ and $\kappa_1 > \dots > \kappa_n$. We then need to consider both sets of spectra for truncation. However, since their corresponding singular vectors may not all be orthogonal, their subspaces may overlap or conflict. Therefore, we combine two singular vector matrices and perform a second round of SVD. Based on this, we can obtain the coarse-graining matrix and the corresponding macro dynamics accordingly by dimension reduction. After these two rounds of SVD, we obtain the final result (detailed in Appendix E.2).

2.4 Extension for nonlinear system

The content discussed above is for linear GIS. For the more universal form of Eq.(A.1), we can perform a local Taylor expansion of $f(x)$, thereby transforming it into the linear form of Eq.(D.1). In this way, we can calculate the quantification of CE ($\Delta \Gamma_\alpha^{x_t}(\epsilon)$) locally (which depends on x_t).

Since most of the dynamics we consider are stationary Markov processes, we can discuss their global CE properties. For this purpose, we can approximate the global properties of CE by averaging the local properties of dynamics. For general problems, if x_{t+1} is approximately distributed within the interval \mathcal{X} , and $A_{x_t}^T \Sigma_{x_t}^{-1} A_{x_t}$ and $\Sigma_{x_t}^{-1}$ do not fluctuate or diverge significantly, we can first randomly sample and then average the parameter matrix to obtain $A^T \Sigma^{-1} A \approx \langle A_{x_t}^T \Sigma_{x_t}^{-1} A_{x_t} \rangle_{x_t \in \mathcal{X}}$ and $\Sigma^{-1} \approx \langle \Sigma_{x_t}^{-1} \rangle_{x_t \in \mathcal{X}}$ to calculate the two global inverse covariance matrices. Finally, we can calculate global CE based on the averaged results of these two matrices (detailed in Appendix A.1).

The above is our theoretical part. In the next section, we show the results of applying our framework to three practical cases.

3 Results

In this section, we present the results of three numerical experimental examples to illustrate the concepts and conclusions derived in the previous sections. The first two are for GIS with known models, and the third is the application on a neural network trained on time series data generated by a Susceptible-Infected-Recovered (SIR) model.

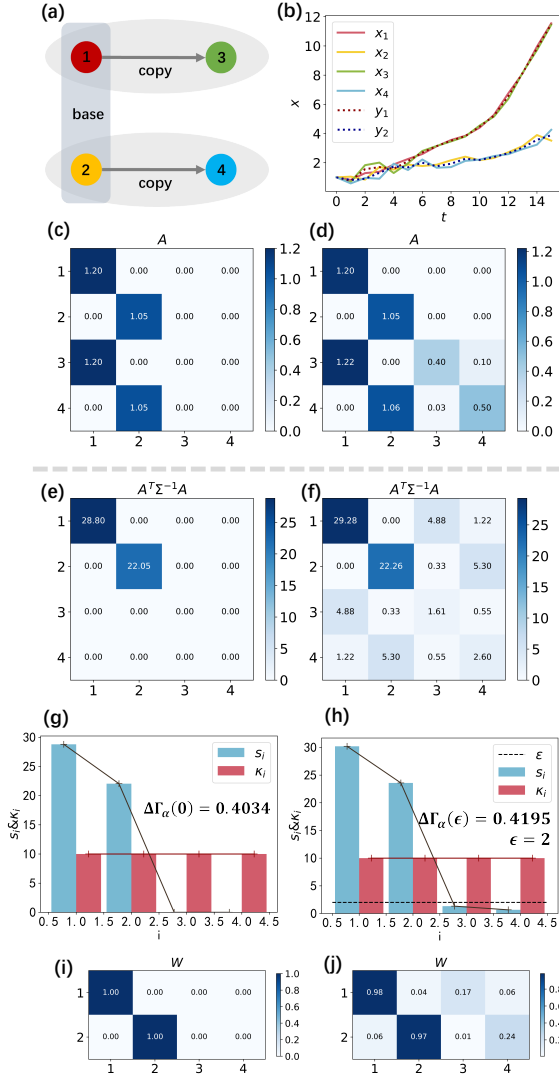
3.1 Malthusian growth models

The first example contains 4 variables, in which the first two variables x_1, x_2 follow the Malthusian growth model [60] with different growth rates of 0.2 and 0.05. To study CE, we define the other two variables x_3, x_4 as the copies of the first two variables shown as Fig.8a, thus, they are redundant dimensions.

If $x = (x_1, x_2, x_3, x_4)$, the evolution of x is a GIS $x_{t+1} = a_0 + Ax_t + \eta_t$, $\eta_t \sim \mathcal{N}(0, \sigma^2 I_4)$ as $x_t, x_{t+1} \in \mathcal{R}^4$, $\sigma^2 = 0.1$, $a_0 = 0$, and A is shown in Fig.8c. Dynamical trajectories of this model are shown in Fig.8b, y_1 and y_2 are theoretical macro-states. In this model, Σ is a full rank matrix, so we only need to study the inverse backward dynamics covariance matrix $A^T \Sigma^{-1} A$ (Fig.8e). This matrix only has two singular values as the singular value spectrum is shown in Fig.8g with $r = 2 < 4$, the horizontal axis represents the sequence number of singular values arranged in descending order as $s_1 \geq \dots \geq s_4$, while the vertical axis represents the magnitude of singular values s_i and κ_i as $\kappa_1 = \dots = \kappa_4 = 10$. So when $r_s = 2 < r_\kappa = 4$, clear CE occurs and the strength can be calculated as $\Delta \Gamma_\alpha(0) = 0.4034$. Fig.8i shows the coarse-graining parameter $W \in \mathcal{R}^{2 \times 4}$ obtained by methods in Section Appendix E, which is equal to remove x_3 and x_4 and only retain x_1 and x_2 to describe the evolution of the growth model since variables x_1 and x_2 hold all the relevant information contained within x_3 and x_4 .

To show the concept of vague CE, we can add some perturbations to A in Fig.8c and obtain A in Fig.8d. Then $A^T \Sigma^{-1} A$ (Fig.8f) is a full rank matrix as $r_s = r_\kappa = n = 4$, and clear CE occurs with the strength $\Delta \Gamma_\alpha(0) = 0$. However, by observing the singular value spectrum in Fig.8h, we can see that only two dimensions have significant

Malthusian growth models



Discretized Brownian motion

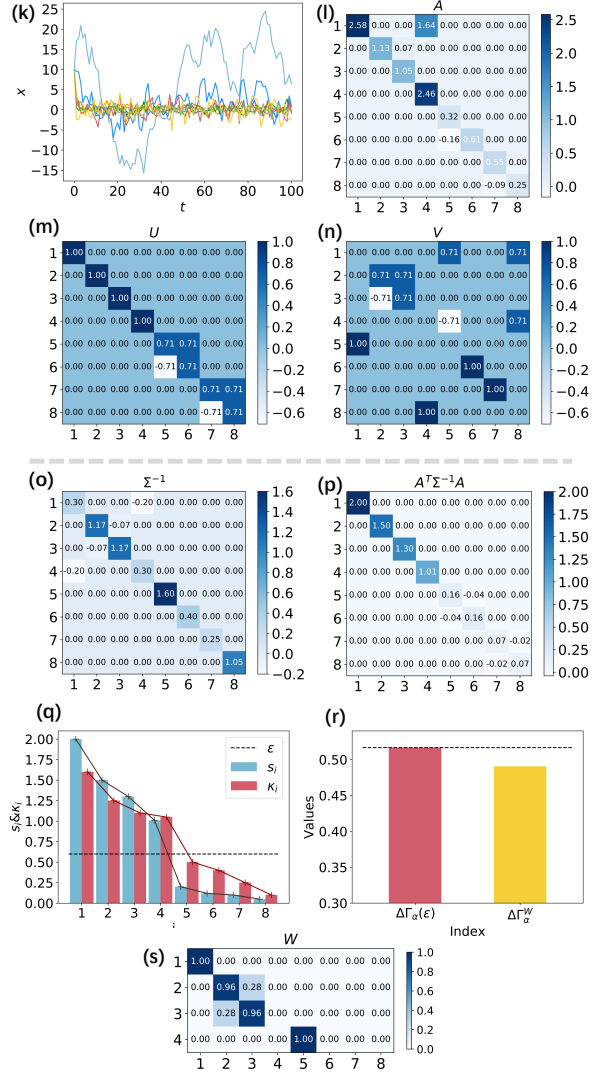


Figure 4: Two examples of dynamics where CE occurs, one's CE is primarily caused by the coefficient A , the other is primarily caused by the covariance Σ . (a) A Malthusian growth model where x_3, x_4 are copies of x_1, x_2 . (b) A sample with growth rates of 0.2 and 0.05. $x_i, i = 1, 2, 3, 4$, are micro-states, while y_1 and y_2 are macro-states we derived by the method mentioned in Section 2.3.1. (c) The original parameter matrix A . (d) Parameter matrix A with perturbations. (e) The original backward dynamics inverse covariance matrix $A^T \Sigma^{-1} A$ with rank $r_s = 2$. (f) $A^T \Sigma^{-1} A$ after random perturbations to A . (g) The singular value spectrum of $A^T \Sigma^{-1} A$ and Σ^{-1} when $A^T \Sigma^{-1} A$ only has two nonzero singular values. Clear CE occurs, and the strength can be calculated as $\Delta \Gamma_\alpha(0) = 0.4034$. (h) The singular value spectrum of $A^T \Sigma^{-1} A$ and Σ^{-1} when A is perturbed. Vague CE occurs, and the strength of this CE is $\Delta \Gamma_\alpha(\epsilon) = 0.4195$ when $\epsilon = 2$. (i) The derived coarse-graining parameter W according to the method mentioned in Section Appendix E and Appendix E.2, where the number of columns represents the macroscopic dimensions, and the number of rows represents the microscopic dimensions. (j) The coarse-graining parameter W for the vague CE case, the first macro-state dimension is determined by x_1, x_3 , and the second macro-state dimension is determined by x_2, x_4 . (k) The samples of trajectories of x_t in Brownian motion. (l) Parameter A of the drift term $f(x_t)$. (m) and (n) show singular matrices U and V . (o) and (p) show the inverse of the covariance matrices of forward and backward dynamics, which are Σ^{-1} and $A^T \Sigma^{-1} A$. (q) Singular value spectra of Σ^{-1} and $A^T \Sigma^{-1} A$ with $\epsilon = 0.6$. (r) Since $\Delta \Gamma_\alpha(\epsilon)$ is the theoretical value of CE, we can use this value to compare with the difference $\gamma_\alpha^W - \gamma_\alpha$ between the γ_α^W of our coarse-grained macro dynamics and the γ_α of the original micro dynamics. Approximate CE based on SVD $\Delta \Gamma_\alpha^W = \gamma_\alpha^W - \gamma_\alpha = 0.4907$ as W is derived from Section Appendix E, which is close to the theoretical value $\Delta \Gamma_\alpha(\epsilon) = 0.5167$. (s) The coarse-graining strategy parameter matrix W derive from methods in Section Appendix E, which preserves the non-conflicting 2nd and 3th dimensions, along with the 1st and 5th dimensions with larger singular values κ_1 and s_1 .

impacts, so we need to select a threshold ($\epsilon = 2$) to truncate the small singular values such that the occurrence of vague CE can be shown. Therefore, the CE strength can be calculated as $\Delta\Gamma_\alpha(\epsilon) = 0.4195$ and $r_\epsilon = 2$ can also be derived. According to Section Appendix E, the coarse-graining parameter W is shown in Fig.8j, the columns represent the macroscopic dimensions, and the rows represent the microscopic dimensions. Due to disturbances, x_3 and x_4 also contain some independent information. Coarse-graining strategy $\phi(x) = Wx$ is to merge x_1 and x_3 , x_2 and x_4 by weighted summation, and the two row-vectors that make up W are exactly equal to the singular vectors corresponding to the two largest singular values s_1, s_2 .

This case illustrates that sometimes high dimensions may reduce the efficiency of reversibility of a system due to dimensional redundancy. Retaining only the maximum r_ϵ singular values of the inverse covariance matrix can improve the efficiency of reversibility and generate CE.

3.2 Discretized Brownian motion

The design of this example is to demonstrate the need to simultaneously filter the two singular value spectra of Σ^{-1} and $A^T\Sigma^{-1}A$. Discretized Brownian motion is an approximation of continuous Brownian motion in discrete time, which is always used for numerical simulation and stochastic process modeling. Eq.(D.1) can be regarded as a discrete version of the Ornstein-Uhlenbeck (OU) [61] process. In this model, $f(x_t) = a_0 + Ax_t$ is the drift vector, which influences the evolution of the state, and A is shown in Fig.8l and $a_0 = 0$. Covariance matrix Σ representing the diffusion coefficient, which determines the magnitude and correlation of random fluctuations across dimensions of η_t like Fig.8k.

As we set A as shown in Fig.8l, after perform SVD on Σ^{-1} and $A^T\Sigma^{-1}A$ in Fig.8o and Fig.8p, as $\Sigma^{-1} = VKV^T$, $A^T\Sigma^{-1}A = USU^T$, we can obtain singular vector matrices $U = (u_1, \dots, u_n)$ and $V = (v_1, \dots, v_n)$ as shown in Fig.8m and n and the diagonal matrices of singular values $S = \text{diag}(2, 1.5, 1.3, 1.01, 0.2, 0.12, 0.1, 0.05)$, $K = \text{diag}(1.6, 1.25, 1.1, 1.05, 0.5, 0.4, 0.25, 0.1)$. After obtaining the singular value spectra in Fig.8q, we specify $\epsilon = 0.6$ to get $\Delta\Gamma_\alpha(\epsilon) = 0.5167$ and the number of macro-states is $r_\epsilon = 4$. Ideally, s_1, \dots, s_4 and $\kappa_1, \dots, \kappa_4$ should be retained.

As we get the singular value spectrum of Σ^{-1} and $A^T\Sigma^{-1}A$ in Fig.8q, we can also calculate the coarse-graining strategy based on SVD. According to Section Appendix E, we can obtain the optimal coarse-graining strategy parameter matrix W in Fig.8s, which preserves the non-conflicting 2nd and 3rd dimensions, along with the 1st and 5th dimensions with larger singular values κ_1 and s_1 . So in reality, we retained s_1, s_2, s_3, s_5 and $\kappa_1, \kappa_2, \kappa_3, \kappa_5$.

Since $\Delta\Gamma_\alpha(\epsilon)$ is the theoretical value of CE, we can use this value to compare with the difference $\gamma_\alpha^W(\epsilon) - \gamma_\alpha$ between the $\gamma_\alpha^W(\epsilon)$ of coarse-grained macro dynamics and the γ_α of the original micro dynamics. The macro dynamics obtained through $\phi = Wx_t$ have their own approximate dynamical reversibility γ_α^W as W is derived from Section 2.3.3. We can obtain an approximate CE based on the coarse-graining strategy $\Delta\Gamma_\alpha^W = \gamma_\alpha^W - \gamma_\alpha = 0.4907$, which is close to the theoretical $\Delta\Gamma_\alpha(\epsilon) = 0.5167$. By comparing in Fig.8r, we can see that $\Delta\Gamma_\alpha^W$ obtained by $\phi(x_t) = Wx_t$ is close to the theoretical value $\Delta\Gamma_\alpha(\epsilon)$.

3.3 SIR based on NN

Except for analytical solutions for CE on known models, this framework can also be applied to observed time series data. Our third case is to show the phenomenon of CE obtained by a well-trained neural network (NN) on time series data generated by the Susceptible-Infected-Recovered (SIR) dynamical model [49] in Fig.9a with the following dynamics:

$$\begin{cases} \frac{dS}{dt} = -\beta SI, \\ \frac{dI}{dt} = \beta SI - \gamma I, \\ \frac{dR}{dt} = \gamma I, \end{cases} \quad (3.1)$$

where $S, I, R \in [0, 1]$ represent the rate of susceptible, infected, and recovered individuals in a population, $\beta = 1$ and $\gamma = 0.5$ are parameters for infection and recovery rates.

To generate the time series data of the micro-state, we adopt the same method as in our previous work of NIS+ [29]. In which we duplicate the macro-state (S_t, I_t) as shown in Fig.9c and add Gaussian random noise to form the micro-state x_t . By feeding the micro-state data into a forward neural network (NN) called **Covariance Learner Network** in Fig.9b, we can use this model to approximate the micro-dynamics of the SIR model (Appendix F.3 shows the details of generating data and the structure of NN).

We can obtain the CE identification result directly by calculating $A_{x_t} = \nabla f(x_t)$ as the Jacobian matrix, and Σ_{x_t} is the covariance matrix that neural networks can directly output at sample x_t . We can randomly generate

SIR models

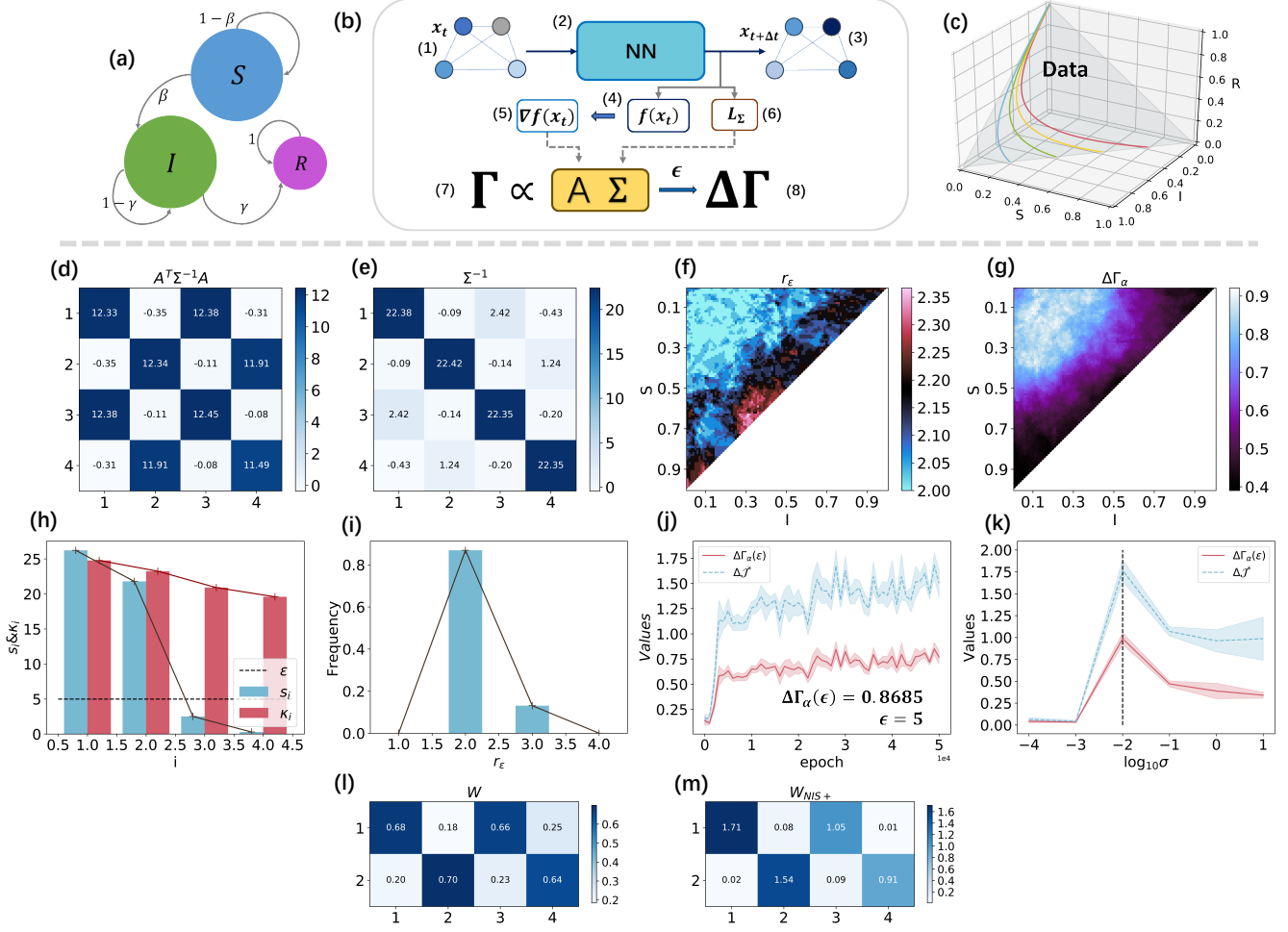


Figure 5: An example of applying machine learning to extract dynamics from data and measure CE of the dynamical system. (a) Schematic diagram of the SIR model. (b) Schematic diagram of learning dynamics and calculating Γ through NN based on data. (1) and (3) are the variables x_t and predicted $x_{t+\Delta t}$ at adjacent time points. (2) NN model for machine learning, whose structure is in Appendix F.3. (4) Dynamics $f(x_t)$ learned by NN model based on data of SIR. (5) $A_{x_t} = \nabla f(x_t)$ is the Jacobian matrix of the trained model at x_t . (6) The output L_Σ of the Covariance Learner Network, the covariance matrix Σ_{x_t} is derived from which. (7) The numerical solution of Γ , which is related to A and Σ . (8) Applying $A^T \Sigma^{-1} A = \langle A_{x_t}^T \Sigma_{x_t}^{-1} A_{x_t} \rangle_{x_t \in \mathcal{X}}$ and $\Sigma^{-1} = \langle \Sigma_{x_t}^{-1} \rangle_{x_t \in \mathcal{X}}$, SVD-based CE $\Delta \Gamma(\epsilon)$ can be calculated under suitable ϵ , \mathcal{X} is the domain of SIR. (c) Training data which is the same as NIS+ [29]. The full dataset (entire triangular region) used for training is displayed, along with four example trajectories with the same infection and recovery or death rates. The method of generating training data can be found in Appendix F.3. (d) $A^T \Sigma^{-1} A = \langle A_{x_t}^T \Sigma_{x_t}^{-1} A_{x_t} \rangle_{x_t \in \mathcal{X}}$ derived by NN trained SIR model. (e) $\Sigma^{-1} = \langle \Sigma_{x_t}^{-1} \rangle_{x_t \in \mathcal{X}}$ derived by NN trained SIR model. (f) Distribution of r_ϵ obtained by traverse the dynamical space of SIR with different (S, I) and x_t generated from which. (g) Distribution of $\Delta \Gamma_\alpha$ under different (S, I) obtained by traverse the dynamical space. (h) The singular value spectra of $A^T \Sigma^{-1} A$ and Σ^{-1} in NN trained SIR model. (i) The frequency of r_ϵ under different samples x_t in test dataset. (j) Maximum $\Delta \Gamma_\alpha(\epsilon) = 0.8685$ when the training period is around 50,000 as $\epsilon = 5$. (k) The changing trend of CE under different σ , the threshold for trend change is around $\sigma = 0.01$. (l) The coarse-graining matrix W derived from Section Appendix E and Appendix E.2 use $A^T \Sigma^{-1} A = \langle A_{x_t}^T \Sigma_{x_t}^{-1} A_{x_t} \rangle_{x_t \in \mathcal{X}}$ and $\Sigma^{-1} = \langle \Sigma_{x_t}^{-1} \rangle_{x_t \in \mathcal{X}}$. (m) The coarse-graining matrix W_{NIS+} derived from NIS+. For the convenience of observation, we have taken absolute values for each dimension in W and W_{NIS+} .

x_t with a uniform distribution on the domain \mathcal{X} of the SIR dynamics and take the average value as Section 2.4 to calculate global $A^T \Sigma^{-1} A$ and Σ^{-1} in Fig.9d and Fig.9e. In Fig.9h, we can see the singular value spectrum of matrices $A^T \Sigma^{-1} A$ and Σ^{-1} in which the horizontal axis represents the sequence number of singular values arranged in descending order, while the vertical axis represents the magnitude of singular values s_i, κ_i . Due to the existence of the copy operation, even the simplest NN can recognize only two dimensions with larger singular values as $r_\epsilon = 2$ when $\epsilon = 5$. In model training, we get the value of Vague CE as $\Delta \Gamma_\alpha(\epsilon) = 0.8685$ as shown in Fig.9j.

Locally, based on directly calculating $r_\epsilon^{x_t}$ by $A_{x_t}^T \Sigma_{x_t}^{-1} A_{x_t}$ and $\Sigma_{x_t}^{-1}$ at samples x_t obtained by traverse the entire SIR dynamic space \mathcal{X} , the resulting matrix shows $r_\epsilon = 2$ at most positions in Fig.9f. Frequency analysis further confirms a similar observation, revealing that $r_\epsilon = 2$ occurs with the highest probability across different samples in the test data of NN training, as shown in Fig.9i. Computing $\Delta \Gamma_\alpha(\epsilon)$ traverses the entire space and visualizing it in Fig.9g, we observe that the regions of highest $\Delta \Gamma_\alpha(\epsilon)$ align closely with the most stable r_ϵ areas in Fig.9f. Both are concentrated within a circle of radius 0.5 centered at $(0, 0)$. It can be observed that due to the stability of the dynamical space, the local and global measures of CE are similar.

We can also compare the results of our framework with those of NIS+ mentioned in [29]. From Fig.9l and Fig.9m, we can see that W obtained by methods in Section Appendix E and W_{NIS+} of the NIS+ are similar as both the values of W and W_{NIS+} are consistent with the copy method (Fig.8a). Additionally, we can examine the changing trend of CE under different σ values. From Fig.9k, we can see that the turning point for CE is around $\sigma = 0.01$, which is consistent with the value obtained by NIS+ [29].

This simple case integrates our new framework with machine learning, providing a fundamental reference for addressing real-world problems with real data.

4 Conclusion and discussion

This work introduces the notion of approximate dynamical reversibility Γ_α and an alternative exact quantification of CE based on it for GIS. Γ_α depends only on the singular values of Σ^{-1} and $A^T \Sigma^{-1} A$ and independent of predefined coarse-graining method. By retaining the top r_ϵ singular values of Σ^{-1} and $A^T \Sigma^{-1} A$, CE can be quantified directly as $\Delta \Gamma_\alpha(\epsilon)$. Compared to EI-based CE, this SVD-based approach offers higher accuracy and computational efficiency, laying the foundation for detecting CE in complex systems.

Meanwhile, the coarse-graining strategy can also be derived directly from the singular vector matrices of Σ^{-1} and $A^T \Sigma^{-1} A$, balancing the preservation of key singular values of two matrices and improving $\Delta \Gamma_\alpha(\epsilon)$. The resulting strategy reveals natural aggregation strategies: correlated dimensions merge (like the copied dimension in the growth model and SIR model), and weak ones are discarded (like the discarded 4th, 6th, 7th, and 8th dimensions with larger noise in Brownian motion). Unlike conventional CE frameworks that maximize EI through manually designed coarse-graining strategies, this method simplifies computation and produces more interpretable, physically grounded macroscopic predictions.

Compared with the SVD-based CE of TPM, $\Delta \Gamma_\alpha$ in GIS more clearly reveals the link between SVD-based and EI-based CE. Analytical results show that $\Delta \Gamma_\alpha(\epsilon) \simeq (1 - \frac{\alpha}{4}) \Delta \mathcal{J}^*$, with equality when the backward dynamics follow a normalized normal distribution. Randomly sampled A and Σ confirm this linear relation. The parameter α further modulates determinism and non-degeneracy. In continuous space, our method can provide theoretical support for some discrete TPM results that can only be obtained through numerical experiments, and can be applied to more real-world systems.

Beyond introducing the CE based on dynamical reversibility, this work also innovates in the use of SVD. SVD has long served as a key tool for analyzing system dynamics—from detecting critical transitions in Earth and market systems [62–65] used ensemble singular values, to model reduction in control theory, neural networks, even the Koopman operator [66–70]. Inspired by these foundations, we extend SVD to stochastic dynamics by applying it to continuous Markovian dynamics, which jointly captures the deterministic mapping A and stochastic covariance Σ . Furthermore, our framework treats the inverse covariance matrices $A^T \Sigma^{-1} A$ and Σ^{-1} as intrinsic information carriers, simultaneously accounting for both forward and backward dynamics. The singular values of the inverse covariance matrices reveal the reversible information embedded in the system, offering a unified view that encompasses certainty, stochasticity, and reversibility to expose the fundamental degrees of freedom driving the evolution of complex systems.

While our approach has made progress, several challenges remain unresolved. The first limitation is that our model is currently restricted to linear GIS, with nonlinear GIS approximated in a locally linear form. However, this approximation introduces stability issues, as the gradient of nonlinear functions may be ill-conditioned. In particular, cases where $\nabla f(x) = 0$ or $\nabla f(x) \rightarrow \infty$ lead to the breakdown of our framework. To address this, incorporating higher-order derivatives as a refined CE metric warrants further investigation.

The second issue arises when time is continuous rather than discrete; the existing CE quantification lacks objective

formulations. The approach in this study discretizes time, converting differential equations into difference equations, where the choice of hyperparameter Δt strongly influences CE. As $\Delta t \rightarrow 0$, state transitions $x_t \rightarrow x_{t+\Delta t}$ exhibit minimal variation, causing the rate of change to vanish. For continuous-time stochastic differential equations, a more principled CE measure is required to account for infinitesimal evolution dynamics.

The third issue is that both SVD-based and EI-based CE quantification methods require training an NN to infer dynamics when the governing equations are unknown. However, NN-based approaches are data-dependent and prone to parameter estimation errors, particularly in capturing interdimensional correlations. In our case, a multivariate Gaussian model approximates both the dynamical function and covariance. Yet, under high noise or limited data, the learned dynamics may deviate from the true system, leading to unreliable CE estimates. For systems with unknown models, it is crucial to develop representations that jointly approximate both the underlying dynamics and noise structure.

Future work will focus on optimizing the existing framework and extending its application to more complex systems. In numerical simulations, machine learning can be leveraged to learn intricate dynamical models, such as Vicsek and Kuramoto, which are analytically intractable. This allows for data-driven CE estimation and the exploration of its relationship with critical states. Additionally, our approach can be applied to real-world datasets, such as meteorological and EEG data, to identify practical problems where CE provides meaningful insights.

5 Supplementary Material

The supplementary material provides detailed calculation processes for effective information EI and approximate dynamical reversibility Γ_α , from the simplest 1-dimensional system to general high-dimensional situations. Especially for EI and Γ_α in cases where A is a full-rank or non-square matrix, we provide computational references. After providing a detailed proof process, we use randomly generated scatter plots to show the linear correlation between two indicators Γ_α and \mathcal{J} , as well as $\Delta\Gamma_\alpha(\epsilon)$ and $\Delta\mathcal{J}^*$ based on which. The original coarse-graining strategy and the coarse-graining strategy of the standardized model, which were not mentioned in the article, have also been discussed in the supplementary material. In the end, we add the case of the Markov Gaussian system, providing ideas for combining our framework with integrated information theory, Markov chain with TPM, and even neural data.

Acknowledgments: This work is inspired by the insightful discussions held in the "Causal Emergence" series reading groups organized by Swarma Club and the "Swarma-Kaifeng" Workshop. Sincere thanks to Mr. Jiayun Wu, Ms. Ruiyang Feng, Mr. Zhang Zhang, Ms. Ruyi Tao, Mr. Keng-Hou Leong, Ms. Wanting Su, Mr. Aobo Lyu, and Mr. Muyun Mou for their suggestions and support on theory, methods, and writing. We would also like to extend our sincere gratitude to Prof. Yizhuang You, Dr. Peng Cui, Dr. Jing He, Dr. Chaochao Lu, and Dr. Yanbo Zhang for their invaluable contributions and insightful discussions. We express our appreciation for the support from the Save 2050 Programme, a joint initiative of Swarma Club and X-OrderSwarma Research. Additionally, we are grateful for the support received from Swarma Research. We also thank the large language models ChatGPT and Deepseek for their assistance in refining our paper writing.

Data Availability Statement: All the codes and data are available at: https://github.com/kilovoltage/SVD-based_CE_Gaussian.

References

- [1] S. E. Jørgensen and F. Müller, "Ecosystems as complex systems," *Handbook of Ecosystem Theories and Management*. CRC Press LLC, Boca Raton, pp. 5–20, 2000.
- [2] R. T. Wicks, S. C. Chapman, and R. Dendy, "Mutual information as a tool for identifying phase transitions in dynamical complex systems with limited data," *Physical Review E*, vol. 75, no. 5, p. 051125, 2007.
- [3] C. Hartman and B. Benes, "Autonomous boids," *Computer Animation and Virtual Worlds*, vol. 17, no. 3-4, pp. 199–206, 2006.
- [4] S. Jingnan, J. He, and X. Gao, "Neurofeedback training of control network improves ssvp-based bci performance in children," 2021.
- [5] O. Sporns, J. Faskowitz, A. S. Teixeira, S. A. Cutts, and R. F. Betzel, "Dynamic expression of brain functional systems disclosed by fine-scale analysis of edge time series," *Network Neuroscience*, vol. 5, no. 2, pp. 405–433, 2021.

- [6] T. F. Varley, *Uncovering Higher-Order Structures in Complex Systems with Multivariate Information Theory*. Indiana University, 2023.
- [7] Z. Wang, Y. Rong, K. Liu, M. Yang, J. Zhang, and J. He, “Causal emergence of consciousness through learned multiscale neural dynamics in mice,” *arXiv preprint arXiv:2509.10891*, 2025.
- [8] Z. Zhao, Y. Zhou, B. Liu, J. He, J. Zhao, Y. Cai, J. Fan, X. Li, Z. Wang, Z. Lu, *et al.*, “Two-photon synthetic aperture microscopy for minimally invasive fast 3d imaging of native subcellular behaviors in deep tissue,” *Cell*, vol. 186, no. 11, pp. 2475–2491, 2023.
- [9] T. Dong, J. He, S. Wang, L. Wang, Y. Cheng, and Y. Zhong, “Inability to activate rac1-dependent forgetting contributes to behavioral inflexibility in mutants of multiple autism-risk genes,” *Proceedings of the National Academy of Sciences*, vol. 113, no. 27, pp. 7644–7649, 2016.
- [10] L. Ma, X.-D. Yang, F. Yang, X.-J. Zhou, and Z.-W. Wu, “Unveiling the early stage evolution of local atomic structures in the crystallization process of a metallic glass,” *Chinese Physics B*, vol. 33, no. 3, p. 036402, 2024.
- [11] H. S. Bennett and J. J. Filliben, “A systematic approach for multidimensional, closed-form analytic modeling: minority electron mobilities in gal-xalxas heterostructures,” *Journal of Research of the National Institute of Standards and Technology*, vol. 105, no. 3, p. 441, 2000.
- [12] A. Albrecht, D. Coulson, P. Ferreira, and J. Magueijo, “Causality, randomness, and the microwave background,” *Physical Review Letters*, vol. 76, no. 9, p. 1413, 1996.
- [13] T. Schreiber, “Measuring information transfer,” *Physical review letters*, vol. 85, no. 2, p. 461, 2000.
- [14] M. G. Rosenblum and A. S. Pikovsky, “Detecting direction of coupling in interacting oscillators,” *Physical Review E*, vol. 64, no. 4, p. 045202, 2001.
- [15] D. Harnack, E. Laminski, M. Schünemann, and K. R. Pawelzik, “Topological causality in dynamical systems,” *Physical review letters*, vol. 119, no. 9, p. 098301, 2017.
- [16] G. Tononi and O. Sporns, “Measuring information integration,” *BMC neuroscience*, vol. 4, pp. 1–20, 2003.
- [17] E. P. Hoel, L. Albantakis, and G. Tononi, “Quantifying causal emergence shows that macro can beat micro,” *Proceedings of the National Academy of Sciences*, vol. 110, no. 49, pp. 19790–19795, 2013.
- [18] E. P. Hoel, “When the map is better than the territory,” *Entropy*, vol. 19, no. 5, p. 188, 2017.
- [19] F. E. Rosas, P. A. M. Mediano, H. J. Jensen, A. K. Seth, A. B. Barrett, R. L. Carhart-Harris, and D. Bor, “Reconciling emergences: An information-theoretic approach to identify causal emergence in multivariate data,” *PLoS Computational Biology*, vol. 16, p. e1008289, Dec 2020.
- [20] L. Barnett and A. K. Seth, “Dynamical independence: discovering emergent macroscopic processes in complex dynamical systems,” *Physical Review E*, vol. 108, no. 1, p. 014304, 2023.
- [21] B. Yuan, J. Zhang, A. Lyu, J. Wu, Z. Wang, M. Yang, K. Liu, M. Mou, and P. Cui, “Emergence and causality in complex systems: A survey of causal emergence and related quantitative studies,” *Entropy*, vol. 26, no. 2, p. 108, 2024.
- [22] E. P. Hoel, L. Albantakis, W. Marshall, and G. Tononi, “Can the macro beat the micro? integrated information across spatiotemporal scales,” *Neuroscience of Consciousness*, vol. 2016, no. 1, p. niw012, 2016.
- [23] S. Bornholdt, “Boolean network models of cellular regulation: prospects and limitations,” *Journal of the Royal Society interface*, vol. 5, no. suppl_1, pp. S85–S94, 2008.
- [24] E. W. Weisstein, “Cellular automaton,” <https://mathworld.wolfram.com/>, 2002.
- [25] M. Yang, Z. Wang, K. Liu, Y. Rong, B. Yuan, and J. Zhang, “Finding emergence in data: causal emergence inspired dynamics learning,” *arXiv preprint arXiv:2308.09952*, 2023.
- [26] P. Chvykov and E. Hoel, “Causal geometry,” *Entropy*, vol. 23, no. 1, p. 24, 2020.
- [27] K. Liu, B. Yuan, and J. Zhang, “An exact theory of causal emergence for linear stochastic iteration systems,” *Entropy*, vol. 26, no. 8, 2024.

- [28] J. Zhang and K. Liu, “Neural information squeezer for causal emergence,” *Entropy*, vol. 25, no. 1, p. 26, 2022.
- [29] M. Yang, Z. Wang, K. Liu, Y. Rong, B. Yuan, and J. Zhang, “Finding emergence in data by maximizing effective information,” *National Science Review*, p. nwae279, 2024.
- [30] C. W. Reynolds, “Flocks, herds and schools: A distributed behavioral model,” in *Proceedings of the 14th annual conference on Computer graphics and interactive techniques*, pp. 25–34, 1987.
- [31] S. M. Smith, K. L. Miller, G. Salimi-Khorshidi, M. Webster, C. F. Beckmann, T. E. Nichols, J. D. Ramsey, and M. W. Woolrich, “Network modelling methods for fmri,” *NeuroImage*, vol. 54, no. 2, pp. 875–891, 2011.
- [32] P. L. Williams and R. D. Beer, “Nonnegative decomposition of multivariate information,” *arXiv preprint arXiv:1004.2515*, 2010.
- [33] A. I. Luppi, P. A. Mediano, F. E. Rosas, D. J. Harrison, R. L. Carhart-Harris, D. Bor, and E. A. Stamatakis, “What it is like to be a bit: an integrated information decomposition account of emergent mental phenomena,” *Neuroscience of consciousness*, vol. 2021, no. 2, p. niab027, 2021.
- [34] J. Song and S. Ermon, “Understanding the limitations of variational mutual information estimators,” 2020.
- [35] C. Kaplanis, P. Mediano, and F. Rosas, “Learning causally emergent representations,” in *NeurIPS 2023 workshop: Information-Theoretic Principles in Cognitive Systems*, 2023.
- [36] D. McSharry, C. Kaplanis, F. Rosas, and P. A. Mediano, “Learning diverse causally emergent representations from time series data,” *Advances in Neural Information Processing Systems*, vol. 37, pp. 119547–119572, 2024.
- [37] Z. C. Chao, Y. Nagasaka, and N. Fujii, “Long-term asynchronous decoding of arm motion using electrocorticographic signals in monkey,” *Frontiers in neuroengineering*, vol. 3, p. 1189, 2010.
- [38] S. D. Muthukumaraswamy and D. T. Liley, “1/f electrophysiological spectra in resting and drug-induced states can be explained by the dynamics of multiple oscillatory relaxation processes,” *NeuroImage*, vol. 179, pp. 582–595, 2018.
- [39] D. Byrne and D. Nelson, “Attraction as a linear function of proportion of positive reinforcements.,” *Journal of personality and social psychology*, vol. 1, no. 6, p. 659, 1965.
- [40] J. Zhang, R. Tao, K. H. Leong, M. Yang, and B. Yuan, “Dynamical reversibility and a new theory of causal emergence based on SVD,” *npj Complexity*, vol. 2, p. 3, Jan. 2025.
- [41] A. Zhang and M. Wang, “Spectral state compression of markov processes,” *IEEE transactions on information theory*, vol. 66, no. 5, pp. 3202–3231, 2019.
- [42] C. Lee and D. J. Wilkinson, “A review of stochastic block models and extensions for graph clustering,” *Applied Network Science*, vol. 4, no. 1, pp. 1–50, 2019.
- [43] K. Liu, X. Lü, F. Gao, and J. Zhang, “Expectation-maximizing network reconstruction and most applicable network types based on binary time series data,” *Physica D: Nonlinear Phenomena*, vol. 454, p. 133834, 2023.
- [44] W. Dunsmuir and E. J. Hannan, “Vector linear time series models,” *Advances in Applied Probability*, vol. 8, no. 2, pp. 339–364, 1976.
- [45] L. Arnold, C. K. Jones, K. Mischaikow, G. Raugel, and L. Arnold, *Random dynamical systems*. Springer, 1995.
- [46] M. I. Jordan *et al.*, “Why the logistic function? a tutorial discussion on probabilities and neural networks,” 1995.
- [47] M. Benedicks and L. Carleson, “The dynamics of the hénon map,” *Annals of Mathematics*, vol. 133, no. 1, pp. 73–169, 1991.
- [48] J. A. Acebrón, L. L. Bonilla, C. J. Pérez Vicente, F. Ritort, and R. Spigler, “The kuramoto model: A simple paradigm for synchronization phenomena,” *Reviews of modern physics*, vol. 77, no. 1, pp. 137–185, 2005.
- [49] J. Satsuma, R. Willox, A. Ramani, B. Grammaticos, and A. S. Carstea, “Extending the sir epidemic model,” *Physica A: Statistical Mechanics and its Applications*, vol. 336, no. 3-4, pp. 369–375, 2004.

- [50] P. J. Wangersky, “Lotka-volterra population models,” *Annual Review of Ecology and Systematics*, vol. 9, pp. 189–218, 1978.
- [51] O. Knill, “Cauchy–binet for pseudo-determinants,” *Linear Algebra and its Applications*, vol. 459, pp. 522–547, 2014.
- [52] Y. Tsutsumi, “Schrodinger equation,” *Funkcialaj Ekvacioj*, vol. 30, pp. 115–125, 1987.
- [53] P. Ao, “Emerging of stochastic dynamical equalities and steady state thermodynamics from darwinian dynamics,” *Communications in theoretical physics*, vol. 49, no. 5, p. 1073, 2008.
- [54] R. Yuan, Y. Tang, and P. Ao, “Sde decomposition and a-type stochastic interpretation in nonequilibrium processes,” *Frontiers of Physics*, vol. 12, pp. 1–9, 2017.
- [55] P. D. Lax, *Functional analysis*. John Wiley & Sons, 2014.
- [56] R. N. Bracewell, “The fourier transform,” *Scientific American*, vol. 260, no. 6, pp. 86–95, 1989.
- [57] B. Klein and E. Hoel, “The emergence of informative higher scales in complex networks,” *Complexity*, vol. 2020, pp. 1–12, 2020.
- [58] E. Hoel, *The world behind the world: Consciousness, Free Will, and the Limits of Science*. Simon and Schuster, 2024.
- [59] R. Comolatti and E. Hoel, “Consilience in causation: Causal emergence is found across measures of causation,” *Entropy*, vol. 27, no. 8, p. 825, 2025.
- [60] O. Galor and D. N. Weil, “Population, technology, and growth: From malthusian stagnation to the demographic transition and beyond,” *American economic review*, vol. 90, no. 4, pp. 806–828, 2000.
- [61] R. A. Maller, G. Müller, and A. Szimayer, “Ornstein–uhlenbeck processes and extensions,” *Handbook of financial time series*, pp. 421–437, 2009.
- [62] Y. Sun, G. Hu, Y. Zhang, B. Lu, Z. Lu, J. Fan, X. Li, Q. Deng, and X. Chen, “Eigen microstates and their evolutions in complex systems,” *Communications in Theoretical Physics*, vol. 73, no. 6, p. 065603, 2021.
- [63] G. Hu, T. Liu, M. Liu, W. Chen, and X. Chen, “Condensation of eigen microstate in statistical ensemble and phase transition,” *Science China Physics, Mechanics & Astronomy*, vol. 62, pp. 1–8, 2019.
- [64] J. Fan, J. Meng, J. Ludescher, X. Chen, Y. Ashkenazy, J. Kurths, S. Havlin, and H. J. Schellnhuber, “Statistical physics approaches to the complex earth system,” *Physics reports*, vol. 896, pp. 1–84, 2021.
- [65] D. Sornette, “Physics and financial economics (1776–2014): puzzles, ising and agent-based models,” *Reports on progress in physics*, vol. 77, no. 6, p. 062001, 2014.
- [66] K. Gallivan, E. Grimme, and P. Van Dooren, “Asymptotic waveform evaluation via a lanczos method,” *Applied Mathematics Letters*, vol. 7, no. 5, pp. 75–80, 1994.
- [67] S. Gugercin, “An iterative svd-krylov based method for model reduction of large-scale dynamical systems,” *Linear Algebra and its Applications*, vol. 428, no. 8-9, pp. 1964–1986, 2008.
- [68] A. C. Antoulas, “An overview of approximation methods for large-scale dynamical systems,” *Annual reviews in Control*, vol. 29, no. 2, pp. 181–190, 2005.
- [69] P. J. Schmid, “Dynamic mode decomposition of numerical and experimental data,” *Journal of fluid mechanics*, vol. 656, pp. 5–28, 2010.
- [70] M. O. Williams, I. G. Kevrekidis, and C. W. Rowley, “A data-driven approximation of the koopman operator: Extending dynamic mode decomposition,” *Journal of Nonlinear Science*, vol. 25, no. 6, pp. 1307–1346, 2015.
- [71] D. Maoutsa, S. Reich, and M. Opper, “Interacting particle solutions of fokker–planck equations through gradient–log–density estimation,” *Entropy*, vol. 22, no. 8, p. 802, 2020.
- [72] L. C. Evans, *An introduction to stochastic differential equations*, vol. 82. American Mathematical Soc., 2012.

- [73] N. Ikeda, S. Watanabe, M. Fukushima, and H. Kunita, *Itô's stochastic calculus and probability theory*. Springer Science & Business Media, 2012.
- [74] M. A. Lifshits, *Gaussian random functions*, vol. 322. Springer Science & Business Media, 2013.
- [75] M. Baldiotti, R. Fresneda, and J. Gazeau, “Dirac distribution and dirac constraint quantizations,” *Physica Scripta*, vol. 90, no. 7, p. 074039, 2015.
- [76] R. Comolatti and E. Hoel, “Causal emergence is widespread across measures of causation,” *arXiv preprint arXiv:2202.01854*, 2022.
- [77] J. Pearl, “Causal inference in statistics: An overview,” 2009.
- [78] E. J. Hannan and L. Kavalieris, “Multivariate linear time series models,” *Advances in Applied Probability*, vol. 16, no. 3, pp. 492–561, 1984.
- [79] J. C. A. Barata and M. S. Hussein, “The moore–penrose pseudoinverse: A tutorial review of the theory,” *Brazilian Journal of Physics*, vol. 42, pp. 146–165, 2012.
- [80] R. A. Horn and C. R. Johnson, *Matrix analysis*. Cambridge university press, 2012.
- [81] A. B. Barrett and A. K. Seth, “Practical measures of integrated information for time-series data,” *PLoS computational biology*, vol. 7, no. 1, p. e1001052, 2011.
- [82] A. K. Seth, A. B. Barrett, and L. Barnett, “Causal density and integrated information as measures of conscious level,” *Philosophical Transactions of the Royal Society A: Mathematical, Physical and Engineering Sciences*, vol. 369, no. 1952, pp. 3748–3767, 2011.
- [83] M. Oizumi, S.-i. Amari, T. Yanagawa, N. Fujii, and N. Tsuchiya, “Measuring integrated information from the decoding perspective,” *PLoS computational biology*, vol. 12, no. 1, p. e1004654, 2016.
- [84] S. Tajima and R. Kanai, “Integrated information and dimensionality in continuous attractor dynamics,” *Neuroscience of consciousness*, vol. 2017, no. 1, p. nix011, 2017.

Supplementary Information for SVD-based Causal Emergence for Gaussian Iterative Systems

The supplementary material provides detailed calculation processes for effective information EI and approximate dynamical reversibility Γ_α , from the simplest one-dimensional system to general high-dimensional situations. Especially for EI and Γ_α in cases where A is full rank or non-square matrices, we provide computational references. After providing a detailed proof process, we use randomly generated scatter plots to show the linear correlation between two indicators Γ_α and \mathcal{J} , as well as $\Delta\Gamma_\alpha(\epsilon)$ and $\Delta\mathcal{J}^*$ based on which. The original coarse-graining strategy and the coarse-graining strategy of the standardized model, which were not mentioned in the article, have also been discussed in the supplementary material. In the end, we add the case of the Markov Gaussian system, providing ideas for combining our framework with integrated information theory, Markov chains with TPM, and even neural data.

Appendix A Linear Gaussian iterative systems

In this Section, we provide some supplements to the content about dynamics in the main text. Many real-world complex systems exhibit dynamical behavior constructed by the interplay of deterministic laws and random disturbances as

$$x_{t+1} = f(x_t) + \eta_t, \eta_t \sim \mathcal{N}(0, \Sigma), \quad (\text{A.1})$$

$x_t \in \mathcal{R}^n, \Sigma \in \mathcal{R}^{n \times n}$, which we called Gaussian iterative systems (GIS) [44]. $f(x_t) : \mathcal{R}^n \rightarrow \mathcal{R}^n$ captures deterministic dynamics, η_t denotes random noise. Some continuous dynamic systems can be approximated in this form.

Appendix A.1 Linearization of nonlinear dynamics

Most of the analysis in the article is based on linear models, but there are also many nonlinear iterative models in reality. We can apply our framework to nonlinear models under certain conditions. Nonlinear stochastic iterative systems like $x_{t+1} = f(x_t) + \eta_t, \eta_t \sim \mathcal{N}(0, \Sigma), x_t \in \mathcal{R}^n, \Sigma \in \mathcal{R}^{n \times n}$, do not have the same known parameter matrix A as linear stochastic iterative systems. However, when $f : \mathcal{R}^n \rightarrow \mathcal{R}^n$ and spatially continuous, the Taylor expansion $f(x) = f(x') + \nabla f(x')(x - x') + o(x - x')$ is very similar to linear function Ax around x' . By using the definition that A is the slope, we can obtain an approximate expression of $A_{x'}$ when $x \approx x'$ as

$$A_{x'} = \frac{f(x) - f(x')}{x - x'} \approx \nabla f(x'). \quad (\text{A.2})$$

So when iterative models are nonlinear, we can replace A with the gradient matrix as $A_{x_t} = \nabla f(x_t) \in \mathcal{R}^{n \times n}$ at x_t to calculate $\Delta\mathcal{J}$ or $\Delta\Gamma_\alpha$. Since causal emergence is related to x_t , to determine the CE of the entire system, we can take the average of Σ^{-1} and $A^T \Sigma^{-1} A$ in x_t 's space \mathcal{X} as

$$\Sigma^{-1} = \frac{1}{|\mathcal{X}|} \int_{\mathcal{X}} \Sigma_{x_t}^{-1} dx_t \quad (\text{A.3})$$

and

$$A^T \Sigma^{-1} A = \frac{1}{|\mathcal{X}|} \int_{\mathcal{X}} \nabla f(x_t)^T \Sigma_{x_t}^{-1} \nabla f(x_t) dx_t \quad (\text{A.4})$$

to calculate the CE of the entire system, $|\mathcal{X}|$ represents the size of \mathcal{X} and Σ_{x_t} is the covariance at x_t .

For the case of sampling, we can change integration to summation. Since most of the dynamics we consider are stationary Markov processes, we can discuss their overall approximate dynamical reversibility and CE properties. For this purpose, we can approximate the overall properties by averaging the properties of each local point in a certain interval. For general problems, if x_{t+1} is approximately distributed within the interval \mathcal{X} , and $A_{x_t}^T \Sigma_{x_t}^{-1} A_{x_t}$ and $\Sigma_{x_t}^{-1}$ do not fluctuate or diverge significantly, we can first randomly sample and then average the parameter matrix to obtain

$$A^T \Sigma^{-1} A \approx \langle A_{x_t}^T \Sigma_{x_t}^{-1} A_{x_t} \rangle_{x_t \in \mathcal{X}} \quad (\text{A.5})$$

and

$$\Sigma^{-1} \approx \langle \Sigma_{x_t}^{-1} \rangle_{x_t \in \mathcal{X}} \quad (\text{A.6})$$

to calculate the two global inverse covariance matrices. Both matrices are dependent only on the spatial \mathcal{X} and are independent of time, deriving the same results regardless of the system's evolution. Finally, we can calculate global CE based on the definition of Γ_α and empirically verify that it better captures the essence of the system's dynamics. Under the condition that \mathcal{X} is stable and limited, this result is approximately equal to the result of calculating the average value of local $\Gamma_\alpha^{x_t}$ first.

Appendix A.2 Discretization of continuous time

Another case requiring special handling is time-continuous systems, where Fokker-plank equations describe dynamics [71] as

$$\frac{\partial p(x_t)}{\partial t} = -\nabla \cdot \left[f(x_t)p(x_t) - \frac{1}{2}\Sigma\nabla p(x_t) \right], \quad (\text{A.7})$$

or equivalent stochastic differential equations [72] as

$$\frac{dx_t}{dt} = f(x_t) + \Sigma^{\frac{1}{2}}\eta_t \quad (\text{A.8})$$

which is also expressed as $dx_t = f(x_t)dt + \Sigma^{\frac{1}{2}}dW_t$, where $x_t \in \mathcal{R}^n$, $\eta_t = dW_t/dt \in \mathcal{R}^n$ and $dW_t \sim \mathcal{N}(0, dtI_n)$. We can approximate the differential of Brownian motion $W_t \in \mathcal{R}^n$ as $dW_t \approx \sqrt{dt}1_n$, $1_n = (1, \dots, 1)_n^T$.

The common method for dealing with this situation is to use finite difference Δx_t approximation for differentiation [73] dx_t as $\Delta x_t = f(x_t)\Delta t + \Sigma^{\frac{1}{2}}\Delta W_t \sim \mathcal{N}(f(x_t)\Delta t, \Delta t\Sigma)$. In this way, we can also approximate the stochastic differential equation in the form of a GIS as

$$x_{t+\Delta t} \approx x_t + \Delta x_t \sim \mathcal{N}(x_t + f(x_t)\Delta t, \Delta t\Sigma). \quad (\text{A.9})$$

We can calculate CE by setting $A = I_n + \nabla f(x_t)\Delta t$ and covariance $\Delta t\Sigma \in \mathcal{R}^{n \times n}$. Due to the need for discretization in continuous models in machine learning, this method can also provide a reference for the effectiveness of machine learning models. However this method has a big problem in that the Δt has a significant impact on the calculation of CE.

Ao et al. [53, 54] presented that through a transformation to a force equation, decomposition of the SDE into three components: potential function $f(x_t)$, dissipative matrix $R(x_t)$, and transverse matrix $T(x_t)$ as

$$[R(x_t) + T(x_t)]\frac{dx_t}{dt} = -\nabla f(x_t) + R^{\frac{1}{2}}(x_t)\eta_t. \quad (\text{A.10})$$

$\nabla f(x_t)$ and $R(x_t)$ happen to be highly correlated in their impact on our matrix A and Σ . So in the future, we can try to find more effective methods just based on three components to find a CE quantization scheme that does not rely on Δt .

Appendix A.3 Backward dynamics of GIS

The third consistent concept is backward dynamics. We can analogy to the approximate dynamical reversibility [40] of TPM to derive the approximate dynamical reversibility of GIS determined by Gaussian mapping [74] like

$$p(x_{t+1}|x_t) = \mathcal{N}(Ax_t + a_0, \Sigma) \equiv \frac{1}{(2\pi)^{\frac{n}{2}} \det(\Sigma)^{\frac{1}{2}}} \exp \left\{ -\frac{1}{2}(x_{t+1} - Ax_t - a_0)^T \Sigma^{-1} (x_{t+1} - Ax_t - a_0) \right\}, \quad (\text{A.11})$$

where, $A \in \mathcal{R}^{n \times n}$ and $\Sigma \in \mathcal{R}^{n \times n}$. In a Markov chain, its TPM is a permutation matrix when the dynamics are reversible. This reversibility can be analogized to GIS. If we treat the Gaussian map defined in Equation (D.17) as a TPM, the state mapping between x_t and x_{t+1} is bijective if the TPM is reversible. Here, we need to define the backward dynamics for GIS in Definition Appendix A.1.

Definition Appendix A.1. (*Backward dynamics*): For a GIS $x_{t+1} = a_0 + Ax_t + \eta_t$, $\eta_t \sim \mathcal{N}(0, \Sigma)$, also presented as $p(x_{t+1}|x_t) = \mathcal{N}(Ax_t + a_0, \Sigma)$, where $x_t \in \mathcal{R}^n$ to $x_{t+1} \in \mathcal{R}^n$, $A \in \mathcal{R}^{n \times n}$ and $\Sigma \in \mathcal{R}^{n \times n}$, it has a unique backward dynamics

$$x_t = A^\dagger x_{t+1} - A^\dagger a_0 - A^\dagger \eta_t, A^\dagger \eta_t \sim \mathcal{N}(0, A^\dagger \Sigma (A^\dagger)^T). \quad (\text{A.12})$$

$A^\dagger \Sigma (A^\dagger)^T$ is the covariance matrix of backward dynamics as A^\dagger is the Moore-Penrose generalized inverse matrix of A .

In continuous space, if the state mapping between two consecutive time points x_t and x_{t+1} is bijective, $r(A) = n$, $\Sigma = 0$ and $A^\dagger \Sigma (A^\dagger)^T = 0$ needs to be satisfied, then the probability distribution would be a Dirac distribution [75], i.e., all the probability mass is concentrated at a single point as

$$p(x_{t+1}|x_t) = \delta(x_{t+1} - Ax_t - a_0) = \begin{cases} \infty, & x_{t+1} = Ax_t + a_0 \\ 0, & x_{t+1} \neq Ax_t + a_0 \end{cases} \quad (\text{A.13})$$

in which $\int_{-\infty}^{+\infty} p(x_{t+1}|x_t) dx_{t+1}^n = 1$, $a_0, x_t, x_{t+1} \in \mathcal{R}^n$, $A, \Sigma \in \mathcal{R}^{n \times n}$. Backward dynamics are the same as $p(x_t|x_{t+1}) = \delta(x_t - A^\dagger x_{t+1} + A^\dagger a_0)$. Then, both mappings can be directly written as linear functions $x_{t+1} = Ax_t + a_0$ and $x_t = A^\dagger x_{t+1} - A^\dagger a_0$, where $A^\dagger = A^{-1}$ in this case.

When A is irreversible or $A^\dagger \Sigma (A^\dagger)^T, \Sigma > 0$, the closer $p(x_{t+1}|x_t)$ and $p(x_t|x_{t+1})$ to Dirac distributions and A to a full-rank matrix, the stronger $p(x_{t+1}|x_t)$'s reversibility. Therefore, when the covariance of both forward and backward dynamics satisfy $\Sigma \rightarrow 0$, $A^\dagger \Sigma (A^\dagger)^T \rightarrow 0$ and A is close to a full-rank matrix, x_{t+1}, x_t are close to bijective and $x_{t+1} = a_0 + Ax_t + \eta_t \rightarrow Ax_t + a_0$, $x_t = A^\dagger x_{t+1} - A^\dagger a_0 - A^\dagger \eta_t \rightarrow A^\dagger x_t - A^\dagger a_0$ are approximate reversible dynamics. From this, we know that we need to find an indicator that includes both Σ and $A^\dagger \Sigma (A^\dagger)^T$ to quantify the approximate reversibility of $p(x_{t+1}|x_t)$. In the next subsection, we provide this indicator Γ_α .

It is not difficult to find that for Gaussian distributions, $\mathcal{N}(0, \sigma^2)$ can be defined for cases where the variance is equal to $\sigma = 0$ or $\sigma = \infty$, rather than simply a singularity. $\sigma = 0$ means that the Gaussian density function is a Dirac distribution, and $\sigma = \infty$ means the probability density function can be seen as a uniform distribution $\mathcal{U}(-\infty, +\infty)$ with a probability density of 0 everywhere. For this, we can specifically define an inverse matrix for the covariance matrix.

Definition Appendix A.2. If Σ is a covariance matrix with a normal distribution and $\Sigma = \tilde{V} \Lambda \tilde{V}^T$, is its eigenvalue (singular value) decomposition $\Lambda = \text{diag}(\lambda_1, \dots, \lambda_n)$, $\tilde{V} = (\tilde{v}_1, \dots, \tilde{v}_n)$, note that singular values here can be set to 0 or infinity as $\infty \geq \lambda_1 \geq \dots \geq \lambda_n \geq 0$. And we define $\kappa_i = 1/\lambda_{n-i+1}$, if $\lambda_{n-i+1} = 0$ then $\kappa_i = \infty$, and if $\lambda_{n-i+1} = \infty$ then $\kappa_i = 0$. We can obtain the singular value matrix of Σ^{-1} as $K = \text{diag}(\kappa_1, \dots, \kappa_n)$, so

$$\Sigma^{-1} = VKV^T \quad (\text{A.14})$$

and $V = (v_1, \dots, v_n)$ as $v_i = \tilde{v}_{n-i+1}$. So, even if the covariance matrix or inverse covariance matrix is not full-rank, we can still perform inverse operations.

The results obtained in this section are also applicable to SDE and NN, but require special processing.

Appendix B Causality

Here, we briefly introduce the theory of causality provided by Hoel et al., which is based on the information-theoretic measure known as Effective Information (EI). Concepts about EI were initially introduced by Tononi et al. in [16] and later used by Hoel et al. to quantify CE in [17, 18, 22, 26, 57, 58, 76]. For a given transitional probability $P(x_{t+1}|x_t)$,

$$EI = I(\tilde{x}_{t+1}, x_t | do(x_t \sim \mathcal{U}(X))), \quad (\text{B.1})$$

where $x_t, \tilde{x}_{t+1}, \forall t \geq 0$ represent the state variables defined on \mathcal{S} at time step t and $t + 1$, respectively. $\mathcal{U}(X)$ means the uniform distribution or maximum entropy distribution on X . The intervention is formalized using Judea Pearl's theory [77] of causality, particularly through $do(\cdot)$ operations, which means artificially defining the probability distribution space of a variable. Consequently, the distribution of x_{t+1} will be indirectly altered by the intervention on x_t through the causal mechanism $P(x_{t+1}|x_t)$. Therefore, \tilde{x}_{t+1} denotes the random variable representing x_{t+1} following the intervention on x_t . To be noticed, Equation (B.1) is only an operational definition and the intervention of $do(\cdot)$ operator is just an imaginary operation to calculate EI but has no real physical meanings. In other words, $do(x_t \sim \mathcal{U}(X))$ is an operator to intervene in the input variable x_t to follow a uniform distribution in its domain X and keep the causal mechanism $P(x_{t+1}|x_t)$ unchanged.

We will introduce the calculation of effective information in different situations in the following subsections.

Appendix B.1 One-dimensional variables

The simplest way to express it is when the variable is in a one-dimensional space as $A = a, \Sigma = \sigma^2$ and $a, \sigma, x_t \in \mathcal{R}^1$. It is particularly emphasized that the effective information can be expressed as

$$EI(a, \sigma^2) = \ln \frac{|a|L}{\sqrt{2\pi e}\sigma}, \quad (\text{B.2})$$

as $do(x_t \sim \mathcal{U}(-L/2, L/2))$, which is the simplest form of effective information for Gaussian iterative systems.

EI can be decomposed into two terms, determinism $-\langle H(p(x_{t+1}|x_t)) \rangle$ and non-degeneracy $H(E_D(x_{t+1}))$ and $EI = -\langle H(p(x_{t+1}|x_t)) \rangle + H(E_D(x_{t+1}))$. Determinism

$$EI_1(a, \sigma^2) = \ln \frac{1}{\sqrt{2\pi e \sigma}}, \quad (\text{B.3})$$

and non-degeneracy

$$EI_2(a, \sigma^2) = \ln |a|L. \quad (\text{B.4})$$

From the formula, we can directly see that the effective information is positively correlated with the parameter a and negatively correlated with the covariance σ .

Appendix B.2 Multidimensional variables

By referring to the one-dimensional calculation method, effective information can be extended to multiple dimensions. Considering the possibility that A may not be a full rank matrix as $r \equiv r(A^T \Sigma^{-1} A) \leq r(A) \leq n$.

$$EI = \ln \left(\frac{|\text{pdet}(A^T \Sigma^{-1} A)|^{\frac{1}{2}} L^n}{(2\pi e)^{\frac{n}{2}}} \right). \quad (\text{B.5})$$

Definition Appendix B.1. (*Dimension averaged effective information for GIS*): For GIS like $x_{t+1} = a_0 + Ax_t + \eta_t$, $\eta_t \sim \mathcal{N}(0, \Sigma)$, $a_0, x_t \in \mathcal{R}^n$, $A, \Sigma \in \mathcal{R}^{n \times n}$ and $r \equiv r(A^T \Sigma^{-1} A) \leq r(A) \leq n$, the **dimension averaged effective information** of the dynamical system is calculated as

$$\mathcal{J} = \frac{EI}{n} = \ln \left(\frac{\text{pdet}(A^T \Sigma^{-1} A)^{\frac{1}{2n}} L}{\sqrt{2\pi e}} \right). \quad (\text{B.6})$$

$\text{pdet}(\cdot)$ represents the generalized determinant value corresponding to matrix \cdot with rank $r(\cdot)$ and singular values $s_i(\cdot), i = 1, \dots, r(\cdot)$, $\text{pdet}(\cdot) = s_1(\cdot)s_2(\cdot)\dots s_{r(\cdot)}(\cdot)$. L represents the size of the probability space with a uniform distribution determined by the do-operator $do(\cdot)$, which is an intervention that enforces $x_t \sim \mathcal{U}([-L/2, L/2]^n)$, where \mathcal{U} represents uniform distribution.

Proof. For the linear stochastic iteration system like $y = Ax + \eta$, $\eta \sim \mathcal{N}(0, \Sigma)$, $y \in \mathcal{R}^m$ follows a normal distribution about $x \in \mathcal{R}^n$, so $y \sim \mathcal{N}(Ax, \Sigma)$, $A \in \mathcal{R}^{m \times n}$, $\Sigma \in \mathcal{R}^{m \times m}$,

$$p(y|x) = \frac{1}{\det(\Sigma)^{\frac{1}{2}} (2\pi)^{\frac{m}{2}}} \exp \left\{ -\frac{1}{2} (y - Ax)^T \Sigma^{-1} (y - Ax) \right\} \quad (\text{B.7})$$

Following the calculation method of causal geometry, assuming η_t is small, $do(x \sim U([-L/2, L/2]^n)) \equiv do(x \sim U)$, then $p(x) = 1/L^n$, $L > 0$, we can calculate the effect distribution

$$\begin{aligned} E_D(y) &= \int_{\mathcal{X}} p(y|x)p(x)d^n x \\ &= \int_{\mathcal{X}} \frac{1}{\det(\Sigma)^{\frac{1}{2}} (2\pi)^{\frac{m}{2}}} \exp \left\{ -\frac{1}{2} (y - Ax)^T \Sigma^{-1} (y - Ax) \right\} \frac{1}{L^n} d^n x \\ &= \int_{\mathcal{X}} \frac{1}{\det(\Sigma)^{\frac{1}{2}} (2\pi)^{\frac{m}{2}}} \exp \left\{ -\frac{1}{2} (x - A^\dagger y)^T A^T \Sigma^{-1} A (x - A^\dagger y) \right\} \frac{1}{L^n} d^n x \\ &= \frac{(2\pi)^{\frac{n-m}{2}}}{|\text{pdet}(A^T \Sigma^{-1} A)|^{\frac{1}{2}} \det(\Sigma)^{\frac{1}{2}}} \int_{\mathcal{X}} \frac{1}{|\text{pdet}(A^T \Sigma^{-1} A)|^{-\frac{1}{2}} (2\pi)^{\frac{n}{2}}} \exp \left\{ -\frac{1}{2} (x - A^\dagger y)^T A^T \Sigma^{-1} A (x - A^\dagger y) \right\} \frac{1}{L^n} d^n x \\ &\approx \frac{(2\pi)^{\frac{n-m}{2}}}{|\text{pdet}(A^T \Sigma^{-1} A)|^{\frac{1}{2}} \det(\Sigma)^{\frac{1}{2}} L^n} \end{aligned} \quad (\text{B.8})$$

According to the properties of information entropy, determinism information

$$\begin{aligned}
-\langle H(p(y|x)) \rangle &= -\left\langle -\int_{\mathcal{X}} p(y|x) \ln(p(y|x)) d^m y \right\rangle \\
&= \int_{\mathcal{X}} \frac{d^n x}{L^n} \int_{\mathcal{X}} \frac{1}{\det(\Sigma)^{\frac{1}{2}} (2\pi)^{\frac{m}{2}}} \exp \left\{ -\frac{1}{2} (x_{t+1} - Ax_t)^T \Sigma^{-1} (x_{t+1} - Ax_t) \right\} \\
&\quad \left[-\ln \left(\det(\Sigma)^{\frac{1}{2}} (2\pi)^{\frac{m}{2}} \right) - \frac{1}{2} (y - Ax)^T \Sigma^{-1} (y - Ax) \right] d^m y \\
&= \left[-\ln \left(\det(\Sigma)^{\frac{1}{2}} (2\pi)^{\frac{m}{2}} \right) - \frac{m}{2} \right] \\
&= \ln \frac{1}{\det(\Sigma)^{\frac{1}{2}} (2\pi e)^{\frac{m}{2}}},
\end{aligned} \tag{B.9}$$

degeneracy information

$$\begin{aligned}
-H(E_D(y)) &= \int_{\mathcal{X}} E_D(y) \ln(E_D(y)) d^m y \\
&= \int_{\mathcal{X}} E_D(y) \ln \left(\frac{(2\pi)^{\frac{n-m}{2}}}{|\text{pdet}(A^T \Sigma^{-1} A)|^{\frac{1}{2}} \det(\Sigma)^{\frac{1}{2}} L^n} \right) \\
&\approx \ln \left(\frac{(2\pi)^{\frac{n-m}{2}}}{|\text{pdet}(A^T \Sigma^{-1} A)|^{\frac{1}{2}} \det(\Sigma)^{\frac{1}{2}} L^n} \right).
\end{aligned} \tag{B.10}$$

It's obvious that

$$EI = -\langle H(p(x_{t+1}|x_t)) \rangle - (-H(E_D(x_{t+1}))) = \ln \left(\frac{|\text{pdet}(A^T \Sigma^{-1} A)|^{\frac{1}{2}} L^n}{(2\pi)^{\frac{n}{2}} e^{\frac{m}{2}}} \right). \tag{B.11}$$

When $m = n$, we can directly calculate dimension averaged effective information for GIS in Eq.(B.6). \square

According to the properties of information entropy, \mathcal{J} can be decomposed into two terms as $\mathcal{J} = \mathcal{J}_1 + \mathcal{J}_2$, determinism

$$\mathcal{J}_1 = -\ln \left(\sqrt{2\pi e} \det(\Sigma)^{\frac{1}{2n}} \right) \tag{B.12}$$

measures how the current state x_t can deterministically (sufficiently) influence the state x_{t+1} in the future, non-degeneracy

$$\mathcal{J}_2 = \ln \left(\text{pdet}(A^T \Sigma^{-1} A)^{\frac{1}{2n}} \det(\Sigma)^{\frac{1}{2n}} L \right), \tag{B.13}$$

measures how exactly we can infer (necessarily) the state x_{t-1} in the past from the current state x_t .

Meanwhile, if matrix A is not of rank, we can directly use the dimension of matrix rank for averaging on EI . EI on a special macro-state dynamics can be obtained when the micro-dynamics matrix A is not full-rank in the following corollary.

Corollary Appendix B.1. *For the linear stochastic iteration systems like Equation (D.1), maximum effective information of the system after coarse-graining $y_t = \phi(x_t) = W x_t$, $W \in \mathcal{R}^{r \times n}$, is calculated as*

$$\mathcal{J}_R = \frac{EI_R}{r} = \ln \left(\frac{|\text{pdet}(A^T \Sigma^{-1} A)|^{\frac{1}{2r}} L}{(2\pi e)} \right). \tag{B.14}$$

Appendix C Dynamical reversibility

Another important property of dynamics that people are concerned about is dynamical reversibility. It is generally believed that the dynamics of the microscopic physical world (such as Newton's second law or the Schrödinger equation in quantum mechanics) are dynamically reversible, while the second law of thermodynamics in the macroscopic world stems from the irreversibility of macroscopic dynamic processes.

Appendix C.1 Approximate dynamical reversibility of TPM

Zhang's previous work [40] has provided an indicator of CE for Markov chains called approximate dynamical reversibility, which describes the proximity of a transitional probability matrix (TPM) to a permutation matrix. This new framework for CE is distinctive for its independence from coarse-grained strategies. The calculation of the approximate dynamical reversibility of TPM P requires solving its singular values as $P \cdot P^T = VZV^T$ and $Z = \text{diag}(\zeta_1, \zeta_2, \dots, \zeta_N)$ as $\zeta_1 \geq \zeta_2 \geq \dots \geq \zeta_N \geq 0$, then the α -ordered approximate dynamical reversibility of P is defined as:

$$\Gamma_\alpha \equiv \sum_i^N \zeta_i^\alpha, \quad (\text{C.1})$$

where $\alpha \in (0, 2)$ is a parameter. The maximum Γ_α can be achieved if P is a permutation matrix. Therefore, Γ_α can be used as an index of the reversibility of TPM and an approximate relationship exists as [40]

$$EI \sim \log \Gamma_\alpha. \quad (\text{C.2})$$

However, this approximate equivalence can only be confirmed through numerical experiments, and there is currently no clear mathematical analytical proof.

Appendix C.2 Approximate dynamical reversibility of GIS in \mathcal{R}^1

In Eq.(D.1), when $\eta_t = 0$ and $f(x_t) = a_0 + Ax_t$ is a reversible bijection mapping on \mathcal{R}^n , we assume that the dynamics of GIS described by Eq.(D.1) is strictly reversible as $x_{t+1} = a_0 + Ax_t$, and the corresponding backward dynamics of Eq.(D.1) can be directly established as $x_t = A^{-1}(x_{t+1} - a_0)$. However, real-world dynamical systems around us are not so simple and perfect.

Similar to the framework in Zhang's article [40], to calculate approximate reversibility, it is necessary to obtain the singular value spectrum of TPM, and the same applies to GIS. For GIS, we need to treat $p(x_{t+1}|x_t)$ as a TPM with continuous states and apply operations from functional analysis [55] to calculate its singular value spectrum. Firstly, we calculate the Gaussian kernel which corresponds to $P \cdot P^T$ of TPM in [40] when the probability space is continuous as

$$K(\mathbf{x}, \mathbf{y}) \equiv \mathcal{K}(\mathbf{x} - \mathbf{y}) = (2\pi)^{-\frac{n}{2}} \det(2\Sigma)^{-\frac{1}{2}} \exp \left\{ -\frac{1}{4}(\mathbf{x} - \mathbf{y})^T (A^T \Sigma^{-1} A)(\mathbf{x} - \mathbf{y}) \right\}. \quad (\text{C.3})$$

Suppose ζ is a singular value of $p(x_{t+1}|x_t)$, then ζ^2 is the eigenvalue of $K(\mathbf{x}, \mathbf{y}) = \mathcal{K}(\mathbf{x} - \mathbf{y})$ and $\psi(\mathbf{x})$ is the eigenfunction corresponding to the eigenvalue ζ^2 . By analogy with the theorem of the spectrum of stochastic integral operators in functional analysis [55], we can derive ζ^2 by $(\mathbf{K}\psi)(\mathbf{x}) = \int_{-\infty}^{\infty} K(\mathbf{x}, \mathbf{y})\psi(\mathbf{y})d\mathbf{y} = \zeta^2\psi(\mathbf{x})$. Based on the properties of the Fourier transform of the convolution function in the integral transform, we can consider the above integral in $(\mathbf{K}\psi)(\mathbf{x})$ as a convolution of $\mathcal{K}(\mathbf{y})$ and $\psi(\mathbf{y})$. Then the eigenvalue spectrum $\zeta^2(\omega)$ in the frequency space is obtained through Fourier transform [56] as $\hat{\mathcal{K}}(\omega)\hat{\psi}(\omega) = \mathcal{F}\{\mathcal{K}(\mathbf{y})\}\mathcal{F}\{\psi(\mathbf{y})\} = \zeta^2\hat{\psi}(\omega)$. From this, we can also obtain the singular value spectrum $\zeta(\omega) = \sqrt{\hat{\mathcal{K}}(\omega)}$ of $p(x_{t+1}|x_t)$ in the frequency space as $\omega \in \mathcal{R}^n$.

Definition Appendix C.1. (*Approximate reversibility*): Suppose the singular value spectrum of GIS $p(x_{t+1}|x_t) = \mathcal{N}(Ax_t + a_0, \Sigma)$ is $\zeta(\omega)$, $a_0, \omega, x_t, x_{t+1} \in \mathcal{R}^n$, $A, \Sigma \in \mathcal{R}^{n \times n}$, then the α -ordered approximate dynamical reversibility of $p(x_{t+1}|x_t)$ is defined as

$$\Gamma_\alpha \equiv \int_{-\infty}^{\infty} \zeta^\alpha(\omega) d\omega \quad (\text{C.4})$$

where $\alpha \in (0, 2)$.

According to Definition Appendix C.1, the approximate dynamical reversibility Γ_α of GIS $x_{t+1} = a_0 + Ax_t + \eta_t$, $\eta_t \sim \mathcal{N}(0, \Sigma)$ is given in following theorems. We can start the deduction process from situations of GIS in \mathcal{R}^1 .

Lemma Appendix C.1. *For Gaussian kernels like*

$$K(\mathbf{x}, \mathbf{y}) = \frac{1}{\sqrt{2\pi}\sigma} \exp \left\{ -\frac{(\mathbf{y} - \mathbf{x})^2}{2\sigma^2} \right\} \quad (\text{C.5})$$

Based on the structure of a Gaussian kernel $K(\mathbf{x}, \mathbf{y}) = \mathcal{K}(\mathbf{x} - \mathbf{y})$, we can perform a convolution operation on the integral, which allows us to perform a Fourier transform on the integral as directly

$$\hat{\mathcal{K}}(\omega)\hat{\psi}(\omega) = \lambda\hat{\phi}(\omega) \quad (\text{C.6})$$

In frequency space, the eigenvalue spectrum can be directly expressed as

$$\lambda(\omega) = \hat{K}(\omega) = \exp \left\{ -\frac{\omega^2 \sigma^2}{2} \right\}. \quad (\text{C.7})$$

Proof. We can perform a Fourier transform on the integral as

$$\begin{aligned} \hat{K}(\omega) \hat{\psi}(\omega) &= \mathcal{F} \{ (\mathbf{K}\psi)(\mathbf{x}) \} = \mathcal{F} \left\{ \int_{-\infty}^{\infty} K(\mathbf{x}, \mathbf{y}) \psi(\mathbf{y}) d\mathbf{y} \right\} = \mathcal{F} \left\{ \int_{-\infty}^{\infty} \frac{1}{\sqrt{2\pi}\sigma} \exp \left\{ -\frac{(\mathbf{x} - \mathbf{y})^2}{2\sigma^2} \right\} \psi(\mathbf{y}) d\mathbf{y} \right\} \\ &= \mathcal{F} \left\{ \frac{1}{\sqrt{2\pi}\sigma} \exp \left\{ -\frac{\mathbf{y}^2}{2\sigma^2} \right\} \right\} \mathcal{F} \{ \psi(\mathbf{y}) \} = \exp \left\{ -\frac{\omega^2 \sigma^2}{2} \right\} \hat{\psi}(\omega). \end{aligned} \quad (\text{C.8})$$

This calculation process is actually a Fourier transform of Gaussian functions, and it is almost the same as the process of finding the characteristic function for Gaussian distribution. \square

Based on the solution of the eigenvalues of the Gaussian kernel function $K(\mathbf{x}, \mathbf{y}) = \mathcal{K}(\mathbf{x} - \mathbf{y})$ mentioned above, we can obtain the singular value of TPM $p(y|x)$.

Theorem Appendix C.1. Suppose the transitional probability from $x \in \mathcal{R}$ to $y \in \mathcal{R}$ is

$$p(y|x) = \frac{1}{\sqrt{2\pi}\sigma} \exp \left\{ -\frac{(y - ax)^2}{2\sigma^2} \right\} \quad (\text{C.9})$$

its singular value spectrum is:

$$\zeta^2(\omega) = \frac{1}{|a|} \exp \left\{ -\frac{\omega^2 2\sigma^2}{2a^2} \right\} \quad (\text{C.10})$$

then the 2-ordered approximate dynamical reversibility of $p(y|x)$ is defined as:

$$\Gamma_2 = \int_{-\infty}^{\infty} \zeta^2(\omega) d\omega = \frac{\sqrt{\pi}}{\sigma} \quad (\text{C.11})$$

Proof. According to the calculation process of calculating the singular values for discrete TPM P is equal to calculating the eigenvalues of PP^T . In continuous space, PP^T for $p(y|x)$ is equal to the Gaussian kernel

$$\begin{aligned} K(\mathbf{x}, \mathbf{y}) &= \int_{-\infty}^{\infty} p(\mathbf{z}|\mathbf{x}) p(\mathbf{z}|\mathbf{y}) d\mathbf{z} = \int_{-\infty}^{\infty} \frac{1}{2\pi\sigma^2} \exp \left\{ -\frac{(\mathbf{z} - a\mathbf{x})^2 + (\mathbf{z} - a\mathbf{y})^2}{2\sigma^2} \right\} d\mathbf{z} \\ &= \int_{-\infty}^{\infty} \frac{1}{2\pi\sigma^2} \exp \left\{ -\frac{2(\mathbf{z} - \frac{a(\mathbf{x}+\mathbf{y})}{2})^2 + \frac{a^2(\mathbf{x}-\mathbf{y})^2}{2}}{2\sigma^2} \right\} d\mathbf{z} \\ &= \frac{1}{\sqrt{2\pi}\sigma} \exp \left\{ -\frac{a^2(\mathbf{x}-\mathbf{y})^2}{4\sigma^2} \right\} \int_{-\infty}^{\infty} \frac{1}{\sqrt{2\pi}\sigma} \exp \left\{ -\frac{(\mathbf{z} - \frac{a(\mathbf{x}+\mathbf{y})}{2})^2}{\sigma^2} \right\} d\mathbf{z} \\ &= \frac{1}{\sqrt{2\pi}(\sqrt{2}\sigma)} \exp \left\{ -\frac{a^2(\mathbf{x}-\mathbf{y})^2}{4\sigma^2} \right\} \int_{-\infty}^{\infty} \frac{1}{\sqrt{2\pi}(\sigma/\sqrt{2})} \exp \left\{ -\frac{(\mathbf{z} - \frac{a(\mathbf{x}+\mathbf{y})}{2})^2}{2(\sigma/\sqrt{2})^2} \right\} d\mathbf{z} \\ &= \frac{1}{|a|} \frac{1}{\sqrt{2\pi}(\sqrt{2}\sigma/|a|)} \exp \left\{ -\frac{(\mathbf{x}-\mathbf{y})^2}{2(\sqrt{2}\sigma/|a|)^2} \right\}. \end{aligned} \quad (\text{C.12})$$

It's also important to be reminded that this is only a special case of linear dynamics. In nonlinear dynamics, we can only get

$$K(\mathbf{x}, \mathbf{y}) = \frac{1}{\sqrt{2\pi}(\sqrt{2}\sigma)} \exp \left\{ -\frac{(f(\mathbf{x}) - f(\mathbf{y}))^2}{2(\sqrt{2}\sigma)^2} \right\}. \quad (\text{C.13})$$

Suppose ζ is a singular value of $p(y|x)$, then ζ^2 is the eigenvalue of $K(\mathbf{x}, \mathbf{y}) = \mathcal{K}(\mathbf{x} - \mathbf{y})$ and $\psi(\mathbf{x})$ is the eigenfunction corresponding to the eigenvalue ζ^2 . By analogy with the theorem of the spectrum of stochastic integral operators in functional analysis, we can derive ζ^2 by

$$(\mathbf{K}\psi)(x) = \zeta^2 \psi(x), \quad (\text{C.14})$$

from which we can get

$$\zeta^2(\omega) = \frac{1}{|a|} \exp \left\{ -\frac{\omega^2}{2} \frac{2\sigma^2}{a^2} \right\}. \quad (\text{C.15})$$

We can see that the calculation process is actually a Fourier transform of Gaussian functions. With integral calculation, we get Γ_α when $\alpha = 2$ as

$$\begin{aligned} \Gamma_2 &= \int_{-\infty}^{\infty} \zeta^2(\omega) d\omega = \int_{-\infty}^{\infty} \frac{1}{|a|} \exp \left\{ -\frac{\omega^2}{2} \frac{2\sigma^2}{a^2} \right\} d\omega \\ &= \frac{1}{|a|} \frac{|a|}{\sqrt{2\sigma}} \int_{-\infty}^{\infty} \exp \left\{ -\frac{\omega^2}{2} \frac{2\sigma^2}{a^2} \right\} d \left(\frac{\sqrt{2\sigma}}{|a|} \omega \right) \\ &= \frac{\sqrt{2\pi}}{\sqrt{2\sigma}} = \frac{\sqrt{\pi}}{\sigma}. \end{aligned} \quad (\text{C.16})$$

Then we can derive the general value of approximate dynamical reversibility Γ_α according to Γ_2 . \square

After knowing the quantitative index of approximate reversibility in the case of $\alpha = 2$, we can extend it to the general case as $\alpha \in (0, 2)$.

Theorem Appendix C.2. *Suppose the transitional probability from $x \in \mathcal{R}$ to $y \in \mathcal{R}$ is*

$$p(y|x) = \frac{1}{\sqrt{2\pi}\sigma} \exp \left\{ -\frac{(y - ax)^2}{2\sigma^2} \right\} \quad (\text{C.17})$$

its α -ordered singular value spectrum is:

$$\zeta^\alpha(\omega) = |a|^{-\frac{\alpha}{2}} \exp \left\{ -\frac{\alpha}{2} \left(\frac{\omega\sigma}{a} \right)^2 \right\} \quad (\text{C.18})$$

then the α -ordered approximate dynamical reversibility of $p(y|x)$ is defined as:

$$\Gamma_\alpha = \int_{-\infty}^{\infty} \zeta^\alpha(\omega) d\omega = \sqrt{\frac{2\pi}{\alpha}} \frac{|a|^{1-\frac{\alpha}{2}}}{\sigma} \quad (\text{C.19})$$

Proof. The α -ordered approximate dynamical reversibility of $p(y|x)$ is defined as:

$$\zeta^\alpha(\omega) = |a|^{-\frac{\alpha}{2}} \exp \left\{ -\frac{\alpha}{2} \left(\frac{\omega\sigma}{a} \right)^2 \right\}. \quad (\text{C.20})$$

So we can get the index of approximate dynamical reversibility as

$$\begin{aligned} \Gamma_\alpha &= \int_{-\infty}^{\infty} \zeta^\alpha(\omega) d\omega = \int_{-\infty}^{\infty} |a|^{-\frac{\alpha}{2}} \exp \left\{ -\frac{\omega^2}{2} \frac{\alpha\sigma^2}{a^2} \right\} d\omega \\ &= \frac{|a|^{1-\frac{\alpha}{2}}}{\sqrt{\alpha}\sigma} \int_{-\infty}^{\infty} \exp \left\{ -\frac{\omega^2}{2} \frac{\alpha\sigma^2}{a^2} \right\} d \left(\frac{\sqrt{\alpha}\sigma}{|a|} \omega \right) \\ &= \frac{\sqrt{2\pi}}{\sqrt{\alpha}\sigma} |a|^{1-\frac{\alpha}{2}} = \sqrt{\frac{2\pi}{\alpha}} \frac{|a|^{1-\frac{\alpha}{2}}}{\sigma}. \end{aligned} \quad (\text{C.21})$$

This is the indicator expression for approximate reversibility in one-dimensional situations. \square

Fig.7b shows the logarithmic relationship between EI and Γ_α . It can be seen that for different noise covariances σ , as Γ_α increases, EI shows an approximate logarithmic growth relationship with Γ_α as $\alpha = 1$. The dimensional average reversible information $\ln \Gamma_\alpha$ and dimensional average effective information \mathcal{J} (Fig.7c), as well as their corresponding determinism (Fig.7d) and non-degeneracy (Fig.7e), are linearly related.

Appendix C.3 Approximate dynamical reversibility of GIS in \mathcal{R}^n

After knowing the approximate reversibility index of random variables in one-dimensional space, we can extend it to multi-dimensional variables as $x \in \mathcal{R}^n$ and $y \in \mathcal{R}^n$. First, we can study the case of the full rank matrix A and Σ .

Theorem Appendix C.3. *Suppose the transitional probability from $x \in \mathcal{R}^n$ to $y \in \mathcal{R}^n$ is*

$$p(y|x) = \frac{1}{(2\pi)^{\frac{n}{2}} \det(\Sigma)^{\frac{1}{2}}} \exp \left\{ -\frac{1}{2} (y - Ax)^T \Sigma^{-1} (y - Ax) \right\} \quad (\text{C.22})$$

$x, y \in \mathcal{R}^n, A \in \mathcal{R}^{n \times n}$, its α -ordered singular value spectrum is:

$$\zeta^\alpha(\omega) = |\det(A)|^{-\frac{\alpha}{2}} \exp \left\{ -\frac{\alpha}{2} (\omega^T (A^{-1})^T \Sigma A^{-1} \omega) \right\} \quad (\text{C.23})$$

$\omega \in \mathcal{R}^n$, the α -ordered approximate dynamical reversibility of $p(y|x)$ is defined as:

$$\Gamma_\alpha = \left(\frac{2\pi}{\alpha} \right)^{\frac{n}{2}} \det(A^T \Sigma^{-1} A)^{\frac{1}{2} - \frac{\alpha}{4}} \det(\Sigma^{-1})^{\frac{\alpha}{4}} \quad (\text{C.24})$$

Besides the first constant, this formula contains two terms: $\det(\cdot)$ of the inverse covariance matrices of the forward and backward dynamics.

Proof. Suppose $y = Ax + \eta, \eta \sim \mathcal{N}(0, \Sigma)$ as the transitional probability from $x \in \mathcal{R}^m$ to $y \in \mathcal{R}^n$ is

$$p(y|x) = \frac{1}{(2\pi)^{\frac{n}{2}} \det(\Sigma)^{\frac{1}{2}}} \exp \left\{ -\frac{1}{2} (y - Ax)^T \Sigma^{-1} (y - Ax) \right\}. \quad (\text{C.25})$$

We calculate the Gaussian kernel, which corresponds to $P \cdot P^T$ of TPM when the probability space is continuous, as

$$K(\mathbf{y}, \mathbf{x}) = \frac{1}{|\det(A)|} \frac{1}{(2\pi)^{\frac{n}{2}} \det(2(A^{-1})^T \Sigma A^{-1})^{\frac{1}{2}}} \exp \left\{ -\frac{1}{2} (\mathbf{y} - \mathbf{x})^T A^T \Sigma^{-1} A (\mathbf{y} - \mathbf{x}) \right\} \quad (\text{C.26})$$

According to $\hat{\mathcal{K}}(\omega) \hat{\psi}(\omega) = \mathcal{F} \{ \mathcal{K}(\mathbf{y}) \} \mathcal{F} \{ \psi(\mathbf{y}) \} = \zeta^2 \hat{\psi}(\omega)$ we can get Eq.(C.23). We can see that the calculation process is actually a Fourier transform of Gaussian functions, so both low dimensional and high-dimensional can directly borrow the form of characteristic functions. When A is full rank, the α -ordered approximate dynamical reversibility of $p(y|x)$ as

$$\begin{aligned} \Gamma_\alpha &= \int_{\mathcal{X}} \zeta^\alpha(\omega) d\omega = \int_{\mathcal{X}} |\det(A)|^{-\alpha/2} \exp \left\{ -\frac{\alpha}{2} \omega^T A^T \Sigma^{-1} A \omega \right\} d\omega \\ &= |\det(A)|^{-\alpha/2} \int_{\mathcal{X}} \exp \left\{ -\frac{1}{2} \omega^T (\alpha A^T \Sigma^{-1} A) \omega \right\} d\omega \\ &= |\det(A)|^{-\alpha/2} \cdot \frac{(2\pi)^{n/2}}{\alpha^{n/2} \cdot \frac{(\det \Sigma)^{1/2}}{|\det(A)|}} = |\det(A)|^{-\alpha/2} \cdot \frac{(2\pi)^{n/2} |\det(A)|}{\alpha^{n/2} (\det \Sigma)^{1/2}} \\ &= \left(\frac{2\pi}{\alpha} \right)^{\frac{n}{2}} \frac{|\det(A)|^{1-\frac{\alpha}{2}}}{\det(\Sigma)^{\frac{1}{2}}}, \end{aligned} \quad (\text{C.27})$$

which can be transformed into the form of Eq.(C.24). □

When we assume A and Σ are reversible matrices, the forward dynamics is $x_{t+1} = a_0 + Ax_t + \eta_t$, and the corresponding backward dynamics is $x_t = A^{-1}(x_{t+1} - a_0 - \eta_t)$. The corresponding conditional probability distributions are $p(x_{t+1}|x_t) = \mathcal{N}(a_0 + Ax_t, \Sigma)$ and $p(x_t|x_{t+1}) = \mathcal{N}(A^{-1}(x_{t+1} - a_0), A^{-1}\Sigma(A^{-1})^T)$, it can be seen that Σ^{-1} and $A^T \Sigma^{-1} A$ represent the inverse covariance matrices of the forward and backward dynamics, respectively.

We can also deal with the case of a non-full rank matrix A , and this method can better reflect the essence of approximate reversibility Γ_α .

Theorem Appendix C.4. Suppose the transitional probability from $x \in \mathcal{R}^m$ to $y \in \mathcal{R}^n$ is

$$p(y|x) = \frac{1}{(2\pi)^{\frac{n}{2}} \det(\Sigma)^{\frac{1}{2}}} \exp \left\{ -\frac{1}{2} (y - Ax)^T \Sigma^{-1} (y - Ax) \right\} \quad (\text{C.28})$$

$x \in \mathcal{R}^m, y \in \mathcal{R}^n, A \in \mathcal{R}^{n \times m}, \Sigma \in \mathcal{R}^{n \times n}$, its α -ordered singular value spectrum is:

$$\zeta^\alpha(\omega) = \left\{ (2\pi)^{\frac{n-m}{2}} \det(\Sigma)^{\frac{1}{2}} \text{pdet}(A^T \Sigma^{-\frac{1}{2}} A)^{\frac{1}{2}} \right\}^{-\frac{\alpha}{2}} \exp \left\{ -\frac{\alpha}{2} (\omega^T (A^T \Sigma^{-1} A)^\dagger \omega) \right\} \quad (\text{C.29})$$

$\omega \in \mathcal{R}^m$, the α -ordered approximate dynamical reversibility of $p(y|x)$ is defined as:

$$\Gamma_\alpha = (2\pi)^{\frac{\alpha(m-n)}{4}} \left(\frac{2\pi}{\alpha} \right)^{\frac{m}{2}} \text{pdet}(A^T \Sigma^{-1} A)^{\frac{1}{2} - \frac{\alpha}{4}} \det(\Sigma^{-1})^{\frac{\alpha}{4}}. \quad (\text{C.30})$$

After that, we can get the indicator for local approximate dynamical reversibility in a general GIS defined as

$$\Gamma_\alpha = \left(\frac{2\pi}{\alpha} \right)^{\frac{n}{2}} \text{pdet}(A^T \Sigma^{-1} A)^{\frac{1}{2} - \frac{\alpha}{4}} \text{pdet}(\Sigma^{-1})^{\frac{\alpha}{4}}, \quad (\text{C.31})$$

Besides the first constant, this formula contains two terms: $\text{pdet}(\cdot)$ of the inverse covariance matrices of the forward and backward dynamics.

Proof. Suppose $y = Ax + \eta, \eta \sim \mathcal{N}(0, \Sigma)$ as the transitional probability from $x \in \mathcal{R}^m$ to $y \in \mathcal{R}^n$ is

$$p(y|x) = \frac{1}{(2\pi)^{\frac{n}{2}} \det(\Sigma)^{\frac{1}{2}}} \exp \left\{ -\frac{1}{2} (y - Ax)^T \Sigma^{-1} (y - Ax) \right\}. \quad (\text{C.32})$$

When A is not a full rank matrix, we need to calculate the Gaussian kernel which corresponds to $P \cdot P^T$ of TPM when probability space is continuous as

$$\begin{aligned} K(\mathbf{x}, \mathbf{y}) &= \int_{-\infty}^{\infty} p(\mathbf{z}|\mathbf{x}) p(\mathbf{z}|\mathbf{y}) d\mathbf{z} = \frac{1}{(2\pi)^{\frac{n}{2}} \det(2\Sigma)^{\frac{1}{2}}} \exp \left\{ -\frac{1}{4} (\mathbf{x} - \mathbf{y})^T (A^T \Sigma^{-1} A) (\mathbf{x} - \mathbf{y}) \right\} \\ &= \frac{\text{pdet}(2(A^T \Sigma^{-1} A)^\dagger)^{\frac{1}{2}}}{(2\pi)^{\frac{n}{2}} \det(2\Sigma)^{\frac{1}{2}} \text{pdet}(2(A^T \Sigma^{-1} A)^\dagger)^{\frac{1}{2}}} \exp \left\{ -\frac{1}{4} (\mathbf{x} - \mathbf{y})^T (A^T \Sigma^{-1} A) (\mathbf{x} - \mathbf{y}) \right\} \\ &= \frac{\text{pdet}(A^T \Sigma^{-1} A)^{-\frac{1}{2}}}{(2\pi)^{\frac{n-m}{2}} \det(2\Sigma)^{\frac{1}{2}} (2\pi)^{\frac{m}{2}} \text{pdet}(2(A^T \Sigma^{-1} A)^\dagger)^{\frac{1}{2}}} \exp \left\{ -\frac{1}{4} (\mathbf{x} - \mathbf{y})^T (A^T \Sigma^{-1} A) (\mathbf{x} - \mathbf{y}) \right\}, \end{aligned} \quad (\text{C.33})$$

By analogy with the theorem of the spectrum of stochastic integral operators in functional analysis, we can derive ζ^2 by

$$\mathbf{K}\psi(x) = \zeta^2 \psi(x) \quad (\text{C.34})$$

and we can get

$$\zeta^\alpha(\omega) = \left\{ (2\pi)^{\frac{n-m}{2}} \det(\Sigma)^{\frac{1}{2}} \text{pdet}(A^T \Sigma^{-\frac{1}{2}} A)^{\frac{1}{2}} \right\}^{-\frac{\alpha}{2}} \exp \left\{ -\frac{\alpha}{2} (\omega^T (A^T \Sigma^{-1} A)^\dagger \omega) \right\} \quad (\text{C.35})$$

the α -ordered approximate dynamical reversibility of $p(y|x)$ is derived from the third line of Eq.(C.27), which changes to

$$\begin{aligned} \Gamma_\alpha &= \left(\frac{2\pi}{\alpha} \right)^{\frac{n}{2}} \left(\frac{\text{pdet}(A^T \Sigma^{-1} A)^{-\frac{1}{2}}}{(2\pi)^{\frac{n-m}{2}} \det(\Sigma)^{\frac{1}{2}}} \right)^{\frac{\alpha}{2}} \text{pdet}(A^T \Sigma^{-1} A) \\ &= (2\pi)^{\frac{\alpha(m-n)}{4}} \left(\frac{2\pi}{\alpha} \right)^{\frac{m}{2}} \text{pdet}(A^T \Sigma^{-1} A)^{\frac{1}{2} - \frac{\alpha}{4}} \det(\Sigma^{-1})^{\frac{\alpha}{4}}. \end{aligned} \quad (\text{C.36})$$

In general dynamics, $m = n$. Considering the situation in Definition Appendix A.2, we can directly use the form in Eq.(C.31) to measure the approximate dynamical reversibility of the dynamics. \square

Γ_α can be considered a measure of approximate dynamical reversibility because when the uncertainty in the system's forward and backward dynamics (i.e., the pseudo-determinant of the covariance matrix) is large, the pseudo-determinants of Σ^{-1} and $A^T\Sigma^{-1}A$ become very small, and the dynamics become highly irreversible. Conversely, if the uncertainty in the system's forward and backward dynamics is very small, or even approaches zero, the pseudo-determinants of Σ^{-1} and $A^T\Sigma^{-1}A$ become very large, or even approach infinity. In this case, the system's dynamics are very close to reversible dynamics, and using the de-noised reversible dynamics to approximate the GIS becomes effective.

To avoid the excessive influence of variable dimension on the reversibility of dynamics, we can use the dimensional average reversible information $\hat{\gamma}_\alpha \equiv \frac{1}{n} \ln \Gamma_\alpha$ to more effectively quantify the approximate dynamical reversibility. After removing the constant term, $\gamma_\alpha = \hat{\gamma}_\alpha - \frac{1}{2} \ln \left(\frac{2\pi}{\alpha} \right)$ is a variable only determined by the singular values after the SVD of Σ^{-1} and $A^T\Sigma^{-1}A$.

Lemma Appendix C.2. (*Dimensional average reversible information based on SVD*) For GIS like Eq.(D.1), we only need to obtain the singular value spectra of inverse covariance matrices $A^T\Sigma^{-1}A$ and Σ^{-1} to quantify the approximate dynamical reversibility. The corresponding indicator is the dimensional average reversibility information after removing the constant term, defined as

$$\gamma_\alpha = \frac{1}{n} \left[\left(\frac{1}{2} - \frac{\alpha}{4} \right) \sum_{i=1}^{r_s} \ln s_i + \frac{\alpha}{4} \sum_{i=1}^{r_\kappa} \ln \kappa_i \right] \quad (\text{C.37})$$

Here r_s, r_κ denote the ranks of matrices $A^T\Sigma^{-1}A, \Sigma^{-1}$, respectively. s_i and κ_i denote the i -th singular value of matrices $A^T\Sigma^{-1}A$ and matrix Σ^{-1} respectively.

Proof. Due to the fact that Γ_α is related to the dimensionality of the input variable and is influenced by a constant that is not related to the variable, we need to average the dimensionality of the input variable by taking the logarithm and eliminate the constant term as

$$\begin{aligned} \gamma_\alpha &\equiv \frac{1}{n} \ln \Gamma_\alpha - \frac{1}{2} \ln \left(\frac{2\pi}{\alpha} \right) \\ &= \frac{1}{n} \ln \text{pdet}(A^T\Sigma^{-1}A)^{\frac{1}{2} - \frac{\alpha}{4}} + \frac{1}{n} \ln \text{pdet}(\Sigma^{-1})^{\frac{\alpha}{4}}. \\ &= \frac{1}{n} \left(\frac{1}{2} - \frac{\alpha}{4} \right) \sum_{i=1}^{r_s} \ln s_i + \frac{\alpha}{4n} \sum_{i=1}^{r_\kappa} \ln \kappa_i \end{aligned} \quad (\text{C.38})$$

to characterize dimensionally independent approximate dynamic reversibility for a more reasonable comparison of iterative systems of different dimensions. As $r(A^T\Sigma^{-1}A) \equiv r_s$, $r(\Sigma^{-1}) \equiv r_\kappa$, $s_i(A^T\Sigma^{-1}A) \equiv s_i$ and $s_i(\Sigma^{-1}) \equiv \kappa_i$, we can get our final results. \square

Appendix C.3.1 Determinism and degeneracy based on Γ_α

As pointed out by [40], Γ_α 's reflection on determinism in Eq.(B.12) and degeneracy in Eq.(B.13) mainly depends on the transformation of hyperparameter α . By adjusting the parameter $\alpha \in (0, 2]$, we can make Γ_α reflect the **determinism** or **degeneracy** of $p(x_{t+1}|x_t) = \mathcal{N}(Ax_t + a_0, \Sigma)$.

As $\alpha \rightarrow 0$,

$$\Gamma_{\alpha \rightarrow 0} = \left(\frac{2\pi}{\alpha} \right)_{\alpha \rightarrow 0}^{\frac{n}{2}} \text{pdet}(A^T\Sigma^{-1}A)^{\frac{1}{2}}, \quad (\text{C.39})$$

in which $\text{pdet}(A^T\Sigma^{-1}A)$ is the Moore-Penrose generalized inverse matrix of $A^\dagger\Sigma(A^\dagger)^T$. $A^\dagger\Sigma(A^\dagger)^T$ is the covariance matrix of the inverse dynamics $x_t = A^\dagger x_{t+1} - A^\dagger a_0 - A^\dagger \eta_t$ of $x_{t+1} = a_0 + Ax_t + \eta_t$. In the calculation of \mathcal{J} , non-degeneracy \mathcal{J}_2 in Eq.(B.13) describes how exactly we can infer the state x_{t-1} in previous time step from the current state x_t which is also the predictability of backward dynamics, so $\Gamma_{\alpha \rightarrow 0}$ resembles the non-degeneracy term in the definition of \mathcal{J} . When $\text{pdet}(A^T\Sigma^{-1}A)$ becomes smaller, $p(x_{t+1}|x_t)$ becomes more degeneracy.

Similarly, as $\alpha \rightarrow 2$, since

$$\Gamma_{\alpha \rightarrow 2} = (\pi)^{\frac{n}{2}} \det(\Sigma^{-1})^{\frac{1}{2}}, \quad (\text{C.40})$$

and covariance matrix Σ of $x_{t+1} = a_0 + Ax_t + \eta_t$ directly determine the determinism term \mathcal{J}_1 in \mathcal{J} which measures how the current state x_t can deterministically influences the state x_{t+1} in next time step, Γ_2 is comparable with

the determinism term. An increase of $\det(\Sigma^{-1})$ leads to higher maximum transition probabilities, reflecting stronger determinism in the underlying dynamics. When $\det(\Sigma^{-1}) \rightarrow \infty$, $p(x_{t+1}|x_t)$ approaches the Dirac distribution, the determinism will tend towards ∞ .

In practice, $\alpha = 1$ is often chosen to balance Γ_α 's emphasis on both determinism and degeneracy. For $\alpha < 1$, Γ_α tends to capture more of the non-degeneracy of $p(x_{t+1}|x_t)$. In contrast, for $\alpha > 1$, Γ_α emphasizes the determinism of $p(x_{t+1}|x_t)$. Given the significance of $\alpha = 1$, we primarily present results for this case, and we will denote

$$\Gamma \equiv \Gamma_1 = (2\pi)^{\frac{n}{2}} \text{pdet}(A^T \Sigma^{-1} A)^{\frac{1}{4}} \det(\Sigma^{-1})^{\frac{1}{4}} \quad (\text{C.41})$$

in the subsequent discussion.

Appendix C.4 Nearly linear relationship

To study the relationship between two CE indicators, we first need to understand the relationship between EI and Γ_α . In continuous systems, approximate equivalence can be analytically proven.

Theorem Appendix C.5. (*Correlation between Γ_α and EI*): When the backward dynamics $p(x_t|x_{t+1}) = \mathcal{N}(A^\dagger x_{t+1} - A^\dagger a_0, A^\dagger \Sigma (A^\dagger)^T)$ is close to a normalized normal distribution as $A^\dagger \Sigma (A^\dagger)^T \approx I_n$, Γ_α and dimension averaged EI are positively correlated as

$$\ln \Gamma_\alpha \simeq n(1 - \frac{\alpha}{4}) \mathcal{J} + C. \quad (\text{C.42})$$

$\ln \Gamma_\alpha$ is the reversible information and measures the degree of approximate reversibility. $C = \frac{n}{2} \ln(\frac{2\pi}{\alpha}) - n(1 - \frac{\alpha}{4}) \ln(\frac{L}{\sqrt{2\pi e}})$ is a constant term independent of A and Σ . When the backward dynamics $p(x_t|x_{t+1})$ is a normalized normal distribution, i.e. $A \in \mathcal{R}^{m \times n}$ is reversible and $A^\dagger \Sigma (A^\dagger)^T = A^{-1} \Sigma (A^{-1})^T = I_n$, the equal sign holds.

Proof. If we only study a single random mapping $p(y|x) = \mathcal{N}(Ax, \Sigma)$, then A may not be a full-rank square matrix. However, coarsening strategies are generally applied to Gaussian iterative systems $x_{t+1} = Ax_t + \eta_t$, where A must be a square matrix to ensure the stability of the system's dimensions. So we need to set $m = n$ and $A, \Sigma \in \mathcal{R}^{n \times n}$. From Eq.(B.5) and (C.30), we can obtain two approximate correlations as

$$\begin{aligned} \ln \Gamma_\alpha &\simeq \frac{n}{2} \ln\left(\frac{2\pi}{\alpha}\right) + (1 - \frac{\alpha}{2}) \frac{1}{2} \ln \text{pdet}(A^T A) + \frac{1}{2} \ln \det(\Sigma)^{-1} = C_1 + \mathbf{a}\mathbf{d}, \\ EI &\simeq n \ln\left(\frac{L}{\sqrt{2\pi e}}\right) + \frac{1}{2} \ln \text{pdet}(A^T A) + \frac{1}{2} \ln \det(\Sigma)^{-1} = C_2 + \mathbf{b}\mathbf{d}, \end{aligned} \quad (\text{C.43})$$

where $\mathbf{a} = ((1 - \frac{\alpha}{2}), 1)$, $\mathbf{b} = (1, 1)$ and $\mathbf{d} = (\frac{1}{2} \ln \text{pdet}(A^T A), \frac{1}{2} \ln \det(\Sigma)^{-1})^T$. The equal sign holds when A is a full rank matrix as $r(A) = n$ or Σ is an identity matrix as $\Sigma = I_n$. At the same time, we can use the generalized inverse matrix to obtain an approximation $\mathbf{d} \simeq \mathbf{b}^\dagger (EI - C_2)$ as $\mathbf{b}^\dagger = (1/2, 1/2)^T$. When $\text{pdet}(A^T A) = \det(\Sigma)^{-1}$, the equal sign holds; the closer $\text{pdet}(A^T A)$ and $\det(\Sigma)^{-1}$ is, the higher the degree of approximation. So we conclude

$$\ln \Gamma_\alpha \simeq C_1 + \mathbf{a}\mathbf{b}^\dagger (EI - C_2) = (1 - \frac{\alpha}{4}) EI + C. \quad (\text{C.44})$$

C_1, C_2 and C are all constants. Fig.7c presents the linear relationship between two indicators as $\alpha = 1$. \square

Appendix D Causal Emergence (CE)

CE refers to a special property of Markov dynamics: if the system's dynamics can yield a macroscopic dynamics with larger EI under a predefined coarse-graining strategy, then the system exhibits CE. However, this definition relies on the selection of coarse-graining strategies. Hoel et al. proposed the principle of maximizing EI [17, 18, 27, 29] to eliminate the arbitrariness of coarse-graining. However, this approach requires solving an often intractable optimization problem to obtain the optimal coarse-graining strategy and derive CE. To overcome this difficulty, Zhang et al. [40] introduced a new measure of CE based on approximate dynamical reversibility with SVD. Independent of coarse-graining, CE can be quantified directly from the singular value spectrum of the system's TPM. In the following section, we will extend this framework to GIS.

Appendix D.1 Causal emergence based on maximizing effective information

We have extended the CE framework to Gaussian iterative systems under Gaussian noise called GIS in the previous article [27], and many definitions and conclusions were drawn from this. A GIS [44] is a sequence of random variables x_t at different times t which usually represent the dynamic evolution of a certain quantity, such as stock prices, temperature changes, traffic flows, etc. This paper mainly focuses on linear high-dimensional stochastic iteration systems [78] to reduce our calculation. For variable $x_t \in \mathcal{R}^n$ at time t in the stochastic iteration system, the evolution of x_t follows the stochastic iterative equation The GIS we discuss is presented as

$$x_{t+1} = a_0 + Ax_t + \eta_t, \eta_t \sim \mathcal{N}(0, \Sigma), \quad (\text{D.1})$$

where, $a_0, x_t \in \mathcal{R}^n, A, \Sigma \in \mathcal{R}^{n \times n}$. We specify the ranks of matrices $\text{rk}(A) = \text{rk}(\Sigma) = n$. $\text{rk}(\cdot)$ means the rank of a matrix. We can easily observe that the probability of x_{t+1} falling in a region centered with Ax_t .

Based on micro-states like Eq.(D.1), we define the macro-state $y_t = \phi(x_t) = Wx_t$, where $W \in \mathcal{R}^{k \times n}$ is the parameter of coarse-graining strategy $\phi(x_t)$. The derived macro-state dynamic is,

$$y_{t+1} = a_{M,0} + A_M y_t + \eta_{M,t}, \eta_{M,t} \sim \mathcal{N}(0, \Sigma_M), \quad (\text{D.2})$$

where $a_{M,0} = Wa_0, A_M = WAW^\dagger, \Sigma_M = W\Sigma W^T$ and $k < n$. In this article, $(\cdot)^\dagger$ is the Moore-Penrose generalized inverse matrix [79, 80] of \cdot .

Obtaining \mathcal{J} , we still have a free parameter L , which is artificially assumed and greatly influences the results of \mathcal{J} . This hyperparameter can be subtracted by calculating dimensional averaged CE as

$$\Delta\mathcal{J} = \mathcal{J}_M - \mathcal{J}, \quad (\text{D.3})$$

where $\mathcal{J}_M \equiv \mathcal{J}(A_M, \Sigma_M)$ is the effective information for the macro-dynamics and $\Delta\mathcal{J}$ is the degree of CE.

After introducing CE $\Delta\mathcal{J}$ for GIS based on EI, it is obvious that one of its shortcomings is the high dependence on coarse-graining $\phi(x) = Wx, W \in \mathcal{R}^{k \times n}$, as

$$\mathcal{J}_M \equiv \mathcal{J}(A_M, \Sigma_M) = \mathcal{J}(WAW^\dagger, W\Sigma W^T). \quad (\text{D.4})$$

Quantifying CE by $\Delta\mathcal{J}$ requires pre-setting coarse-graining strategies ϕ and optimizing its parameters $W \in \mathcal{R}^{k \times n}$, k is the pre-defined macro dimension as $k < n$. Then, our problem can be formulated as

$$\begin{aligned} \max \quad & \Delta\mathcal{J}(W) \\ \text{s.t.} \quad & W \in \mathcal{W} \subseteq \mathcal{R}^{k \times n}. \end{aligned} \quad (\text{D.5})$$

Appendix D.1.1 Maximizing effective information by optimizing coarse-graining

When optimizing W , we must specify a subset \mathcal{W} of $\mathcal{R}^{k \times n}$ in advance as a limited range to avoid \mathcal{J}_M being divergent in Eq.D.5, which is very subjective and complicated. At the end of [27], a coarse-grained strategy that ensures stable information entropy is presented as $W^\dagger = W^T$. In this case, we can optimize W to obtain optimal macro-states and theoretical maximum $\Delta\mathcal{J}^*$ in [27] as

$$\Delta\mathcal{J}^* = \frac{1}{2k} \sum_{i=1}^k \ln s_i - \frac{1}{2n} \sum_{i=1}^n \ln s_i, \quad (\text{D.6})$$

where $s_i, i = 1, \dots, n$, are the singular values of $A^T \Sigma^{-1} A$. The pre-setting and optimization of W increases computational complexity and reduces accuracy. Even after the optimization of W , it is difficult to obtain the optimal $\Delta\mathcal{J}^*$ in Eq.(D.6) numerically based on data. We need to find a way to explore the potential of CE in GIS directly.

It is worth noting that Erik Hoel's effective information method suffers from a flaw in its calculation of non-degeneracy. This definition of degeneracy essentially involves iterating the Markov dynamics to obtain x_{t+1} when x_t is known, and then calculating the determinism of the state \tilde{x}_t at the previous moment, rather than directly inferring the previous moment x_t from the knowledge of the next moment x_{t+1} . This lack of effective simplification makes it difficult to detect the problem when calculating the discrete TPM matrix EI [17, 18, 22]. However, this flaw is particularly evident in Eq.(B.13), which first multiplies the covariance matrix of the forward dynamics and then divides it by the covariance matrix of the inverse dynamics. Consequently, when the determinism and non-degeneracy are added together, the covariance matrix of the forward dynamics is eliminated. When W is a unitary matrix, the SVD decomposition matrix $A^T \Sigma^{-1} A$ is actually the inverse covariance matrix of the inverse dynamics. The

coarse-graining strategy obtained by maximizing EI ignores the covariance of the forward dynamics in the original dynamics, resulting in a suboptimal coarse-graining of the forward dynamics in the new macro dynamics. Therefore, blindly maximizing effective information as in [26, 27] is not always reasonable.

Proof of Equation (D.3)

Proof. For the micro dynamical systems like Equation (D.1) and macro dynamical systems like Equation (D.2) after coarse-graining, we can calculate the micro effective information \mathcal{J}_m and macro effective information \mathcal{J}_M of two kinds of dynamical systems separately. In this way, causal emergence

$$\begin{aligned}
\Delta\mathcal{J} &= \mathcal{J}_M - \mathcal{J}_m = \frac{EI_M}{k} - \frac{EI_m}{n} \\
&= \frac{1}{k} \ln \frac{|\det(A_M)|L^k}{\det(\Sigma_M)^{\frac{1}{2}}(2\pi e)^{\frac{k}{2}}} - \frac{1}{n} \ln \frac{|\det(A)|L^n}{\det(\Sigma)^{\frac{1}{2}}(2\pi e)^{\frac{n}{2}}} \\
&= \frac{1}{k} \left(\ln \frac{1}{\det(\Sigma_M)^{\frac{1}{2}}(2\pi e)^{\frac{k}{2}}} + \ln(|\det(A_M)|L^k) \right) \\
&\quad \text{DeterminismInformation} \quad \text{DegeneracyInformation} \\
&\quad - \frac{1}{n} \left(\ln \frac{1}{\det(\Sigma)^{\frac{1}{2}}(2\pi e)^{\frac{n}{2}}} + \ln(|\det(A)|L^n) \right) \\
&= \ln \frac{|\det(WAW^\dagger)|^{\frac{1}{k}}}{|\det(A)|^{\frac{1}{n}}} + \ln \frac{|\det(\Sigma)|^{\frac{1}{2n}}}{|\det(W\Sigma W^T)|^{\frac{1}{2k}}}. \\
&\quad \text{DegeneracyEmergence} \quad \text{DeterminismEmergence}
\end{aligned} \tag{D.7}$$

□

Proof of Equation (D.6)

Proof. According to Jensen's inequality, we can obtain inequalities

$$|\det(W\Sigma W^\dagger)|^{-\frac{1}{2}} = \left[\sum (\gamma_m \prod \kappa_i) \right]^{-\frac{1}{2}} \leq \left[\sum \gamma_m \left(\prod \kappa_i \right)^{-\frac{1}{2}} \right] = |\det(W\Sigma^{-\frac{1}{2}}W^\dagger)|, \tag{D.8}$$

if and only if the eigenvalues are equal, the equal sign holds. By utilizing this inequality and combining it with the relevant properties of linear algebra, we can conclude that

$$\begin{aligned}
\Delta\mathcal{J} &= \ln \frac{|\det(WAW^\dagger)|^{\frac{1}{k}}}{|\det(W\Sigma W^\dagger)|^{\frac{1}{2k}}} - \ln \frac{|\det(A)|^{\frac{1}{n}}}{|\det(\Sigma)|^{\frac{1}{2n}}} \\
&= \frac{1}{k} \ln(|\det(W\Sigma W^\dagger)|^{-\frac{1}{2}} |\det(WAW^\dagger)|) - \frac{1}{n} \ln |\Sigma^{-\frac{1}{2}}A| \\
&\leq \frac{1}{k} \ln(|\det(W\Sigma^{-\frac{1}{2}}W^\dagger)| |\det(WAW^\dagger)|) - \frac{1}{n} \ln |\Sigma^{-\frac{1}{2}}A| \\
&= \frac{1}{k} \ln |\det(W\Sigma^{-\frac{1}{2}}W^\dagger WAW^\dagger)| - \frac{1}{n} \ln |\Sigma^{-\frac{1}{2}}A| \\
&\quad (\Sigma=VKV^T, A=V\Lambda V^T) \leq \frac{1}{k} \ln |\det(W\Sigma^{-\frac{1}{2}}AW^\dagger)| - \frac{1}{n} \ln |\Sigma^{-\frac{1}{2}}A| \\
&\quad (W=(\tilde{W}_k, O_{k \times (n-k)})V^T) \leq \frac{1}{k} \sum_{i=1}^k \ln |\tilde{d}_i| - \frac{1}{n} \sum_{i=1}^n \ln |\tilde{d}_i| \\
&= \frac{1}{2k} \sum_{i=1}^k \ln s_i - \frac{1}{2n} \sum_{i=1}^n \ln s_i,
\end{aligned} \tag{D.9}$$

When A and Σ share the same n eigenvectors, $|\tilde{d}_1| \geq \dots \geq |\tilde{d}_n|$ are n eigenvalues of $A\Sigma^{-1/2}$. That is to say, $\Sigma = VKV^T$ and $A = V\Lambda V^T$, where V is the matrix formed by the shared eigenvectors, and K and Λ are the eigenvalues for A and Σ , respectively. $\kappa = (\kappa_1, \dots, \kappa_n)$ and $\lambda = (\lambda_1, \dots, \lambda_n)$. The eigenvalues of $\Sigma^{-1/2}A$ are equal to the product of the eigenvalues of A and $\Sigma^{-1/2}$. $W = (\tilde{W}_k, O_{k \times (n-k)})V^T$ represents that both A and $\Sigma^{-1/2}$ retain the eigenvalues with the highest norm, the second and third unequal signs can also be taken as equal signs. $s_i, i = 1, \dots, n$, are the singular values of $A^T \Sigma^{-1} A$, we can directly get $\Delta\mathcal{J}^*$ in Eq.(D.6). □

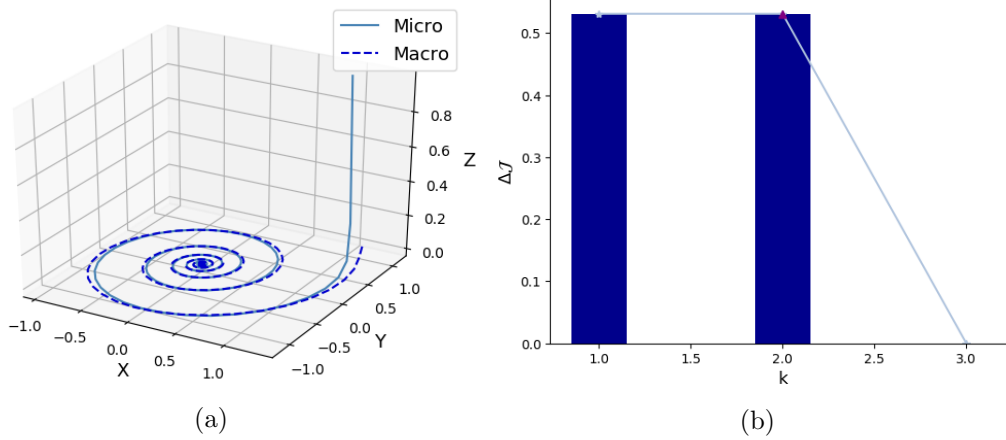


Figure 6: Experimental results of spiral rotating. Assuming the direction vector of the rotation axis is $u_0 = (0, 0.1, 1)^T$, after normalization as $u = u_0/\|u_0\|$, the rotation axis u can be obtained. At the same time, we specify the rotation angle $\theta = \pi/16$ and $\eta = 0$ as the dimension averaged Shannon entropy of both x_t and y_t remains the same. Through θ and u , we can get the rotation matrix R . By changing Ψ , we will obtain causal emergence in different forms. in Fig.6c, when $\Psi = \text{diag}(0.99, 0.97, 0.2)$ and $x_0 = (1, 1, 1)^T$, the path of x_t will first shrink to a plane perpendicular to u . In 6d, we project x_t onto the plane as the macro-state, where $k = 2$, $\Delta\mathcal{J} = 0.5295$. The reason why we do not take $k = 1$ here is that the more dimensionality we reduce, the greater the information loss. Therefore, in the absence of further improvement in causal emergence, we do not need to continue the dimensionality reduction of the system. (a) The spiral curve when $\Psi = \text{diag}(0.99, 0.97, 0.2)$ and $x_0 = (1, 1, 1)^T$, the trajectory of x_t is compressed to a plane perpendicular to u at the initial stage. (b) We can project x_t on the plane as a macro-state, where $k = 2$, $\Delta\mathcal{J} = 0.5295$.

Appendix D.1.2 Selection of k

In general, we choose the dimension macro k by comparing the maximum $\Delta\mathcal{J}^*$ after optimization under different dimensions k . Then, our problem can be formulated as

$$\begin{aligned} \max \quad & \Delta\mathcal{J}(W) \\ \text{s.t.} \quad & W \in \mathcal{W} \subseteq \mathcal{R}^{k \times n} \\ & k = 1, \dots, n \end{aligned} \quad (\text{D.10})$$

It can be seen that if k is not specified in advance, in the process of maximizing causal emergence, k will also be optimized along with W to obtain the result. So when we optimize $\Delta\mathcal{J}(W)$ under different k , we can get a sequence $\{\Delta\mathcal{J}_i^*\}$ as $i = 1, \dots, n$. Equally, our problem can also be presented as solving

$$k = \arg \max_i \Delta\mathcal{J}_i^*. \quad (\text{D.11})$$

to select the final macro dimension k . If there are two dimensions with equal $\Delta\mathcal{J}^*$, to minimize information loss, we choose the slightly higher dimension. For example, in the rotation model in Fig.6, we choose $k = 2$ as the macro dimension.

Appendix D.2 Causal emergence based on approximate dynamical reversibility with SVD

We have now demonstrated that the approximate dynamical reversibility of GIS can be quantified directly based on SVD of Σ^{-1} and $A^T \Sigma^{-1} A$, and has an approximately linear relationship with maximized EI. We also know that traditional EI-based CE relies on coarse-graining strategies and macro dynamics, but after maximizing EI when W is a unitary matrix, CE can also be obtained by eliminating the singular values of $A^T \Sigma^{-1} A$. So, can we directly define a metric for CE based on the singular value spectrum, bypassing the search for the optimal coarse-graining solution W ? This is the basic idea of the quantitative definition of SVD-based CE.

Appendix D.2.1 SVD-based CE for TPM

According to Zhang's previous work [40], since Γ_α is size-dependent, we need to normalize them by dividing the size of P as $\gamma_\alpha = \Gamma_\alpha/N$, to characterize the size-independent approximate dynamical reversibility. There is an integer $i \in [1, N)$ such that $\zeta_i > \epsilon$, then there is **vague causal emergence** with the level of vagueness ϵ occurred in the system as

$$\Delta\Gamma_\alpha(\epsilon) = \frac{\sum_{i=1}^{r_\epsilon} \zeta_i^\alpha}{r_\epsilon} - \frac{\sum_{i=1}^N \zeta_i^\alpha}{N}, \quad (\text{D.12})$$

where $r_\epsilon = \max\{i | \zeta_i > \epsilon\}$. ϵ can be selected according to the relatively clear cut-offs in the spectrum of singular values. When $\epsilon = 0$, if $r \equiv \text{rank}(P) < N$ then **clear causal emergence** occurs, and the degree is $\Delta\Gamma_\alpha(0)$. This definition is independent of any coarse-graining strategy and reflects the inherent property of the Markov chain.

Finally, a concise coarse-graining method based on the SVD of P to obtain a macro-level reduced TPM can be obtained by projecting the row vectors $P_i, \forall i \in [1, N]$ in P onto the sub-spaces spanned by the eigenvectors of $P \cdot P^T$ such that the major information of P is conserved, as well as Γ_α is kept unchanged.

Appendix D.2.2 SVD-based CE for GIS

From the definition of dimensional average reversible information $\hat{\gamma}_\alpha$, we can obtain that its final value depends on two spectra, one is the spectrum $s_1 \geq \dots \geq s_n$ of $A^T \Sigma^{-1} A$, and the other is the spectrum $\kappa_1 \geq \dots \geq \kappa_n$ of Σ^{-1} . Therefore, following the quantitative equation of CE (Eq.(D.6)), we can define CE based on approximate dynamical reversibility from the distribution of these two spectra.

One of the main contributions of this article is the new quantification of CE for GIS based on approximate dynamical reversibility under SVD following the definition of TPM in [40], which depends only on the system's parameters and does not require the optimization of coarse-graining strategies. Because Γ_α is calculated based on generalized determinants $\text{pdet}(A^T \Sigma^{-1} A)$, removing zero singular values will not change the first term of γ_α .

Because Γ_α is calculated based on generalized determinants $\text{pdet}(A^T \Sigma^{-1} A)$, removing zero singular values will not change γ_α . If $r \equiv \min\{r_s, r_\kappa\} < n$, we can directly replace n with r to obtain the macro-state dimension averaged reversibility information as

$$\gamma_\alpha(0) = \frac{1}{r} \left(\frac{1}{2} - \frac{\alpha}{4} \right) \sum_{i=1}^{r_s} \ln s_i + \frac{\alpha}{4r} \sum_{i=1}^{r_\kappa} \ln \kappa_i. \quad (\text{D.13})$$

Definition Appendix D.1. For GIS like Eq.(D.1), if $r \equiv \min\{r_s, r_\kappa\} < n$ then **clear causal emergence** occurs in this system. The degree of causal emergence is

$$\begin{aligned} \Delta\Gamma_\alpha(0) &= \gamma_\alpha(0) - \gamma_\alpha \\ &= \frac{1}{r} \left(\frac{1}{2} - \frac{\alpha}{4} \right) \sum_{i=1}^{r_s} \ln s_i + \frac{\alpha}{4r} \sum_{i=1}^{r_\kappa} \ln \kappa_i \\ &\quad - \frac{1}{n} \left(\frac{1}{2} - \frac{\alpha}{4} \right) \sum_{i=1}^{r_s} \ln s_i - \frac{\alpha}{4n} \sum_{i=1}^{r_\kappa} \ln \kappa_i. \end{aligned} \quad (\text{D.14})$$

Fig.7f and g shows the distribution of $\Delta\mathcal{J}_R^*$ and $\Delta\Gamma_\alpha(0)$ with a_2 and σ_2 in two-dimensional iterative systems as

$$A = \begin{pmatrix} a_1 & 0 \\ 0 & a_1 \end{pmatrix}, \Sigma = \begin{pmatrix} \sigma_1^2 & 0 \\ 0 & \sigma_2^2 \end{pmatrix}. \quad (\text{D.15})$$

It can be seen that when a_2 is large and σ_2 is small, there will be larger values for both, and their distributions are very close.

However, clear CE is difficult to directly detect in reality because it is unlikely for the parameter matrix derived from the data to have strictly zero singular values. So it is difficult to find a strict non-full rank matrix, even if the singular value of $A^T \Sigma^{-1} A$ is quite small and cannot be directly treated as a strict non-full rank matrix. On the other hand, Σ^{-1} may have very small singular values. So more often than not, we need to establish a lower bound for singular values as ϵ , where only singular values $s_i, \kappa_i \geq \epsilon$ are considered effective. Due to the information loss caused by deleted singular values $s_i, \kappa_i \leq \epsilon$, ϵ also determines the upper limit of the system's loss of information. The number of effective singular values is called the effective rank $r_\epsilon(A^T \Sigma^{-1} A)$ and $r_\epsilon(\Sigma^{-1})$. Based on global effective rank of the whole system as $r_\epsilon = \min\{r_\epsilon(A^T \Sigma^{-1} A), r_\epsilon(\Sigma^{-1})\}$, we can define vague macro reversibility as

$$\gamma_\alpha(\epsilon) = \frac{1}{r_\epsilon} \left(\frac{1}{2} - \frac{\alpha}{4} \right) \sum_{i=1}^{r_\epsilon} \ln s_i + \frac{\alpha}{4r_\epsilon} \sum_{i=1}^{r_\epsilon} \ln \kappa_i \quad (\text{D.16})$$

Definition Appendix D.2. For GIS like Eq.(D.1), suppose the singular values of $A^T \Sigma^{-1} A$ are $s_1 \geq s_2 \geq \dots \geq s_{r_s} \geq 0$. For a given real value $\epsilon \in [0, s_1]$, if there is an integer $i \in [1, r_s]$ such that $s_i \equiv s_i(A^T \Sigma^{-1} A) > \epsilon$, then there is **vague causal emergence** with the level of vagueness ϵ occurred in the system. We define

$$r_\epsilon \equiv \min\{r_\epsilon(A^T \Sigma^{-1} A), r_\epsilon(\Sigma^{-1})\} \quad (\text{D.17})$$

and the degree of causal emergence is:

$$\begin{aligned} \Delta \Gamma_\alpha(\epsilon) &= \gamma_\alpha(\epsilon) - \gamma_\alpha \\ &= \frac{1}{r_\epsilon} \left(\frac{1}{2} - \frac{\alpha}{4} \right) \sum_{i=1}^{r_\epsilon} \ln s_i + \frac{\alpha}{4r_\epsilon} \sum_{i=1}^{r_\epsilon} \ln \kappa_i \\ &\quad - \frac{1}{n} \left(\frac{1}{2} - \frac{\alpha}{4} \right) \sum_{i=1}^{r_s} \ln s_i - \frac{\alpha}{4n} \sum_{i=1}^{r_\kappa} \ln \kappa_i \end{aligned} \quad (\text{D.18})$$

where $r_\epsilon = \max\{i | s_i > \epsilon\}$.

Fig.7j and i shows the distribution of $\Delta \mathcal{J}^*$ and $\Delta \Gamma_\alpha(\epsilon)$ with a_2 and σ_2 in two-dimensional iterative systems and their distributions are very close.

Appendix D.3 Equivalence between $\Delta \Gamma_\alpha$ and $\Delta \mathcal{J}^*$

The third important contribution of this article is the rigorous proof of the positive correlation between $\Delta \Gamma_\alpha$ and $\Delta \mathcal{J}^*$.

Theorem Appendix D.1. (Correlation between $\Delta \Gamma_\alpha(\epsilon)$ and $\Delta \mathcal{J}^*$): When the backward dynamics $p(x_t | x_{t+1}) = \mathcal{N}(A^\dagger x_{t+1} - A^\dagger a_0, A^\dagger \Sigma (A^\dagger)^T)$ is close to a normalized normal distribution as $A^\dagger \Sigma (A^\dagger)^T \approx I_n$, $\Delta \Gamma_\alpha(\epsilon)$ and $\Delta \mathcal{J}^*$ are approximately linear and positively correlated as

$$\Delta \Gamma_\alpha(\epsilon) \simeq \left(1 - \frac{\alpha}{4}\right) \Delta \mathcal{J}^*. \quad (\text{D.19})$$

The equal sign holds when the inverse dynamics $p(x_t | x_{t+1}) = \mathcal{N}(A^\dagger x_{t+1} - A^\dagger a_0, A^\dagger \Sigma (A^\dagger)^T)$ is a normalized normal distribution as $A^\dagger \Sigma (A^\dagger)^T = A^{-1} \Sigma (A^{-1})^T = I_n$.

Proof. We can compare $\Delta \mathcal{J}$ and $\Delta \Gamma_\alpha(\epsilon)$. When $W^\dagger = W^T$, $r = r_s$ is the rank of $A^T \Sigma^{-1} A$, the CE of linear Gaussian iterative systems satisfy

$$\begin{aligned} \Delta \mathcal{J} &= \frac{1}{2k} \ln \det(A_M^T \Sigma_M^{-1} A_M) - \frac{1}{2n} \ln \text{pdet}(A^T \Sigma^{-1} A) \\ &\leq \frac{1}{2k} \sum_{i=1}^k \ln s_i - \frac{1}{2n} \sum_{i=1}^r \ln s_i \equiv \Delta \mathcal{J}^*. \end{aligned} \quad (\text{D.20})$$

Similar to Eq.(C.43), when A approximates full rank or $\Sigma \approx \sigma^2 I_n$, $\sum_{i=1}^r \ln s_i \simeq \sum_{i=1}^r \ln a_i + \sum_{i=1}^n \ln \kappa_i$. If the coupling degree between A and Σ^{-1} spaces is high as $s_i = a_i \kappa_i, i = 1, \dots, n$, the macro-state will also satisfy the same approximation properties. In this way, when $k = r_\epsilon$, $m = n$ and $r = r_s$, we can obtain two approximate forms of CE as

$$\begin{aligned} \Delta \mathcal{J}^* &\simeq \frac{1}{2k} \sum_{i=1}^k \ln a_i - \frac{1}{2n} \sum_{i=1}^r \ln a_i + \frac{1}{2k} \sum_{i=1}^k \ln \kappa_i - \frac{1}{2n} \sum_{i=1}^n \ln \kappa_i, \\ \Delta \Gamma_\alpha(\epsilon) &\simeq \frac{1}{2r_\epsilon} \left(1 - \frac{\alpha}{2}\right) \sum_{i=1}^k \ln a_i - \frac{1}{2n} \left(1 - \frac{\alpha}{2}\right) \sum_{i=1}^r \ln a_i + \frac{1}{2r_\epsilon} \sum_{i=1}^k \ln \kappa_i - \frac{1}{2n} \sum_{i=1}^n \ln \kappa_i, \end{aligned} \quad (\text{D.21})$$

where $a_1 \geq a_2 \geq \dots \geq a_r$ are singular values of $A^T A$. The equal sign holds when $r(A) = n$ and $s_i = a_i \kappa_i$ or $\Sigma = \sigma^2 I_n$.

Based on the monotonicity of elementary functions and matrix theory like Eq.(C.44), we can conclude that $\Delta \Gamma_\alpha(\epsilon)$ and $\Delta \mathcal{J}^*$ are approximately linear and positively correlated as Theorem Appendix D.1 shows. The equal sign is established when (1) $\Sigma = \sigma^2 I_n$ and (2) $\text{pdet}(A^T A) = \det(\Sigma)^{-1}$. Otherwise, 3 conditions must be met together: (1) $r(A) = n$, (2) $s_i = a_i \kappa_i, i = 1, \dots, n$, (3) $\text{pdet}(A^T A) = \det(\Sigma)^{-1}$. If the model approaches either of the above two sets of conditions, the approximation is effective. Fig.7f,g and j presents the linear relationship between $\Delta \mathcal{J}^*$ and $\Delta \Gamma_\alpha(0)$. Fig.7h,i and l presents the linear relationship between $\Delta \mathcal{J}^*$ and $\Delta \Gamma_\alpha(\epsilon)$ as $\alpha = 1$. We can see that the scatter points are very close to the slope and theoretical value of the curve. \square

From a logical perspective, our definition of CE is actually an approximate necessary condition for maximizing EI-based CE as defined by Hoel et al. [17, 18]. In other words, for any Markov dynamics, if we want to find a coarse-graining strategy that maximizes EI, we can actually perform SVD on the dynamics first. For example, the discussion at the end of [27] on the case where W is a unitary matrix actually transforms the coarse-graining strategy into a screening of singular values of the matrix $A^T \Sigma^{-1} A$, which is part of the calculation of SVD-based CE, namely the SVD of the inverse covariance matrix $A^T \Sigma^{-1} A = USU^T$ of backward dynamics. If the singular values $S = \text{diag}(s_1, \dots, s_n)$, and the orthogonal singular vector matrix $U = (u_1, \dots, u_n)$, in order to preserve the maximum k singular values, we only need to preserve the dimensions corresponding to these singular vectors $U_1 = (u_1, \dots, u_k)$ and discard $U_2 = (u_{k+1}, \dots, u_n)$. Due to the orthogonality of U , we can directly obtain $U_1^T A^T \Sigma^{-1} A U_1 = U_1^T U S U^T U_1 = \text{diag}(s_1, \dots, s_k)$. It can be seen that we only need to multiply the coarse-graining parameter matrix $W = U_1^T$ by the original variables to make the inverse covariance matrix $W A^T \Sigma^{-1} A W^T$ of the macroscopic backward dynamics become a diagonal matrix that only retains s_1, \dots, s_k . The singular vectors u_1, \dots, u_k corresponding to those larger singular values actually correspond to the optimal coarse-graining strategy we are looking for.

Although there is a high likelihood that the two frameworks overlap, they are not entirely equivalent because the coarse-graining strategy obtained by maximizing EI ignores the covariance of forward dynamics. So, we propose an algorithm that constructs a coarse-graining strategy based on SVD, considering both the inverse covariance matrices Σ^{-1} and $A^T \Sigma^{-1} A$ of the forward and backward dynamics, and attempts to preserve the maximum singular values of the two matrices as much as possible. In this way, it can ensure that the coarse-graining strategy matrix W is unitary, and only the singular values of the inverse covariance matrix will be screened without changing the singular values, so that the probability space retained by the macro dynamics and the corresponding micro dynamics has the same probability distribution, and it can also ensure that both forward and backward dynamics are taken into account in the calculation of the coarse-graining strategy at the same time without only focusing on one side.

Appendix E Coarse-graining strategy based on SVD

Firstly, we need to review the coarse-grained strategy based on SVD for discrete TPM, which is mainly based on the singular vectors corresponding to the largest few singular values.

Appendix E.1 Coarse-graining strategy based on SVD of TPM

Although clear or vague CE phenomena can be defined and quantified without coarse-graining, a simpler coarse-grained description for the original system is needed to compare with the results derived from EI. Therefore, we also provide a concise coarse-graining method based on the singular value decomposition of P to obtain a macro-level reduced TPM. The basic idea is to project the row vectors $P_i, \forall i \in [1, N]$ in P onto the sub-spaces spanned by the eigenvectors of $P \cdot P^T$ such that the major information of P is conserved, as well as Γ_α is kept unchanged.

Concretely, the coarse-graining method contains five steps:

1) We first make SVD decomposition for P (suppose P is irreducible and recurrent such that stationary distribution exist):

$$P = U \cdot \Sigma \cdot V^T, \quad (\text{E.1})$$

where, U and V are two orthogonal and normalized matrices with dimension $N \times N$, and $\Sigma = \text{diag}(\sigma_1, \sigma_2, \dots, \sigma_N)$ is a diagonal matrix which contains all the ordered singular values.

2) Selecting a threshold ϵ and the corresponding r_ϵ according to the singular value spectrum;

3) Reducing the dimensionality of row vectors P_i in P from N to r by calculating the following Equation:

$$\tilde{P} \equiv P \cdot V_{N \times r}, \quad (\text{E.2})$$

where $V_{N \times r} = (V_1^T, V_2^T, \dots, V_r^T)$.

4) Clustering all row vectors in \tilde{P} into r groups by K-means algorithm to obtain a projection matrix Φ , which is defined as:

$$\Phi_{ij} = \begin{cases} 1 & \text{if } \tilde{P}_i \text{ is in the } r\text{th group} \\ 0 & \text{otherwise,} \end{cases} \quad (\text{E.3})$$

for $\forall i, j \in [1, N]$.

5) Obtain the reduced TPM according to P and Φ .

To illustrate how we can obtain the reduced TPM, we will first define a matrix called stationary flow matrix as follows:

$$F_{ij} \equiv \mu_i \cdot P_{ij}, \forall i, j \in [1, N], \quad (\text{E.4})$$

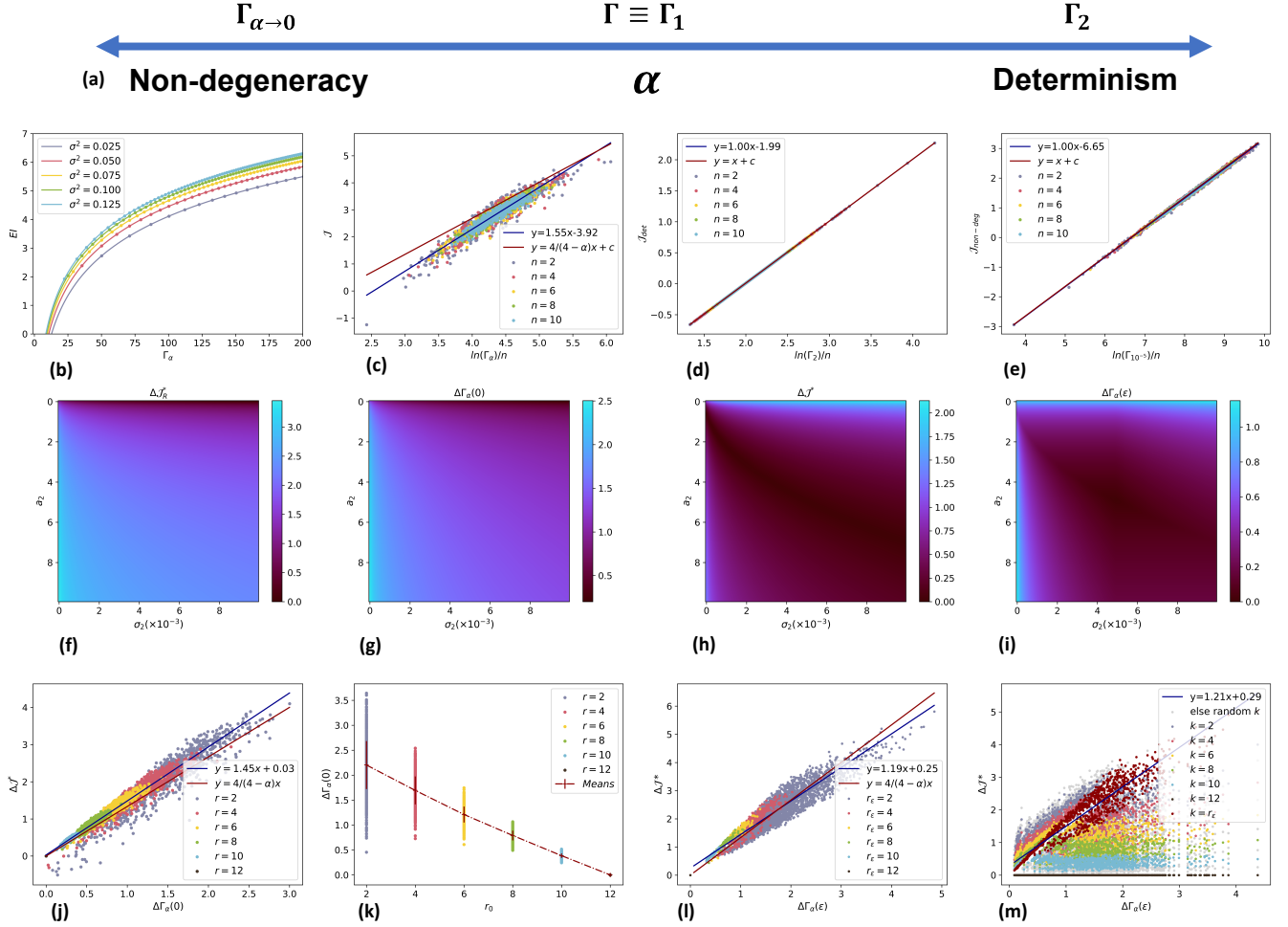


Figure 7: (a) $\alpha = 1$ is often chosen to balance Γ_α 's emphasis on both determinism and degeneracy. For $\alpha < 1$, Γ_α tends to capture more non-degeneracy of $p(x_{t+1}|x_t)$. For $\alpha > 1$, Γ_α emphasizes the determinism. (b) The logarithmic relationship between EI and Γ_α . It can be seen that for different noise covariances σ , as Γ_α increases, EI shows an approximate logarithmic growth relationship with Γ_α as $\alpha = 1$. (c) The linear relationship between two indicators \mathcal{J} and Γ_α as $\alpha = 1$. (d) the linear relationships between determinism to Γ_α as $\alpha \rightarrow 2$. (e) the linear relationships between non-degeneracy to Γ_α as $\alpha \rightarrow 0$. The dimensional average reversible information $\ln \Gamma_\alpha$ and dimensional average effective information \mathcal{J} , as well as their corresponding determinism and non-degeneracy, are all linearly related. (f), (g), (h) and (i) shows the distribution of $\Delta \mathcal{J}_R^*$, $\Delta \Gamma_\alpha(0)$, $\Delta \mathcal{J}$ and $\Delta \Gamma_\alpha(\epsilon)$ with a_2 and σ_2 in two-dimensional iterative systems. (j) The linear relationship between $\Delta \mathcal{J}_R^*$ and $\Delta \Gamma_\alpha(0)$ as $\alpha = 1$. (k) $\Delta \Gamma_\alpha(0)$ under different fixed r . (l) The linear relationship between $\Delta \mathcal{J}_R^*$ and $\Delta \Gamma_\alpha(\epsilon)$ as $\alpha = 1$. (l) The relationship between $\Delta \mathcal{J}_R^*$ and $\Delta \Gamma_\alpha(\epsilon)$ as $\alpha = 1$ under different k and r_ϵ .

where μ is the stationary distribution of P which satisfies $P \cdot \mu = \mu$.

Secondly, we will derive the reduced flow matrix according to Φ and F :

$$F' = \Phi^T \cdot F \cdot \Phi, \quad (\text{E.5})$$

where, F' is the reduced stationary flow matrix. Finally, the reduced TPM can be derived directly by the following formula:

$$P'_i = F'_i / \sum_{j=1}^N (F'_i)_j, \forall i \in [1, N]. \quad (\text{E.6})$$

Finally, P' is the coarse-grained TPM.

Appendix E.2 Coarse-graining strategy based on SVD of GIS

After learning that $\Delta\Gamma_\alpha$ and $\Delta\mathcal{J}^*$ are approximately positively correlated and only determined by the difference in singular values of $A^T\Sigma^{-1}A$ and Σ^{-1} , we need to find the optimal coarse-graining strategy $\phi(x_t) = Wx_t$ defined by $W \in \mathcal{R}^{r_\epsilon \times n}$, based on SVD, which is determined by the singular vectors of $A^T\Sigma^{-1}A$ and Σ^{-1} . Since both $A^T\Sigma^{-1}A$ and Σ^{-1} are symmetric matrices, the SVD of them are $A^T\Sigma^{-1}A = USU^T$, $\Sigma^{-1} = VKV^T$, $S = \text{diag}(s_1, \dots, s_n)$ and $K = \text{diag}(\kappa_1, \dots, \kappa_n)$, $s_1 \geq \dots \geq s_n$, $\kappa_1 \geq \dots \geq \kappa_n$, are singular value matrices of $A^T\Sigma^{-1}A$ and Σ^{-1} . Corresponding singular vector matrices $U = (u_1, \dots, u_n)$ and $V = (v_1, \dots, v_n)$. Due to the filtering of singular values when calculating $\Delta\Gamma_\alpha(\epsilon)$, we need to redefine the singular vectors corresponding to the retained and discarded singular values during coarse-graining.

The optimal coarse-graining strategy $\phi(x_t) = Wx_t$ requires considering both $A^T\Sigma^{-1}A$ and Σ^{-1} to balance forward and backward dynamics, so it is necessary to construct W based on the vectors of U and V together. Since $U \neq V$, we generally cannot guarantee that $s_i, \dots, s_{r_\epsilon}$ and $\kappa_i, \dots, \kappa_{r_\epsilon}$ are retained together. Therefore, when constructing W , we need a classified discussion of the span spaces of U and V . Here we present an algorithm to achieve this.

Appendix E.2.1 Algorithm

This section presents the algorithm for constructing a coarse-graining strategy based on SVD.

Input: Matrices A, Σ

Step 1: Perform SVD on $A^T\Sigma^{-1}A$ and Σ^{-1} :

$$\begin{aligned} USU^T &= A^T\Sigma^{-1}A, \\ VKV^T &= \Sigma^{-1}, \end{aligned}$$

Step 2: Combine $S = \text{diag}(s_1, \dots, s_n)$ and $K = \text{diag}(\kappa_1, \dots, \kappa_n)$, then sort $s_1 \geq \dots \geq s_n$ and $\kappa_1 \geq \dots \geq \kappa_n$ in descending order to get $\tilde{S} = \text{diag}(\tilde{s}_1, \dots, \tilde{s}_{2n})$ as $\tilde{s}_1 \geq \dots \geq \tilde{s}_{2n}$.

Step 3: Truncate \tilde{S} with a threshold ϵ , and keep corresponding singular vectors and values:

$$\tilde{S}_1 = \text{Truncate}(\tilde{S}, \epsilon), \quad (\text{E.7})$$

Retaining $\tilde{S}_1 = (\tilde{s}_1, \dots, \tilde{s}_{r_{\epsilon 1}})$, $\tilde{s}_1 > \dots > \tilde{s}_{r_{\epsilon 1}} > \epsilon$, and keeps the corresponding singular vectors from $U = (u_1, \dots, u_n)$ and $V = (v_1, \dots, v_n)$, which are combined as $\tilde{U}_1 = (\tilde{u}_1, \dots, \tilde{u}_{r_{\epsilon 1}}) \in \mathcal{R}^{n \times r_{\epsilon 1}}$. $r_{\epsilon 1} < 2n$ is the effective rank we get from SVD for the first time.

Step 4: Apply SVD on the matrix $\tilde{U}_1\tilde{S}_1 \in \mathcal{R}^{n \times r_{\epsilon 1}}$:

$$\hat{U}\hat{S}\hat{V}^T = \tilde{U}_1\tilde{S}_1, \quad (\text{E.8})$$

$\hat{S} \in \mathcal{R}^{n \times r_{\epsilon 1}}$ contains singular values of matrix $\tilde{U}_1\tilde{S}_1$, $\hat{U} \in \mathcal{R}^{n \times n}$ are the corresponding singular vectors.

Step 5: Truncate \hat{U} and \hat{S} using the same threshold ϵ , and keep the retained singular vectors as $\hat{U}_1 \in \mathcal{R}^{n \times r_{\epsilon 2}}$. Use these to obtain the final quantization strategy as

$$W = \hat{U}_1^T, \quad (\text{E.9})$$

where $r_{\epsilon 2} < n$ is the effective rank we get from SVD for the second time, which can be regarded as the final dimension of macro states r_ϵ .

Output: Coarse-graining function $\phi(x) = Wx$.

Appendix E.2.2 Explanation

According to [40], the reversibility of dynamics analyzed with the SVD method relates directly to maximizing EI in macroscopic dynamics. The singular vectors corresponding to the largest singular values of the TPM align with the directions that maximize macroscopic EI. For continuous systems, we decompose the deterministic and non-degenerate terms with SVD separately and then analyze and screen the combined singular value spectra. In this process, coarse-graining based on determinism and that based on non-degeneracy do not necessarily remain independent, so \tilde{U}_1 may fail to stay orthogonal and linearly independent. For example, if A is the identity matrix, the U and V obtained in the first step are identical. This results in different macroscopic variables that actually correspond to the same microscopic variables. To prevent this issue, we perform a second SVD to decouple the different coarse-graining directions, thus forming a unified coarse-graining scheme.

Specifically, when dealing with known models, we can get the global effective rank r_ϵ in advance, so we can directly specify $r_{\epsilon 1} = n$ and $r_{\epsilon 2} = r_\epsilon$ to complete our coarse-graining operation. What's more, when $\Sigma \approx \sigma^2 I$ or $A^\dagger \Sigma (A^\dagger)^T \approx (\sigma^2/a^2)I$, as a and σ are constants, our parameter is equivalent to $W = U_1^T$ or $W = V_1^T$ as $U_1 = (u_1, \dots, u_{r_\epsilon}), V_1 = (v_1, \dots, v_{r_\epsilon})$.

Appendix F Experiments

Here are some supplements to the experiments in the main text.

Appendix F.1 Details of Malthusian growth models

In a dynamical system, the degrees of freedom represent the number of independent variables needed to fully describe its state. When strong correlations or constraints exist between different dimensions (e.g., state variables), they no longer evolve independently. This interdependence, which can arise from conservation laws, synchronization, or other mathematical constraints, implies that the value of one variable can be determined by the others. Consequently, the system's effective degrees of freedom are reduced. Instead of exploring the full high-dimensional space, the system's trajectory is confined to a lower-dimensional manifold, simplifying its overall behavior.

The first example contains 4 variables, in which the first two variables x_1, x_2 follow the Malthusian growth model [60] with different growth rates of 0.2 and 0.05. To study CE, we define the other two variables x_3, x_4 as the copies of the first two variables shown as Fig.8a, thus, they are redundant dimensions. If $x = (x_1, x_2, x_3, x_4)$, the evolution of x is a GIS $x_{t+1} = a_0 + Ax_t + \eta_t, \eta_t \sim \mathcal{N}(0, \sigma^2 I_4)$ as $x_t, x_{t+1} \in \mathcal{R}^4, \sigma^2 = 0.1, a_0 = 0$, and

$$A = \begin{pmatrix} 1.2 & 0 & 0 & 0 \\ 0 & 1.05 & 0 & 0 \\ 1.2 & 0 & 0 & 0 \\ 0 & 1.05 & 0 & 0 \end{pmatrix}. \quad (\text{F.1})$$

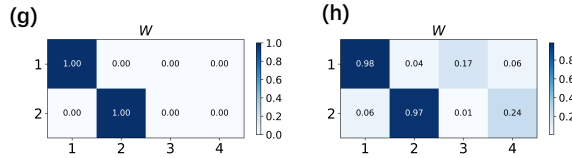
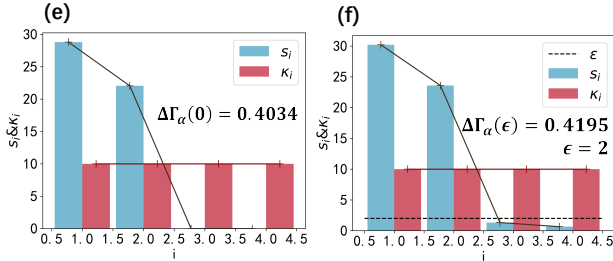
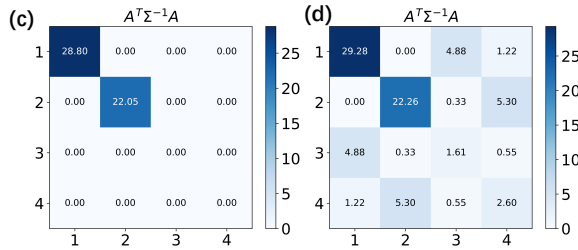
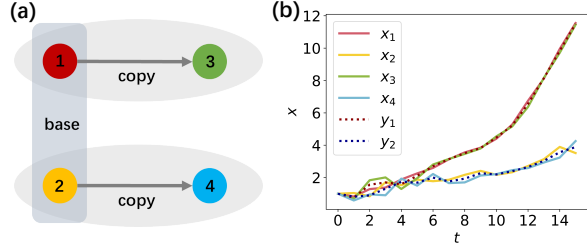
A sample of evolutionary trajectories generated by this model is shown in Fig.8b. In this model, $\Sigma = \sigma^2 \cdot I_4$ is a full rank matrix, so we only need to study the backward dynamics covariance matrix $A^T \Sigma^{-1} A$ (Fig.8c). This matrix only has two singular values as the singular value spectrum is shown in Fig.8e with $r = 2 < 4$, the horizontal axis represents the sequence number of singular values arranged in descending order as $s_1 \geq \dots \geq s_4$, while the vertical axis represents the magnitude of singular values s_i , so clear CE can be calculated as $\Delta \Gamma_\alpha(0) = 0.4034$. Fig.8g shows the coarse-graining parameter $W \in \mathcal{R}^{2 \times 4}$ obtained by truncating the orthogonal matrix U after SVD of $A^T \Sigma^{-1} A$. When clear CE exists, variables x_1 and x_2 hold all the relevant information contained within x_3 and x_4 . Therefore, the role of $\phi(x) = Wx$ is to remove the last two dimensions and only retain the first two dimensions of x to describe the evolution of the growth model.

To show the concept of vague CE, we can add some perturbations to A and obtain

$$A = \begin{pmatrix} 1.2 & 0 & 0 & 0 \\ 0 & 1.05 & 0.001 & 0 \\ 1.22 & 0 & 0.4 & 0.1 \\ 0 & 1.06 & 0.03 & 0.5 \end{pmatrix} \quad (\text{F.2})$$

and $A^T \Sigma^{-1} A$ (Fig.8d) is a full rank matrix as $r = n = 4$. Then clear CE $\Delta \Gamma_\alpha(0) = 0$. However, by observing the singular value spectrum in Fig.8f, we can see that only two dimensions have significant impacts, so we need to calculate vague CE. By using the threshold selection as $\epsilon = 2$, vague CE can be calculated as $\Delta \Gamma_\alpha(\epsilon) = 0.4195$. The coarse-graining parameter W is shown in Fig.8h, the columns represent the macroscopic dimensions, and the rows

Malthusian growth models



Markovian Gaussian systems

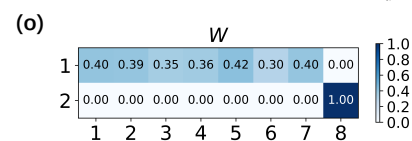
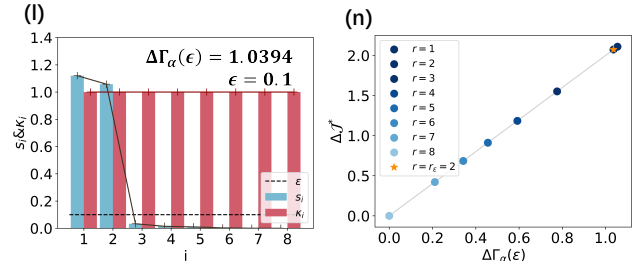
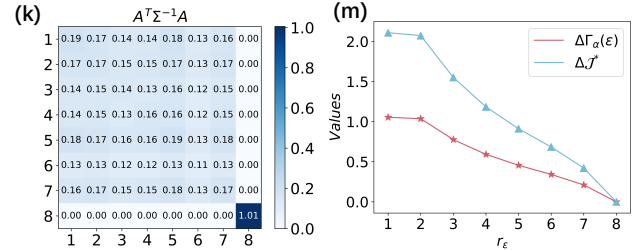
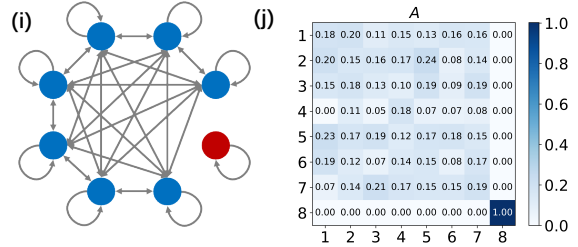


Figure 8: Analytical solutions obtained from numerical simulations of known models. (a) A Malthusian growth mode where x_3, x_4 are copies of x_1, x_2 . (b) A sample of trajectory generated by the Malthusian growth models with growth rates of 0.2 and 0.05. $x_i, i = 1, 2, 3, 4$, are micro-states, while y_1 and y_2 are theoretical macro-states obtained by coarse-graining. (c) The backward dynamics covariance matrix $A^T \Sigma^{-1} A$ when $r(A) = 2$. (d) The singular value spectrum of $A^T \Sigma^{-1} A$ when $A^T \Sigma^{-1} A$ only has two singular values. Clear CE can be calculated as $\Delta \Gamma_\alpha(0) = 0.4034$. (e) Coarse-graining parameter W obtained by truncating U in the presence of Clear CE, the number of columns represents the macroscopic dimension, and the number of rows represents the microscopic dimension. (f) $A^T \Sigma^{-1} A$ after random perturbations to A . (g) The singular value spectrum of $A^T \Sigma^{-1} A$ when A is perturbed. The degree of Vague CE is $\Delta \Gamma_\alpha(\epsilon) = 0.4195$ when $\epsilon = 2$. (h) The coarse-graining parameter W for vague CE case, combined x_1 and x_3 , x_2 and x_4 . (i) A Markov Gaussian system. (j) The connectivity matrix A of the Markov Gaussian system with the first 7 variables are dependent each other and the 8th variable is isolated. (k) The backward dynamics covariance matrix $A^T \Sigma^{-1} A$ of the Markov Gaussian system. (l) The singular value spectrum of $A^T \Sigma^{-1} A$ in the Markov Gaussian system has two larger singular values and the cut off can be taken at $\epsilon = 0.1$. Vague CE occurs, and the degree of CE is $\Delta \Gamma_\alpha(\epsilon) = 1.0394$. (m) The dependence of $\Delta \mathcal{J}^*$ and $\Delta \Gamma_\alpha(\epsilon)$ with the manually setting r_ϵ . (n) The correlation between $\Delta \mathcal{J}^*$ and $\Delta \Gamma_\alpha(\epsilon)$ by varying r_ϵ . (o) The coarse-graining parameter W obtained by the singular vector with the largest singular values, it merges the first seven dimensions of Markov Gaussian system to form a new macro-variable, and keep the last variable as another macro-variable.

represent the microscopic dimensions. Due to disturbances, x_3 and x_4 also contain some independent information. $\phi(x) = Wx$, $W = U_1^T$, is to merge x_1 and x_3 , x_2 and x_4 by weighted summation and the two row-vectors that make up W are exactly equal to the singular vectors corresponding to the two largest singular values s_1, s_2 .

This case illustrates that sometimes high dimensions may reduce the efficiency of reversibility of a system due to dimensional redundancy. Retaining only the maximum r_ϵ singular values of the covariance matrix can improve the efficiency of reversibility and generate CE.

Appendix F.2 Markovian Gaussian systems

In addition to directly copying, the system also has information redundancy if there are several dimensions with strong correlations. In this situation, CE will also be evident. A classic case here is the Markov Gaussian system [81–84], which can be seen as a Markov chain in a continuous state space. The example systems are characterized by the dynamics $x_{t+1} = Ax_t + \eta_t$, where x_t contains n variables, $A = (a_{ij})_{n \times n}$ is the connectivity matrix and $\eta_t \sim \mathcal{N}(0, I_n)$. $0 \leq a_{ij} \leq 1$ reflects whether there is a connection between i and j and the strength of the connection. In this way, the system’s state fluctuates within a stable region, and the Markovian Gaussian system can model EEG data [6, 81] to study consciousness-related issues. The relevant data can be transformed into a 0-1 time series and studied using TPM, but the information is lost.

We considered a system with $n = 8$ and connectivity as shown in Figure. Connection strengths between the first seven nodes are $1/7$ and the eighth node is a self-ring with a connection strength of 1. To avoid $\gamma_\alpha = 0$ caused by singular values all being 1, we can add some perturbations to A , such as

$$A \sim \mathcal{N} \left(\begin{pmatrix} 1/7 & 1/7 & 1/7 & 1/7 & 1/7 & 1/7 & 1/7 & 0 \\ 1/7 & 1/7 & 1/7 & 1/7 & 1/7 & 1/7 & 1/7 & 0 \\ 1/7 & 1/7 & 1/7 & 1/7 & 1/7 & 1/7 & 1/7 & 0 \\ 1/7 & 1/7 & 1/7 & 1/7 & 1/7 & 1/7 & 1/7 & 0 \\ 1/7 & 1/7 & 1/7 & 1/7 & 1/7 & 1/7 & 1/7 & 0 \\ 1/7 & 1/7 & 1/7 & 1/7 & 1/7 & 1/7 & 1/7 & 0 \\ 1/7 & 1/7 & 1/7 & 1/7 & 1/7 & 1/7 & 1/7 & 0 \\ 0 & 0 & 0 & 0 & 0 & 0 & 0 & 1 \end{pmatrix}, 0.05I_8 \right). \quad (\text{F.3})$$

As Fig.8i showed, the first seven dimensions of the system have the same connection strength and equal correlation. The eighth dimension is independent of the first seven dimensions and without correlation. After randomly generating a matrix A , we can calculate $A^T \Sigma^{-1} A$, from Fig.8j and 8k we can see that matrix $A^T \Sigma^{-1} A$ can also be approximately divided into two independent parts as A . By observing the singular value spectrum in Fig.8l, we can observe that $A^T \Sigma^{-1} A$ has two larger singular values and $r_\epsilon = 2$ as $\epsilon = 0.0552$. Vague CE can be calculated as $\Delta \Gamma_\alpha(\epsilon) = 1.0394$. The coarse-graining parameter W is shown in Fig.8o, $\phi(x) = Wx$ can merge the first seven dimensions of the Markov Gaussian system to obtain a system where the efficiency of reversibility is improved.

We can also analyze the optimal value of r_ϵ by balancing the enhancement of reversibility efficiency and information loss. Analyzing the impact of manually setting effective rank r_ϵ on CE in Fig.8m, we find that from $r_\epsilon = 8$ to $r_\epsilon = 2$, $\Delta \mathcal{J}^*$ and $\Delta \Gamma_\alpha(\epsilon)$ significantly increases as r_ϵ decreases. But comparing $r_\epsilon = 2$ with $r_\epsilon = 1$, we found that due to the close similarity in the size of the first two singular values and the weights of the two dimensions, CE when $r_\epsilon = 1$ cannot be significantly improved compared to CE when $r_\epsilon = 2$. The property of information entropy based on Gaussian distribution, the loss of information entropy in the inverse dynamics of macro-states $y_t = Wx_t$ and micro-states x_t is $H(x_t|x_{t+1}) - H(y_t|y_{t+1}) = \sum_{i=r_\epsilon}^n \ln s_i$, if $r_\epsilon < 2$, the loss will be significantly increased. This can explain why $r_\epsilon = 2$ is the optimal effective rank, and the optimal macro-state dimension is also 2 dimensions. If we coarsen the system into one dimension, not only will CE not be significantly improved, but the model may also lose too much information. At the same time, in Fig.8n we can also confirm that there is a linear relationship between $\Delta \mathcal{J}^*$ and $\Delta \Gamma_\alpha(\epsilon)$ under different r_ϵ .

Appendix F.3 Details of SIR based on NN

Most systems in reality are unable to obtain precise dynamic models to calculate analytical solutions for CE, as demonstrated in the previous two examples. However, we can train a neural network to obtain approximate dynamics from observed time series data. Our third case is to show the phenomenon of CE obtained by a well-trained neural network (NN) on the training time series data generated by a Susceptible-Infected-Recovered (SIR) dynamical model

SIR models

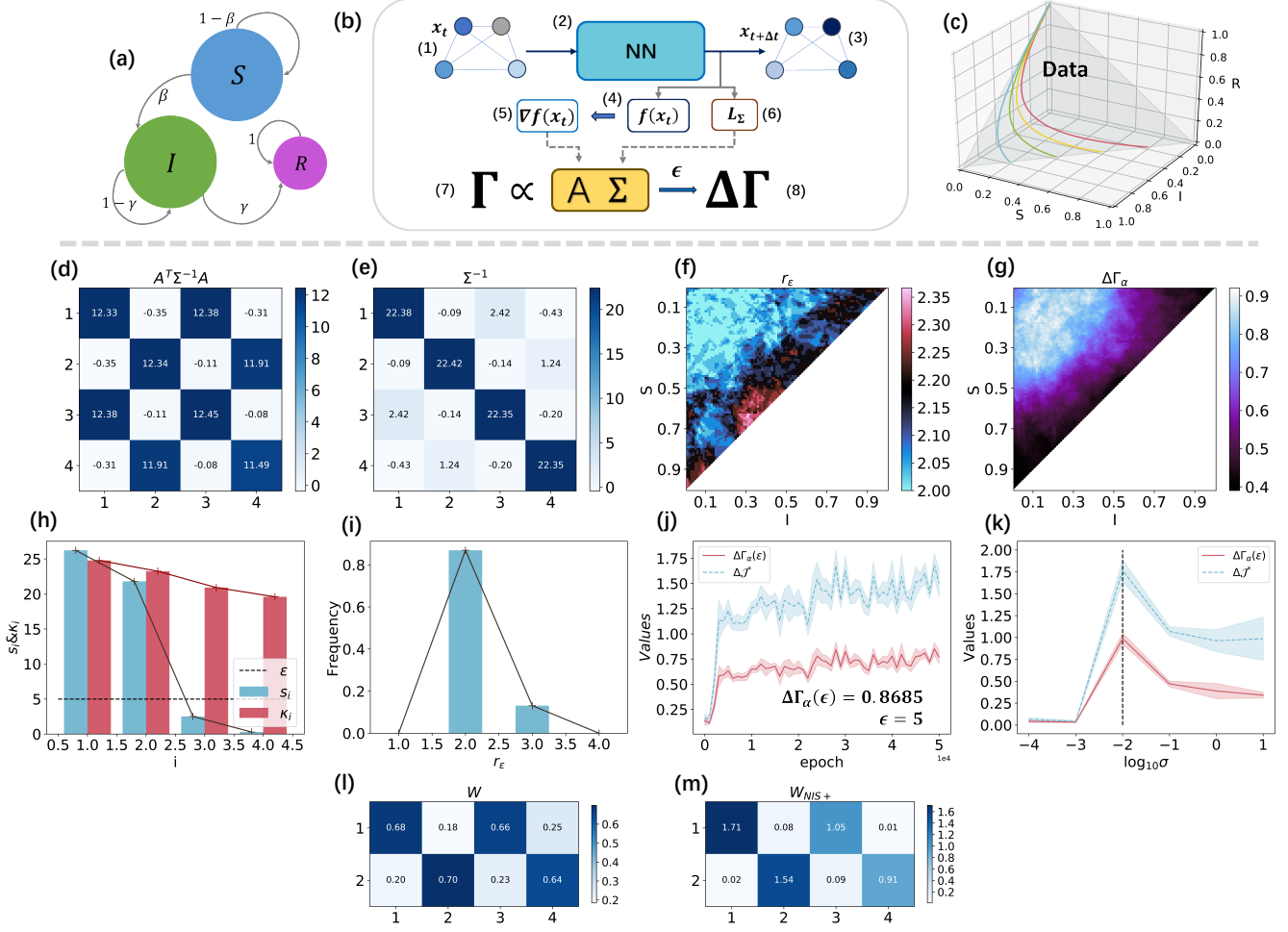


Figure 9: An example of applying machine learning to extract dynamics from data and measure CE of the dynamical system. (a) Schematic diagram of the SIR model. (b) Schematic diagram of learning dynamics and calculating Γ through NN based on data. (1) and (3) are the variables x_t and predicted $x_{t+\Delta t}$ at adjacent time points. (2) NN model for machine learning, whose structure is in Appendix F.3. (4) Dynamics $f(x_t)$ learned by NN model based on data of SIR. (5) $A_{x_t} = \nabla f(x_t)$ is the Jacobian matrix of the trained model at x_t . (6) The output L_Σ of the Covariance Learner Network, the covariance matrix Σ_{x_t} is derived from which. (7) The numerical solution of Γ , which is related to A and Σ . (8) Applying $A^T \Sigma^{-1} A = \langle A_{x_t}^T \Sigma_{x_t}^{-1} A_{x_t} \rangle_{x_t \in \mathcal{X}}$ and $\Sigma^{-1} = \langle \Sigma_{x_t}^{-1} \rangle_{x_t \in \mathcal{X}}$, SVD-based CE $\Delta \Gamma(\epsilon)$ can be calculated under suitable ϵ , \mathcal{X} is the domain of SIR. (c) Training data which is the same as NIS+ [29]. The full dataset (entire triangular region) used for training is displayed, along with four example trajectories with the same infection and recovery or death rates. The method of generating training data can be found in Appendix F.3. (d) $A^T \Sigma^{-1} A = \langle A_{x_t}^T \Sigma_{x_t}^{-1} A_{x_t} \rangle_{x_t \in \mathcal{X}}$ derived by NN trained SIR model. (e) $\Sigma^{-1} = \langle \Sigma_{x_t}^{-1} \rangle_{x_t \in \mathcal{X}}$ derived by NN trained SIR model. (f) Distribution of r_ϵ obtained by traverse the dynamical space of SIR with different (S, I) and x_t generated from which. (g) Distribution of $\Delta \Gamma_\alpha$ under different (S, I) obtained by traverse the dynamical space. (h) The singular value spectra of $A^T \Sigma^{-1} A$ and Σ^{-1} in NN trained SIR model. (i) The frequency of r_ϵ under different samples x_t in test dataset. (j) Maximum $\Delta \Gamma_\alpha(\epsilon) = 0.8685$ when the training period is around 50,000 as $\epsilon = 5$. (k) The changing trend of CE under different σ , the threshold for trend change is around $\sigma = 0.01$. (l) The coarse-graining matrix W derived from Section Appendix E and Appendix E.2 use $A^T \Sigma^{-1} A = \langle A_{x_t}^T \Sigma_{x_t}^{-1} A_{x_t} \rangle_{x_t \in \mathcal{X}}$ and $\Sigma^{-1} = \langle \Sigma_{x_t}^{-1} \rangle_{x_t \in \mathcal{X}}$. (m) The coarse-graining matrix W_{NIS+} derived from NIS+. For the convenience of observation, we have taken absolute values for each dimension in W and W_{NIS+} .

[49] as shown in Fig.9b with the following dynamics:

$$\begin{cases} \frac{dS}{dt} = -\beta SI, \\ \frac{dI}{dt} = \beta SI - \gamma I, \\ \frac{dR}{dt} = \gamma I, \end{cases} \quad (\text{F.4})$$

as shown in Fig.9a, where $S, I, R \in [0, 1]$ represent the rate of susceptible, infected, and recovered individuals in a population, $\beta = 1$ and $\gamma = 0.5$ are parameters for infection and recovery rates.

To generate the time series data of the micro-state, we adopt the same method as in our previous work of NIS+ [29]. We generate data by converting $dS/dt, dI/dt$ into $\Delta S/\Delta t, \Delta I/\Delta t$ as $\Delta t = 0.01$ and $(S_{t+\Delta t}, I_{t+\Delta t}) \approx (S_t, I_t) + (dS_t/dt, dI_t/dt)\Delta t$. Then we duplicate the macro-state (S_t, I_t) as shown in Fig.9c and added Gaussian random noise to form the micro-state x_t as

$$x_t = (S_t, I_t, S_t, I_t) + \xi_t, \quad (\text{F.5})$$

where $\xi_t \sim N(0, \Sigma)$ and

$$\Sigma = \sigma^2 \begin{pmatrix} 1 & -\frac{1}{2} & 0 & 0 \\ -\frac{1}{2} & 1 & 0 & 0 \\ 0 & 0 & 1 & -\frac{1}{2} \\ 0 & 0 & -\frac{1}{2} & 1 \end{pmatrix}. \quad (\text{F.6})$$

as $\sigma^2 = 0.04$.

By feeding the micro-state data into a forward neural network (NN) called **Covariance Learner Network**, we can use this model to approximate the micro-dynamics of the SIR model. The model we trained has the following structure:

- **Input layer:** The NN has $n = 4$ input neurons, corresponding to the size of the input vector x_t .
- **Hidden layers:** The network contains two hidden layers. The first hidden layer has *hidden_size* = 64 neurons, followed by a *LeakyReLU* activation function. The second hidden layer also has *hidden_size* = 64 neurons, followed by another *LeakyReLU* activation.
- **Output layer:** The output layer contains two parts. The first part, f_μ , outputs a mean vector μ of size n . The second part, f_L , outputs the elements of the lower triangular part of the Cholesky decomposition of the covariance matrix, with size $n \times n$.

Formally, given an input, the network applies a series of transformations:

$$\begin{aligned} h_1 &= \text{LeakyReLU}(B_1 x_t + b_1), \\ h_2 &= \text{LeakyReLU}(B_2 h_1 + b_2), \\ \mu &= B_\mu h_2 + b_\mu, \\ L_\Sigma &= B_L h_2 + b_L, \end{aligned} \quad (\text{F.7})$$

where B and b denote trainable weight matrices and biases. The predicted $f(x_t)$ and final covariance matrix are then computed as:

$$\begin{aligned} f(x_t) &= \mu, \\ \Sigma_{x_t} &= L_\Sigma L_\Sigma^T. \end{aligned} \quad (\text{F.8})$$

After that, we use a negative logarithmic likelihood loss function (NLL) as

$$NLL = \frac{1}{2} \left[(x_{t+1} - f(x_t))^T \Sigma_{x_t}^{-1} (x_{t+1} - f(x_t)) + \ln \det(\Sigma_{x_t}) + n \ln(2\pi) \right] \quad (\text{F.9})$$

to train the parameters of the dynamical function $f(x_t)$ and the covariance matrix Σ_{x_t} simultaneously.

Since the quantification of our CE framework does not require a pre-setting coarse-grained strategy and the coarse-grained function can be directly obtained from the SVD of $A^T \Sigma^{-1} A$ after setting r_ϵ , we can directly calculate the degree of CE by $\Delta \Gamma_\alpha$ and ignore the learning processes of encoder, decoder and macro-dynamics in NIS+ as mentioned in [29]. Due to the nonlinearity of the SIR dynamics, we cannot directly use the CE quantification method of linear GIS. Instead, we approximate NN as a linear mapping at different input x_t by Taylor expansion

(see the method in Appendix D.1). We can obtain the CE identification result and the final coarse-graining strategy directly by calculating $A_{x_t} = \nabla f(x_t)$ as the Jacobian matrix of the trained NN model at x_t . And Σ_{x_t} is the covariance matrix that neural networks can directly output. Due to the differences under different x_t , we can randomly generate x_t with a uniform distribution on the domain \mathcal{X} of the SIR dynamics and take the average value as $A^T \Sigma^{-1} A \approx \langle A_{x_t}^T \Sigma_{x_t}^{-1} A_{x_t} \rangle_{x_t \in \mathcal{X}}$ and $\Sigma^{-1} \approx \langle \Sigma_{x_t}^{-1} \rangle_{x_t \in \mathcal{X}}$ to calculate $\Delta \Gamma_\alpha$ of the system. Fig.9b visualizes the method of computation for $\Delta \Gamma$ on a multivariate Gaussian model.

Using the data in Fig.9c, we can perform SVD on matrices $A^T \Sigma^{-1} A$ and Σ^{-1} in Fig.9d and Fig.9e. In Fig.9h, we can see the singular value spectrum of matrices $A^T \Sigma^{-1} A$ and Σ^{-1} in which the horizontal axis represents the sequence number of singular values arranged in descending order, while the vertical axis represents the magnitude of singular values s_i, κ_i . Due to the existence of the copy operation, even the simplest NN can recognize only two dimensions with larger singular values as $r_\epsilon = 2$ when $\epsilon = 5$. If we directly calculate r_ϵ by $A_{x_t}^T \Sigma_{x_t}^{-1} A_{x_t}$ as x_t is sampled from the test data set and plot r_ϵ as a matrix related to S, I in Fig.9f, we can see that most positions satisfy $r_\epsilon = 2$. By calculating the frequency of r_ϵ under different samples $A_{x_t}^T \Sigma_{x_t}^{-1} A_{x_t}$, from Fig.9i we can find that $r_\epsilon = 2$ has the highest frequency.

From Fig.9h, $A^T \Sigma^{-1} A$ has two larger singular values and $r_\epsilon = 2$ as $\epsilon = 5$. In model training, we get the value of Vague CE as $\Delta \Gamma_\alpha(\epsilon) = 0.8685$ when the training period is 50,000, which is shown in Fig.9j. We can also directly calculate $\Delta \Gamma_\alpha(\epsilon)$ by $A_{x_t}^T \Sigma_{x_t}^{-1} A_{x_t}$ as x_t is sampled from the test data set and plot $\Delta \Gamma_\alpha$ as a matrix related to S, I in Fig.9g. Comparing Fig.9f and Fig.9g, we can see that the most stable region of r_ϵ and the region with the highest $\Delta \Gamma_\alpha(\epsilon)$ are almost identical as (S, I) roughly located within a circle with a radius of 0.5 and a center of $(0, 0)$.

We can also compare the results of our framework and NIS+ mentioned in [29]. From Fig.9l and Fig.9m, we can see that the coarse-graining matrix W obtained through the singular vectors and the Jacobian matrix W_{NIS+} of the NIS+ coarse-graining encoder are similar. For the convenience of observation, we have taken absolute values for each dimension in W and W_{NIS+} . Both coarse-graining methods indicate that the first and the third micro-state dimensions mainly influence the first macro-state dimension, while the second and fourth micro-state dimensions mainly influence the second macro-state dimension. Both the values of W and W_{NIS+} are consistent with the copy method (Fig.8a), which is used during data generation. In addition, we can test the changing trend of CE under different σ . From Fig.9k, When $\sigma < 0.01$, $\Delta \Gamma_\alpha(\epsilon)$ is positively correlated with σ , and when $\sigma > 0.01$, the two are negatively correlated. We can see that the turning point for CE is around $\sigma = 0.01$, which is consistent with the value obtained by NIS+ [29].

However, our framework addresses the decline in training efficiency associated with encoder training in NIS+, leading to a more streamlined and effective approach to model training and CE detection.

Appendix G Methods

Appendix G.1 System and observation noises

The noise $\eta \sim \mathcal{N}(0, \Sigma)$ in our model $y = Ax + \eta$ can be decomposed into system noise e and observation noise ξ . For the GIS like $\mathbf{y} = \mathbf{Ax} + e, e \sim \mathcal{N}(0, E)$ is pure noise inherent in the system, $\mathbf{y} \in \mathcal{R}^n$ follows a normal distribution about $\mathbf{x} \in \mathcal{R}^n$, so $\mathbf{y} \sim \mathcal{N}(A\mathbf{x}, E)$, $A \in \mathcal{R}^{n \times n}$, $E \in \mathcal{R}^{n \times n}$. We can add observation noise as

$$x = \mathbf{x} + \xi_{\mathbf{x}}, \xi_{\mathbf{x}} \sim \mathcal{N}(0, \Xi_{\mathbf{x}}) \quad (\text{G.1})$$

$$y = \mathbf{y} + \xi_{\mathbf{y}}, \xi_{\mathbf{y}} \sim \mathcal{N}(0, \Xi_{\mathbf{y}}) \quad (\text{G.2})$$

Since $\mathbf{y} = \mathbf{Ax} + e, y = A(x - \xi_{\mathbf{x}}) + e + \xi_{\mathbf{y}} \sim \mathcal{N}(Ax_t, \Xi_{\mathbf{y}} + A\Xi_{\mathbf{x}}A' + E) = \mathcal{N}(Ax_t + a_0, \Sigma)$, in which

$$\Sigma = \Xi_{\mathbf{y}} + A\Xi_{\mathbf{x}}A' + E \in \mathcal{R}^{n \times n} \quad (\text{G.3})$$

is the combination of covariance matrixes of system and observation noises and

$$\eta = -A\xi_{\mathbf{x}} + e + \xi_{\mathbf{y}} \in \mathcal{R}^n \quad (\text{G.4})$$

is the combination of two types of noise. In real data, Ξ is more common than E and it's difficult to distinguish between the two directly. The SIR model in this article only has observation noise ξ and the first two cases only have system noises e , all included in η .